


For Reference

NOT TO BE TAKEN FROM THIS ROOM

Ex LIBRIS
UNIVERSITATIS
ALBERTAENSIS





Digitized by the Internet Archive
in 2022 with funding from
University of Alberta Library

<https://archive.org/details/Al1984>

THE UNIVERSITY OF ALBERTA

TRANSPORT PROPERTIES OF RARE EARTH
HEXABORIDES AND ALLOYS

by



NAUSHAD ALI

A THESIS

SUBMITTED TO THE FACULTY OF GRADUATE STUDIES AND RESEARCH
IN PARTIAL FULFILLMENT OF THE REQUIREMENTS FOR THE DEGREE
OF DOCTOR OF PHILOSOPHY

DEPARTMENT OF PHYSICS

EDMONTON, ALBERTA

FALL, 1984

A faint, circular stamp is visible in the bottom right corner of the page, but its details are illegible.

ABSTRACT

We have measured the low temperature electrical resistivity, thermoelectric power and magnetoresistance of antiferromagnetic rare earth hexaborides (REB_6 , $\text{RE} = \text{La}, \text{Ce}, \text{Pr}, \text{Nd}, \text{Gd}$ and Dy), $[\text{La}, \text{Gd}]_x\text{B}_6$ and $[\text{La}, \text{Dy}]_x\text{B}_6$ alloys and dilute yttrium-rare earth alloys. CeB_6 is found to be a "dense Kondo" system and could be understood at least qualitatively in the "Kondo Lattice" model. A T^2 dependence in resistivity of magnetic REB_6 at the lowest temperatures is interpreted to be caused by an electron-electron scattering of Baber-type. The magnetic resistivity, of the REB_6 compounds in the antiferromagnetic phase, has a temperature dependence of T^3 or T^4 , which is consistent with the theoretical predictions. The thermoelectric power of REB_6 has a non-linear behaviour in T at low temperatures that is associated with the phonon drag and magnon drag effects. We have determined the critical exponents from critical resistivity studies and have found that the temperature derivatives of the resistivity and the thermoelectric power in the vicinity of T_N are linearly related.

We have measured the magnetoresistance (MR) of the antiferromagnetic REB_6 in the magnetically ordered state as well as in the paramagnetic state and have found the field (H) and the temperature (T) dependence of the MR. The anisotropy in the longitudinal and the transverse magnetoresistance is associated with the anisotropic conduction

electron-f-electron scattering.

We have found, from the resistivity and the thermoelectric power studies, $[\text{La},\text{Gd}]\text{B}_6$ and $[\text{La},\text{Dy}]\text{B}_6$ alloys to be spin glasses at low temperatures even for concentrations of rare earths as high as 28 at. %. Dilute Y-RE alloys exhibit various properties depending on concentration and nature of rare earth impurities. YCe (Ce = 3%) is a Kondo alloy whereas YCe (15 at. %) shows coexistence of spin glass and Kondo effect. For YDy alloys, 2% Dy is sufficient to produce a spin-glass effect. We observe an antiferromagnetic behaviour in YSm (Sm = 3%) and YTB (Tb = 3%).

ACKNOWLEDGEMENTS

First and foremost I would like to thank Prof. S.B. Woods for his continued guidance during the entire course of this work. He has been very kind and patient with me all the time. Indeed I am very grateful to him for giving me independence to work on my own, yet he was always there whenever I needed his help and guidance. I wish to thank Dr. R.L. Singh from whom I learnt experimental techniques during the first two months of this project. For technical help, I am thankful to Mr. T. Valian.

Finally, I thank my wife Donna for her understanding and patience particularly during the final stages of this thesis.

TABLE OF CONTENTS

	<u>Page</u>
CHAPTER 1 INTRODUCTION	1
CHAPTER 2 BASIC CONCEPTS AND THEORETICAL BACKGROUND	8
2.1 The RKKY Interaction	8
2.2 Resistivity	12
2.2.1 Resistivity in the paramagnetic state ($T > T_O$)	13
2.2.2 Resistivity in the ordered state ($T < T_O$)	14
2.2.3 Critical resistivity	17
2.3 Thermoelectric Power (TEP)	19
2.4 Magnetoresistance (MR)	24
2.5 Spin Glass	29
CHAPTER 3 EXPERIMENTAL DETAILS	33
3.1 The Cryostat	33
3.2 Thermometry	37
3.3 Resistance Measurements	38
3.4 Thermoelectric Power Measurement	40
3.5 <u>AuFe</u> Thermocouple	42
3.6 Specimens	46
CHAPTER 4 REB_6 COMPOUNDS	47
4.1 Properties of the Compounds	47
4.2 Experimental Results and Discussion	52

	<u>Page</u>
CHAPTER 4 (cont'd)	
4.2.1 CeB ₆	54
4.2.2 Antiferromagnetic REB ₆ (RE = Pr, Nd, Gd and Dy)	65
4.2.2a Resistivity	65
4.2.2b Thermoelectric power	86
4.2.2c Magnetoresistance	102
CHAPTER 5 [La,Gd]B ₆ AND [La,Dy]B ₆ ALLOYS	130
CHAPTER 6 Y-RE ALLOYS	140
CHAPTER 7 CONCLUDING REMARKS	157
BIBLIOGRAPHY	160

LIST OF TABLES

<u>Table</u>	<u>Description</u>	<u>Page</u>
4.1	Crystallographic and magnetic data	49
4.2	Values of parameter A for CeB_6	64
4.3	RRR values for REB_6 compounds	66
4.4	Temperature range of T^2 and T^4 or T^3 dependence for REB_6	73
4.5	Values of critical exponent (α) of REB_6 compounds	85
4.6	Values of S_{\min} and T_{\min} for REB_6 compounds	91
4.7	Values of parameter A for PrB_6	112
4.8	Values of parameter A for NdB_6	115
4.9	Values of parameter A for GdB_6	115
4.10	Values of parameter A for DyB_6	118
5.1	RRR values for $[\text{La},\text{Gd}]\text{B}_6$ and $[\text{La},\text{Dy}]\text{B}_6$ alloys	131
5.2	Values of T_O , T_{\max} and S_{\max} for $[\text{La},\text{Gd}]\text{B}_6$ and $[\text{La},\text{Dy}]\text{B}_6$	137
6.1	RRR values for Y-Re alloys	141
6.2	Values of S_{\max} , T_{\max} and T_O for Y-RE alloys	145

LIST OF FIGURES

<u>Figure</u>	<u>Description</u>	<u>Page</u>
2.1	ρ vs T of a magnetic metal	15
2.2	Anisotropy in $\Delta\rho/\rho_0$ vs H	28
3.1	Cryostat and Specimen Holder	35
3.2	Circuit diagram of d.c. comparator	39
3.3	Diagram showing polarity of thermo-electric voltage	41
3.4	Sensitivity of AuFe thermocouple vs T	43
3.5	Arrangement for measuring thermoelectric voltage	45
4.1	Structure of REB_6	48
4.2	T_N vs atomic number	51
4.3	$(\Gamma_{\text{RE}}/\Gamma_{\text{Gd}})^2$ vs atomic number	53
4.4	r vs log T for CeB_6	55
4.5	S vs T for CeB_6	59
4.6	$\Delta\rho/\rho_0$ vs H for CeB_6	61
4.7	$\Delta\rho/\rho_0$ vs H^2 for CeB_6	63
4.8	r vs T for LaB_6 , PrB_6 and NdB_6	68
4.9	r vs T for GdB_6 and DyB_6	69
4.10	r vs T in range 4-12K for GdB_6	70
4.11	ρ vs T^2 for PrB_6 , NdB_6 , GdB_6 and DyB_6	72
4.12	ρ vs T^4 for PrB_6 and NdB_6	76
4.13	ρ vs T^3 for GdB_6 and DyB_6	77
4.14	r vs T and r' vs T for PrB_6	79
4.15	r vs T and r' vs T for NdB_6	80
4.16	r vs T and r' vs T for GdB_6	81

<u>Figure</u>	<u>Description</u>	<u>Page</u>
4.17	r vs T and r' vs T for DyB_6	82
4.18	S vs T for LaB_6 , PrB_6 and NdB_6	87
4.19	S vs T for LaB_6 , GdB_6 and DyB_6	88
4.20	(a) S vs T (b) S_e , S_{gN} and S_{gU} vs T	90
4.21	S_{spd} vs T for PrB_6 and NdB_6	93
4.22	S_{spd} vs T for GdB_6 and DyB_6	94
4.23	r' and S' vs T for PrB_6 around T_N	96
4.24	r' and S' vs T for NdB_6 around T_N	97
4.25	r' and S' vs T for GdB_6 around T_N	98
4.26	S' vs r' in the vicinity of T_N of PrB_6	99
4.27	S' vs r' in the vicinity of T_N of NdB_6	100
4.28	S' vs r' in the vicinity of T_N of GdB_6	101
4.29	$\Delta\rho/\rho_0$ vs H for PrB_6	103
4.30	$\Delta\rho/\rho_0$ vs H for NdB_6	104
4.31	$\Delta\rho/\rho_0$ vs H for GdB_6	105
4.32	$\Delta\rho/\rho_0$ vs H for DyB_6	106
4.33	$\Delta\rho/\rho_0$ vs T for PrB_6	108
4.34	$\Delta\rho/\rho_0$ vs T for NdB_6	109
4.35	$\Delta\rho/\rho_0$ vs T for GdB_6	110
4.36	$\Delta\rho/\rho_0$ vs T for DyB_6	111
4.37	A/H^2 vs H for PrB_6	113
4.38	$\Delta\rho_{\text{AN}}$ vs T for PrB_6	120
4.39	$\Delta\rho_{\text{AN}}$ vs T for NdB_6	121
4.40	$\Delta\rho_{\text{AN}}$ vs T for DyB_6	122
4.41	r vs T for GdB_6 at various H	125

<u>Figure</u>	<u>Description</u>	<u>Page</u>
4.42	$(\Delta\rho/\rho_0)_{ }$ vs H for GdB_6 at $T \leq 12\text{K}$	127
4.43	$(\Delta\rho/\rho_0)_{\perp}$ vs H for GdB_6 at $T \leq 12\text{K}$	129
5.1	r vs T for $[\text{La},\text{Gd}]\text{B}_6$	132
5.2	r vs T for $[\text{La},\text{Dy}]\text{B}_6$	133
5.3	S vs T for $[\text{La},\text{Gd}]\text{B}_6$	135
5.4	S vs T for $[\text{La},\text{Dy}]\text{B}_6$	136
5.5	S vs T parameterized in S_{max} , T_{max} and T_0	138
6.1	r vs T for YCe (Ce = 3% and 15%)	142
6.2	S vs T for YRE alloys	143
6.3	r vs T for YDy (Dy = 2% and 10%)	146
6.4	r vs T for YSm (3% Sm) and YTb (3% Tb)	148
6.5	S vs T for YSm (3% Sm) and YRb (3% Tb)	149
6.6	$\Delta\rho/\rho_0$ vs H for YCe (3% Ce)	152
6.7	$\Delta\rho/\rho_0$ vs H for YDy (2% Dy)	154
6.8	$\Delta\rho/\rho_0$ vs H for YTb (3% Tb)	156

CHAPTER 1

INTRODUCTION

Recently there has been considerable interest in the broad range of physical properties encompassed by the rare earth hexaborides (REB_6 , RE = rare earth), generated by the work of Matthias and coworkers (1968, 1968a). At present the physical properties of these hexaborides are neither completely determined nor understood. These materials exhibit a variety of magnetic and electronic properties.

LaB_6 is non-magnetic and becomes superconducting below $\sim 2\text{K}$, CeB_6 is antiferromagnetic below $\sim 2.4\text{K}$ and is considered to be a "dense Kondo" material, SmB_6 exhibits valence fluctuating properties while other REB_6 (RE = Pr, Nd, Gd, Dy, Tb and Ho) order antiferromagnetically at low temperatures. The REB_6 compounds have a CsCl crystal structure with a rare earth ion at each corner of the cube and a B_6 -octahedron at the body centre. The trivalent rare earth ions in REB_6 compounds contribute one electron towards the conduction band and two electrons to the valence band. It is clear that the trivalent REB_6 are monovalent metals from the Fermi surface information and band structure calculation for LaB_6 by Ishizawa et al (1977).

The magnetic properties of CeB_6 have been investigated recently by Kasuya et al (1981) and it has been found to be a "dense Kondo" material in the sense that the

resistivity decreases as $\log T$ from $\sim 3.3\text{K}$ to room temperature. Kasuya and his coworkers at Tohoku University (Japan) are actively involved in a detailed magnetic study of CeB_6 . There has been an experimental study of the magnetic susceptibility of PrB_6 , NdB_6 , GdB_6 and DyB_6 (Paderno et al, 1967; Hacker et al, 1971; and Hacker and Lin, 1968). Specific heat studies (Westrum et al, 1968; Westrum, 1968; McCarthy et al, 1980; and Lee et al, 1970) have shown that PrB_6 , NdB_6 and GdB_6 go through a second order phase transition in ordering from the paramagnetic phase to an antiferromagnetic phase at low temperatures. A recent study by McCarthy et al (1980) has shown that PrB_6 has another phase below $\sim 4\text{K}$ in the antiferromagnetic regime. Although resistivity and magnetic torque measurements by Nozaki et al (1980) on single crystal GdB_6 have shown the presence of a lower temperature phase below $\sim 7\text{K}$, the detail of the magnetic structure of GdB_6 is not yet known. The recent neutron-diffraction studies on PrB_6 and NdB_6 by McCarthy et al (1980) and McCarthy and Thompson (1980) have identified two phases for PrB_6 and one phase for NdB_6 in their antiferromagnetic regimes. Resistivity measurements by Fisk and Johnston (1977) and Fisk (1976) on PrB_6 and NdB_6 , with particular interest in the temperature region above the Nèel temperatures (T_N), have shown that the resistivity data of PrB_6 can be well explained if one takes into account the aspherical Coulomb interaction between the conduction electrons and the f-electrons. It is believed that such

anisotropic scattering in NdB_6 is not significant. At the same time their fit to the data in the ordered state below T_N was not at all satisfactory.

It is believed that the interaction between magnetic moments of rare earth ions is not due to direct exchange interaction. Magnetic f-electrons in a rare earth ion are well localized and there is no significant overlap of the charge distribution of f-electrons on different rare earth ions. It is thought that in metallic REB_6 the magnetic moments interact mainly via the conduction electrons. Such an interaction is called the RKKY (Ruderman, Kittel, Kasuya and Yoshida) interaction, borrowing the initials of the people who developed the mathematical model for such an interaction.

There is little experimental data for REB_6 , particularly in the ordered state. To determine and understand the physical properties of REB_6 , we have conducted experimental studies of the transport properties (e.g. resistivity, thermoelectric-power and magneto-resistance) with particular interest in the magnetically ordered state. From measurements on non-magnetic LaB_6 it is known that the resistivity does not change significantly below $\sim 30\text{K}$. This means that the phonon resistivity of LaB_6 and therefore of the other isostructural hexaborides below $\sim 30\text{K}$ is very weak. Since all the REB_6 studied here have their antiferromagnetic-to-paramagnetic phase-transition temperature (T_N) below $\sim 25\text{K}$, it is possible to extract the magnetic contribution

to the resistivity easily. At the same time, since these compounds are cubic, the resistivity is expected to be isotropic, hence polycrystalline samples could be used for the study.

The critical scattering (i.e. the scattering in the vicinity of a magnetic phase transition temperature) of antiferromagnetic metals is neither clearly understood nor has there been much accurate and detailed experimental work done. We have measured the critical resistivity and the thermoelectric power of the antiferromagnetic REB_6 metals in the vicinity of their Néel temperatures. A comparison of these data with the present theoretical predictions provides the first comprehensive test of the resistivity calculations and of the theoretical prediction of a universal critical behaviour of all the transport coefficients.

According to the theoretical and experimental studies of Fert and coworkers (1977, 1977a, 1974 and 1980) there is an anisotropic interaction between the conduction electrons (k) and f -electrons in a rare earth system with $L \neq 0$ (where L is the total orbital angular momentum of the rare earth ion). Anisotropic k - f scattering exhibits itself as anisotropy in the magnetoresistance (MR), that is, the dependence of the MR on the direction of the external magnetic field with respect to the direction of the sample current.

The MR of antiferromagnetic metals with localized magnetic moments, has been investigated theoretically by Yamada and Takada (1973, 1973a) a decade ago. There is no theoretical work, to our knowledge, on the MR of antiferromagnets with localized moments where the dominant magnetic interaction is of RKKY type. We have done a systematic experimental study of the MR of antiferromagnetic REB_6 .

From the susceptibility work on dilute alloys of $[\text{La}_{1-x}\text{Gd}_x]\text{B}_6$ by Felsh (1978) it is known that these alloys with $0.0035 \leq x \leq 0.0812$ show a spin-glass behaviour. A spin-glass is a random dilute magnetic alloy that shows a magnetic transition at a well defined temperature T_f below which the spins become locked in time but oriented in random directions. There have been extensive experimental studies of spin-glasses of dilute 3d transition metal impurities in noble metals such as AuFe, CuMn and CuCo etc. The theoretical formalism of spin-glasses is still a matter of active discussion. It is believed that the interaction between the magnetic moments responsible for random locking of the spins below T_f is via the conduction electrons and is of RKKY type. This interaction is best suited for systems with well localized magnetic moments, such as the rare earth ions. The noble metal-transition metal alloys suffer from complications because the direct d-d exchange interaction is larger and at the same time these alloys frequently exhibit a resistance minimum at low temperatures, more commonly known as the Kondo effect. For these reasons

there is need to study dilute alloys where rare earth ions form the randomly distributed spin systems.

We have studied the transport properties (resistivity and thermoelectric power) of various $[\text{La}_{1-x}\text{Gd}_x]\text{B}_6$ and $[\text{La}_{1-x}\text{Dy}_x]\text{B}_6$ alloys. To our surprise we have observed spin-glass behaviour for even 28 atomic percent of Gd^{3+} in $[\text{La}_{1-x}\text{Gd}_x]\text{B}_6$ alloys. We have also studied dilute yttrium-rare earth alloys. These alloys are also spin-glasses for low concentration of rare earths as shown by Sarkissian and Coles (1976) except for Y-Ce which displays the Kondo effect at low concentrations. Y falls one period earlier than La in the periodic table and has the same electronic structure as La in its outer shell and is therefore a useful element with which to dilute the rare earth interactions.

We have undertaken the present study keeping in mind that there is a need to have a better understanding of and to determine the variety of physical properties displayed by the rare earth hexaborides, their alloys and the Y-RE alloys.

The next five chapters of this thesis include respectively a theoretical background relevant to the rare earths and their transport properties (Chapter 2), a description of the experimental procedure and techniques used (Chapter 3), the presentation of the experimental results and the analysis and discussion of the experimental results

of REB_6 compounds (Chapter 4), $[\text{La}, \text{RE}]\text{B}_6$ alloys (Chapter 5) and Y-RE alloys (Chapter 6). Finally, Chapter 7 contains a summary of the results and conclusion.

CHAPTER 2

BASIC CONCEPTS AND THEORETICAL BACKGROUND

2.1 The RKKY Interaction

The first row of rare earth elements in the Periodic Table, also known as the 'Lanthanides', have very similar chemical properties. The electronic structure in the atomic state is given by

$$(1s - 4d) 4f^n 5s^2 5p^6 5d^1 6s^2 ,$$

where n runs from one to fourteen. The trivalent rare earth ions (RE^{3+}) have the same valence electrons ($5d^1 6s^2$) responsible for the similar chemical properties.

It is the unfilled f-electron states that are responsible for magnetic properties in rare earth systems. These f-electrons are screened by filled outer electron shells. The mean radius of the 4f shells is one tenth of the interionic spacing in rare earth metals. Hence, even in the metallic state 4f-electrons retain their localized atomic character. This is the basis for most of the magnetic properties of the rare earths, their alloys and compounds.

The localization of 4f-electrons suggests that the direct exchange interaction between the magnetic moments of different lattice sites would be too weak to account for the magnetic properties of these materials. The exchange interaction for coupling between localized

magnetic moments is thought instead to be indirect. This indirect exchange interaction in metallic systems is mediated by the spin polarization of the conduction electrons. The way in which conduction electrons can polarize and propagate was dealt with first by Ruderman and Kittel (1954). The theory was further developed and extended to s-f and s-d interactions by Kasuya (1956) and Yosida (1957) and is now commonly known as RKKY theory. The spin polarization of the conduction electrons is found to oscillate with distance and has a long range.

In the RKKY approximation an s-f interaction can be described in a simple way as follows. The exchange interaction between a conduction electron spin \vec{S} at a distance \vec{r} and an ionic spin \vec{S} at site \vec{R} can be written as

$$H_{s-f} = -A(\vec{r}-\vec{R})\vec{S}\cdot\vec{S} \quad . \quad (2.1)$$

In the RKKY approximation $A(\vec{r}-\vec{R}) = A_0 \delta(\vec{r}-\vec{R})$ where A is the exchange coupling constant for the s-f interaction. The Hamiltonian H_{s-f} is spin dependent, hence conduction electrons of different spins respond differently to the perturbation created by a single ionic spin \vec{S} . The result will be the spin polarization of the conduction-electron gas. In the RKKY approximation the spin polarization of the conduction electron at site R' in the free-electron-gas model will be given by

$$\vec{S}(\vec{R}') = A_0 \sum_{\vec{q}} \chi(\vec{q}) \exp[i\vec{q} \cdot (\vec{R}' - \vec{R})] \vec{S}, \quad (2.2)$$

where the wave vector $\vec{q} = \vec{R}' - \vec{R}$ and $\chi(\vec{q})$ is given by the expression,

$$\chi(\vec{q}) = \frac{mK_f}{4\pi^2 \hbar^2} \left(1 + \frac{4K_f^2 - q^2}{4K_f^2 q} \ln \left| \frac{q + 2K_f}{q - 2K_f} \right| \right). \quad (2.3)$$

The polarization produced by one ionic spin at \vec{R}_i will interact with another spin at \vec{R}_j through H_{s-f} . The effective exchange interaction between the two magnetic ions can be shown to be

$$H_{ij} = -J(\vec{R}_i - \vec{R}_j) \vec{S}_i \cdot \vec{S}_j, \quad (2.4)$$

where

$$J(\vec{R}_i - \vec{R}_j) = \frac{9\pi^2 z^2 A_0^2}{2\Omega^2 E_f} \phi(K_f |\vec{R}_i - \vec{R}_j|). \quad (2.5)$$

In the above expression z is the number of conduction electrons per atom, Ω is the atomic volume and the function $\phi(x)$ is given by

$$\phi(x) = \frac{\sin x - x \cos x}{x^4}. \quad (2.6)$$

It is evident that the RKKY result has a long range, oscillatory behaviour falling off as $\cos(2K_f r)/r^3$. There are two important consequences of this magnetic coupling. First, the magnetic interaction has a long range character, much longer range than any direct exchange interaction. Second, a large variation of the coupling strength

and even reversal of its sign is possible with small changes in the relationship between the interionic distance and the periodicity of the spin density.

The exchange interaction is always between the spins \vec{S} . In the case of rare earth ions there is strong spin-orbit coupling in the 4f shells and \vec{S} is not a good quantum number. In such a situation the ion is specified by its total angular momentum \vec{J} . Upon eliminating \vec{L} (the total orbital angular momentum) between the relations, $\vec{L} + 2\vec{S} = g\vec{J}$ (g = Lande g -factor) and $\vec{L} + \vec{S} = \vec{J}$, the spin (\vec{S}) may be replaced by $\vec{S} = (g-1)\vec{J}$. Then the exchange Hamiltonian H_{i-j} can be rewritten as

$$H_{i-j} = -J(\vec{R}_i - \vec{R}_j) (g-1)^2 \vec{J}_i \cdot \vec{J}_j \quad . \quad (2.7)$$

The interaction between two ions is much more complex if the anisotropic terms are included in H_{s-f} . There has been some work to include anisotropic terms by Kaplan and Lyons (1962) and Specht (1967). However, thus far the isotropic exchange interaction (RKKY type) has been found to be fairly good for a qualitative understanding of experimental results.

An exchange interaction, such as the RKKY interaction, which alternates in sign with increasing interionic distances is potentially capable of accounting for various kinds of magnetic ordering. If $J(q)$ has a maximum at $q=0$ then it favours a ferromagnetic alignment but if the

maximum occurs at the edge of the Brillouin zone then the exchange interaction favours antiferromagnetism. A maximum in $J(q)$ between the origin and the zone boundary can account for spiral-spin arrangements.

2.2 Resistivity

In a non-magnetic metal the conduction electrons are scattered by two processes, namely by lattice imperfections and by phonons. Assuming that these scattering processes are independent, the individual resistivity contributions will be additive (Matthiessen's rule) and the total resistivity of a non-magnetic metal can be expressed as

$$\rho = \rho_0 + \rho_{ph} \quad , \quad (2.8)$$

where ρ_0 is the residual resistivity due to impurities and static crystal imperfections. The phonon resistivity ρ_{ph} arises due to electron-phonon scattering and may be approximated by $\rho_{ph} \propto T^n$ at low temperatures and $\rho_{ph} \propto T$ above the Debye temperature. A general expression for ρ_{ph} is given by the Bloch-Grüneisen law (Ziman, 1960). In some metals (e.g. Li, K, etc.) at very low temperatures another contribution to the resistivity has been found due to electron-electron interaction (ρ_{e-e}). This ρ_{e-e} has been found, at low enough temperatures that ρ_{ph} is negligible, to have a temperature dependence of T^2 .

In magnetic metals an additional contribution to the resistivity has to be taken into account. The contribution ρ_{mag} describes the scattering processes of conduction electrons due to the disorder in the arrangement of the magnetic moments. Therefore, the total resistivity of a magnetic metal (assuming that Matthiessen's rule is valid) can be written as

$$\rho(T) = \rho_0 + \rho_{\text{ph}}(T) + \rho_{\text{mag}}(T) . \quad (2.9)$$

The resistivity of a magnetic material could be conveniently studied in three temperature regimes. These refer to the paramagnetic state (when $T > T_0$), the magnetically ordered state (when $T < T_0$) and the critical resistivity in the vicinity of the ordering temperature (T_0).

2.2.1 Resistivity in the paramagnetic state ($T > T_0$)

The indirect exchange interaction between the localized magnetic moments via the conduction electrons (discussed in previous section) leads to a scattering process which is dependent on the ionic spin. In the paramagnetic state where all possible spin orientations are equally probable, the magnetic contribution to the resistivity (called the spin-disorder resistivity, ρ_{spd}) has been calculated by de Gennes (1962) and Dekker (1965) and can be written as

$$\rho_{\text{spd}} = \frac{3\pi m^* A_0^2}{8\hbar e^2 \Omega E_f} (g-1)^2 J(J+1) , \quad (2.10)$$

where m^* is the average effective mass of the conduction electrons. The above result shows that well above T_0 the spin-disorder resistivity is temperature independent. Another important conclusion that can be drawn from the above expression is that ρ_{spd} is proportional to $(g-1)^2 J(J+1)$ (called the de Gennes factor). For rare earth metals this relationship holds fairly well and implies that for localized magnetic moment system the RKKY theory is applicable and gives at least a qualitative understanding of the magnetic behaviour.

For temperatures above T_0 the increase in resistivity is due to the electron-phonon interaction. To get an estimate of ρ_{spd} , linear extrapolation of the resistivity above T_0 to zero temperature can be done as shown schematically in Fig. 2.1.

2.2.2 Resistivity in the ordered state ($T < T_0$)

At low temperatures ($T < T_0$) the magnetic scattering is best discussed in terms of a spin-wave model. When all spins are in the ordered state, the spin-wave excitations are negligible and there is no spin-wave contribution to the resistivity. But as the temperature is raised the spin alignment is disturbed, leading to thermally excited spin waves and hence the resistivity due to electron-spin-wave scattering increases. The electrical resistivity due to spin-wave scattering in ferromagnetic metals has been calculated by Kasuya (1959) and Mannari (1959). More

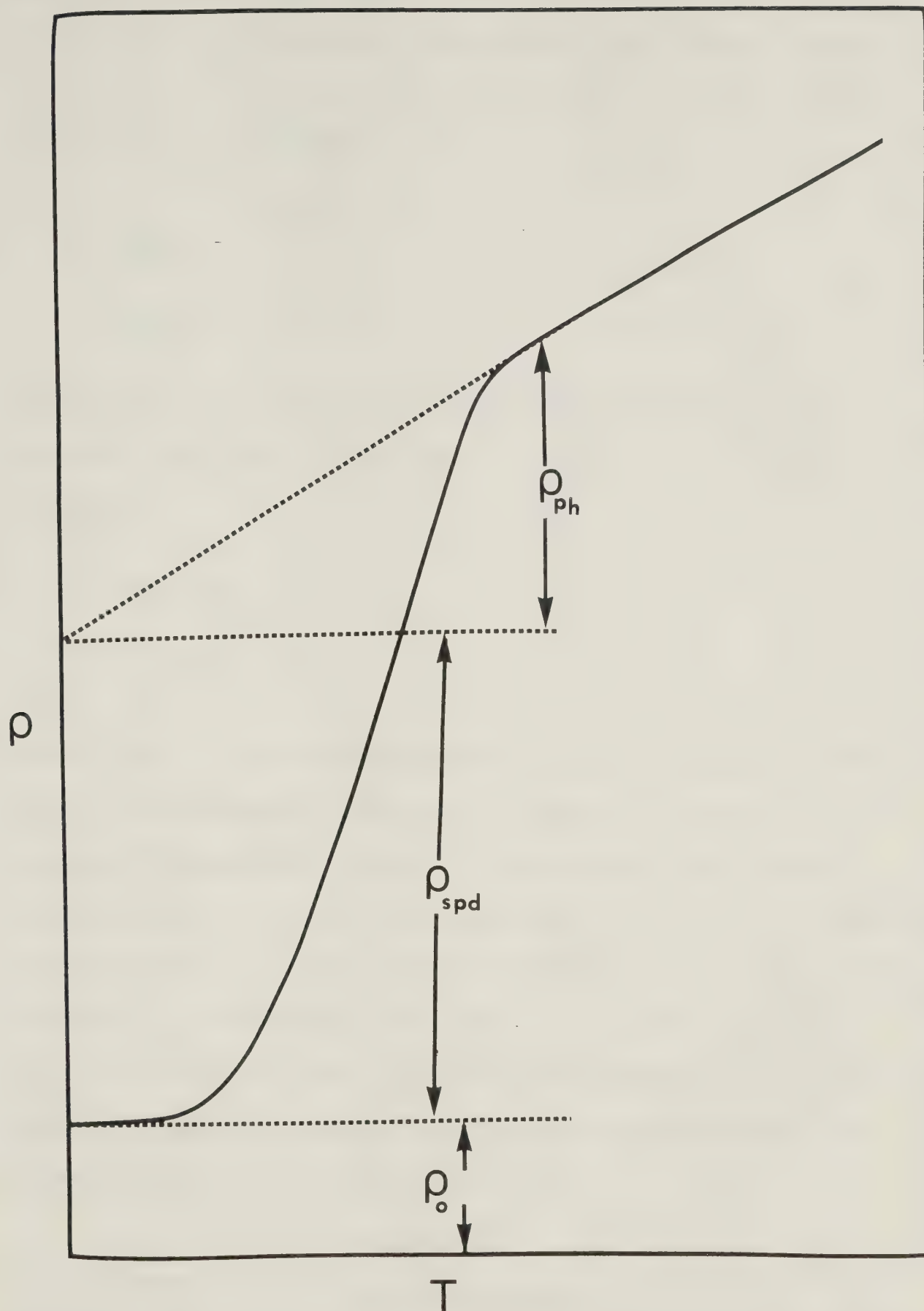


Fig. 2.1 The variation of the resistivity (ρ) of a magnetic metal with temperature (T), showing the various contributions to the resistivity.

recently, Rivier and Mensah (1977) have calculated the resistivity of a magnetic material in the ordered state. According to them the resistivities of a magnetic metal or alloy can be expressed as

$$\left. \begin{aligned} \rho_{\text{metal}} &\sim T^{(2p+4)/n} \\ \rho_{\text{alloy}} &\sim T^{(2p+3)/n} \end{aligned} \right\} , \quad (2.11)$$

where n and p are defined by the dispersion relation of the spin-wave excitations and the form factor (F_K) as follows,

$$\left. \begin{aligned} E_K &= D K^n \\ F_K &= F K^p \end{aligned} \right\} , \quad (2.12)$$

where D and F are constants and K is a wave vector. For simple ferromagnetic and antiferromagnetic materials, the spin-wave dispersion relation is quadratic and linear respectively, i.e., for a ferromagnet $n=2$ and for an antiferromagnet $n=1$. The form factor becomes a constant with $p=0$ when it is assumed that there is a point exchange interaction between the conduction electrons and localized magnetic moments. Hence, the spin-wave resistivity for magnetic materials can be written as

$$\rho_{\text{metal}} \sim \left. \begin{aligned} T^2 & \text{ Ferromagnet} \\ T^4 & \text{ Antiferromagnet} \end{aligned} \right\} \quad (2.13)$$

$$\rho_{\text{alloy}} \sim \left. \begin{array}{ll} T^{3/2} & \text{Ferromagnet} \\ T^3 & \text{Antiferromagnet} \end{array} \right\} \quad (2.14)$$

2.2.3 Critical resistivity

During the past few years there has been considerable interest in studies of the critical scattering of the conduction electrons near magnetic phase transitions. The first account of critical resistivity was given by de Gennes and Friedel (1958) using a simple model in which free electrons are linearly coupled to localized spins. Fisher and Langer (1968) have shown that the magnetic resistivity of a ferromagnetic metal in the vicinity of the ferromagnetic to paramagnetic transition temperature (T_C) is due to short-range spin fluctuations. Hence the temperature derivative of the resistivity and the magnetic specific heat (C_m) should vary as $t^{-\alpha}$ for $T \rightarrow T_C$ (i.e. $T \geq T_C$), where the reduced temperature $t = |(T - T_C)/T_C|$.

Present theoretical studies (Fisher and Langer, 1968; Richard and Geldart, 1977; Geldart and Richard, 1975; and Alexander et al, 1976) suggest that the critical resistivity of a ferromagnetic as well as antiferromagnetic metal should have the temperature dependence of the magnetic energy. Hence, in the vicinity of T_C (or T_N) (for both, above and below the ordering temperature)

$$\frac{d\rho}{dt} \propto C_m \propto t^{-\alpha} . \quad (2.15)$$

One therefore expects a divergence at T_C (or T_N) in the

temperature derivative of the resistivity. The temperature derivative of resistivity of antiferromagnetic metals has been found to have a negative or positive divergence at T_N depending on the material and crystallographic orientations. The sign of the divergence is found to be determined by the Fermi surface geometry and the magnetic reciprocal lattice vector Q of the ordered state (Richard and Geldart, 1977; Balberg, 1977; and Balberg and Maman, 1979). Richard and Geldart (1977) have shown that for $Q < 2K_f$ and for $Q > 2K_f$ (K_f is the Fermi wave vector) the divergence in $d\rho/dT$ at T_N will have a negative and positive sign respectively. Materials with negative divergence are classified as type I and those with positive divergence are classified as type II antiferromagnets.

Renormalization-group theoretical studies suggest that for the temperature region where the short-range spin fluctuations are dominant, the critical exponents depend only on the physical dimension (d) of the lattice and the number of degrees of freedom of the spins (n). There have been theoretical calculations of the critical exponents for $d=3$ systems with several values of n (Bak and Mukamel, 1976; and Leguillon and Zinn-Justin, 1980).

2.3 Thermoelectric Power (TEP)

The thermoelectric power (TEP) of a simple metal can be written as

$$S(T) = S_e(T) + S_g(T) , \quad (2.16)$$

where S_e is the thermoelectric power due to electron diffusion and S_g is the phonon drag contribution to the TEP.

The standard expression for S_e for a cubic metal is given by

$$S_e(T) = \frac{\pi^2 K_B^2}{3e} T \left(\frac{\partial \ln \sigma(\epsilon)}{\partial \epsilon} \right)_{\epsilon=\epsilon_f} , \quad (2.17)$$

where e is the electronic charge, $\sigma(\epsilon)$ the conductivity as a function of electron energy ϵ . Starting from

$$\sigma = \frac{1}{4\pi^3} \frac{e^2}{\hbar} \frac{1}{3} \int \ell d\Lambda ,$$

where the integration is to be carried out over the whole Fermi surface, one considers σ to be a function of energy and writes

$$\frac{\partial \ln \sigma(\epsilon)}{\partial \epsilon} = \frac{\partial \ln \ell}{\partial \epsilon} + \frac{\partial \ln \Lambda}{\partial \epsilon} , \quad (2.18)$$

where ℓ is the electron mean free path and Λ is the area of the Fermi surface. The first term on the right hand side of equation (2.18) is positive since more energetic electrons are less easily scattered than slower electrons and thus have longer paths. But the second term depends on the detailed geometry of the Fermi surface and it can be positive or negative. The electron diffusion TEP is expected

to be linear in T for simple metals as predicted by equation (2.17).

At low temperatures the TEP of even the simplest metal has been found to deviate from linearity. This deviation has usually been attributed to the phenomenon of phonon drag. This process can be described in a simple way as follows. Any temperature gradient gives rise to a flow of phonons which through the electron-phonon interaction drag electrons with them creating a potential difference between the hot and cold end of a metal. Also an electric current carried by the electrons in an isothermal metal transfers some of its momentum to the phonons and drags them along with it.

Theoretical studies of the phonon drag TEP (S_g) have been done by Bailyn (1962) and Guénault (1971). They found that S_g varies as T^3 , that is, it is proportional to the lattice specific heat. The sign of S_g depends on whether the electron-phonon interaction is predominantly of 'Normal' or 'Umklapp' character. In the case of N-processes the phonon current can drift in the same direction as that of the electron, leading to a negative S_g whereas U-processes may lead to a positive S_g .

At high temperatures the phonon-phonon scattering dominates the electron-phonon interaction. This leads to quenching of S_g at higher temperatures as shown by Guénault (1971), hence according to equation (2.17) a linear temperature dependence of the TEP is expected at

high temperatures, which is consistent with the experimental results.

For magnetic metals containing localized magnetic moments there has not been much theoretical investigation of the TEP. The magnetic contribution to the TEP of a ferromagnetic metal in a molecular field approximation has been calculated by Kasuya (1959). In magnetic materials the possibility exists that the electron may be driven along the temperature gradient by the magnon thermal current, thus creating an additional contribution to the TEP, namely the magnon drag S_m . Assuming that the various contributions are independent, the total TEP for a magnetic metal can then be expressed as

$$S(T) = S_e(T) + S_g(T) + S_m(T) . \quad (2.19)$$

The effect of the magnon drag was first discussed by Bailyn (1967). He found that the expression for S_m is very similar to that of phonon drag (S_g) with the same temperature dependence (T^3) and can have negative or positive sign depending on the dominance of N-processes or U-processes respectively.

In magnetic metals the TEP at higher temperatures will have a contribution due to spin disorder scattering (S_{spd}). To our knowledge there has not been any theoretical calculation of S_{spd} . In order to estimate the contribution of S_{spd} , following Gratz (1981) and Gratz and Zuckermann (1982), one can analyze the experimental data

using the Nordheim-Gorter rule:

$$S = \sum_i \frac{\rho_i}{\rho} S_i , \quad (2.20)$$

where i , ρ_i and S_i respectively denote the scattering mechanism, the resistivity and the TEP due to that mechanism. For a non-magnetic metal one can write,

$$S^{nm} = \frac{\rho_o}{\rho} S_o + \frac{\rho_g}{\rho} S_g , \quad (2.21)$$

and for a magnetic material,

$$S^m = \frac{\rho_o}{\rho} S_o + \frac{\rho_g}{\rho} S_g + \frac{\rho_{spd}}{\rho} S_{spd} , \quad (2.22)$$

where S_o , S_g and S_{spd} are the contributions to the TEP due to impurity scattering, phonon scattering and spin disorder scattering respectively and ρ , ρ_o , ρ_g and ρ_{spd} represent the total resistivity, the residual resistivity, the phonon resistivity and the spin disorder resistivity respectively. With the assumption that the impurity and phonon contributions for the isostructural magnetic and non-magnetic metals are the same to the first approximation, one can write an expression for S_{spd} as,

$$S_{spd} = (S^m - S^{nm}) \rho / \rho_{spd} . \quad (2.23)$$

Such a technique has been used by Gratz (1981) and Gratz and Zuckermann (1982) for some intermetallic rare earth compounds and S_{spd} have been found to be linear in temperature with positive as well as negative signs, depending on the material.

The TEP anomalies observed at ferromagnetic and antiferromagnetic ordering temperatures are characterized by the specific-heat-like divergences in the temperature derivative of the TEP. The elastic and inelastic contributions to the TEP in the vicinity of the ordering temperature were shown by Helman and Balberg (1978) to have the critical temperature dependence of the static spin-spin correlation function (i.e. the temperature dependence of the magnetic energy). With the assumption that the non-critical contributions to the TEP in the vicinity of T_C (or T_N) are only weakly temperature dependent, the temperature derivative of the TEP has the same temperature dependence as that of the magnetic specific heat C_m , i.e.,

$$\frac{dS}{dT} \propto C_m . \quad (2.24)$$

From the earlier discussion on the critical resistivity we know that

$$\frac{d\rho}{dT} \propto C_m . \quad (2.25)$$

Hence, the behaviour of the temperature dependence of dS/dT and that of $d\rho/dT$ are intimately related and, as predicted by Ausloos (1977, 1978) and Helman and Balberg (1978), they possess a universal behaviour irrespective of the scattering processes. One expects a divergence in dS/dT at T_C (or T_N) which has the same behaviour as that of $d\rho/dT$ and one can examine this result in the vicinity of T_C (or T_N) where

$$\frac{dS}{dT} \propto \frac{d\rho}{dT} . \quad (2.26)$$

Experimentally, such a behaviour has been found for several ferromagnetic metals but the situation for antiferromagnetic metals is still far from clear.

2.4 Magnetoresistance (MR)

The change in the resistivity of a metal in a magnetic field, called the magnetoresistance, transverse (TMR) when the specimen current and field are perpendicular and longitudinal (LMR) when they are parallel, is expressed as the ratio

$$\frac{\Delta\rho}{\rho_0} = \frac{\rho(H,T) - \rho(0,T)}{\rho(0,T)} , \quad (2.27)$$

where $\rho_0 = \rho(0,T)$ is the resistivity at zero field and temperature T and $\rho(H,T)$ is the resistivity at field H and temperature T . The magnetoresistance, being a second-order effect, is not well understood at present. However, for magnetoresistance one general rule, known as Kohler's rule (Kohler, 1938), usually describes the experimental results for non-magnetic metals. This rule can be expressed as

$$\frac{\Delta\rho}{\rho_0} = F(H/\rho_0) , \quad (2.28)$$

where F is a function that depends only on the geometrical configuration and the metal.

A simple calculation shows that in the free electron model the TMR vanishes and for an electron system with spherical symmetry the LMR cannot exist (Ziman, 1960). However, with a more complicated theory, particularly using the method of Jones and Zener (1934) it was shown by Ziman (1960) that where the conduction electrons may be considered to be in two bands the MR could be written as

$$\left. \begin{aligned} (\Delta\rho/\rho_o)_{\perp} &= B_{\perp} H^2 \\ (\Delta\rho/\rho_o)_{\parallel} &= B_{\parallel} H^2 \end{aligned} \right\} \quad (2.29)$$

where B_{\perp} and B_{\parallel} are transverse and longitudinal coefficients. This suggests that the longitudinal and transverse MR are of the same order of magnitude for non-magnetic metals.

In the case of dilute magnetic alloys and rare earth metals there are several theoretical investigations of MR (Kondo, 1962 and Yosida, 1957). The emphasis has been for ferro or paramagnetic spin ordering which leads to negative MR. This comes from the suppression of the localized spin fluctuations by the external magnetic field. Here, we shall concern ourselves mainly with antiferromagnetic metals in which the situation is far less clear. To our knowledge the only theoretical calculation of the MR of an antiferromagnetic metal with localized magnetic moments, has been done by Kamada and Takada (1973,

1973a). They have used the random phase approximation (RPA) for localized spin systems described by the Heisenberg model. They have done the MR calculation for the s-d model within the assumption that the s-d scattering strength (J) is much smaller than the Néel temperature, i.e. $T_N \gg J$. In the rare earth (f-electron) systems the magnetic interaction between localized magnetic moments is via the conduction electrons and the s-f exchange strength $J \sim T_N$, hence the Yamada and Takada results cannot be used for quantitative analysis of experimental results. However, some of the ideas could be used at least qualitatively to obtain some understanding of the MR results. According to Yamada and Takada (1973, 1973a) for $T < T_N$ the MR is positive and increases with increasing field (H) up to a critical field H_C , the antiferromagnetic to paramagnetic transition point. There is a rapid increase in the MR at H_C , then in the paramagnetic phase the MR decreases monotonically with increasing field just as it does for ferromagnets. The positive MR in the antiferromagnetic phase has been associated with an increase in the total number of excited magnons in the presence of an external magnetic field and the field induced enhancement of the spin fluctuations which increases with increasing field below H_C . Above H_C the negative MR is due to field induced alignments of the magnetic moments in an external field, which suppresses spin fluctuations.

Magnetoresistance measurements by Fert and coworkers (1977, 1977a, 1974, 1980) on dilute rare earth impurities in noble metals have shown a difference in the longitudinal and transverse magnetoresistances. This anisotropy vanishes for Gd impurities and changes its sign in the middle of the heavy rare earth series between Ho and Er. It has been shown that this anisotropy is due to an aspherical Coulomb interaction between the conduction electron (k) and f-electrons and it is mainly due to a quadrupolar term in the scattering.

The k-f interaction between the conduction electrons and f-electrons can be expressed according to Fert et al (1980) by the potential

$$V = V_o + V_{ex} + V_{an} , \quad (2.30)$$

where V_o is the isotropic potential, V_{ex} is the isotropic s-f exchange term and the V_{an} term comes from the anisotropic Coulomb interaction between the conduction electrons and the f-electrons. This last term vanishes for an S-ion (e.g. Gd^{3+}). A general expression for V is given by Hirst (1978). It has been shown by Fert et al (1977) that the anisotropic part of V is mainly due to the quadrupolar scattering and can be written as

$$V_{an} \sim V_{qd} \sim \alpha_J O_2(\vec{\ell}_c) \cdot O_2(\vec{J}) , \quad (2.31)$$

where α_J is the Stevens multiplication factor of the quadrupolar operators, O_2 is a quadrupolar tensor, $\vec{\ell}_c$ is

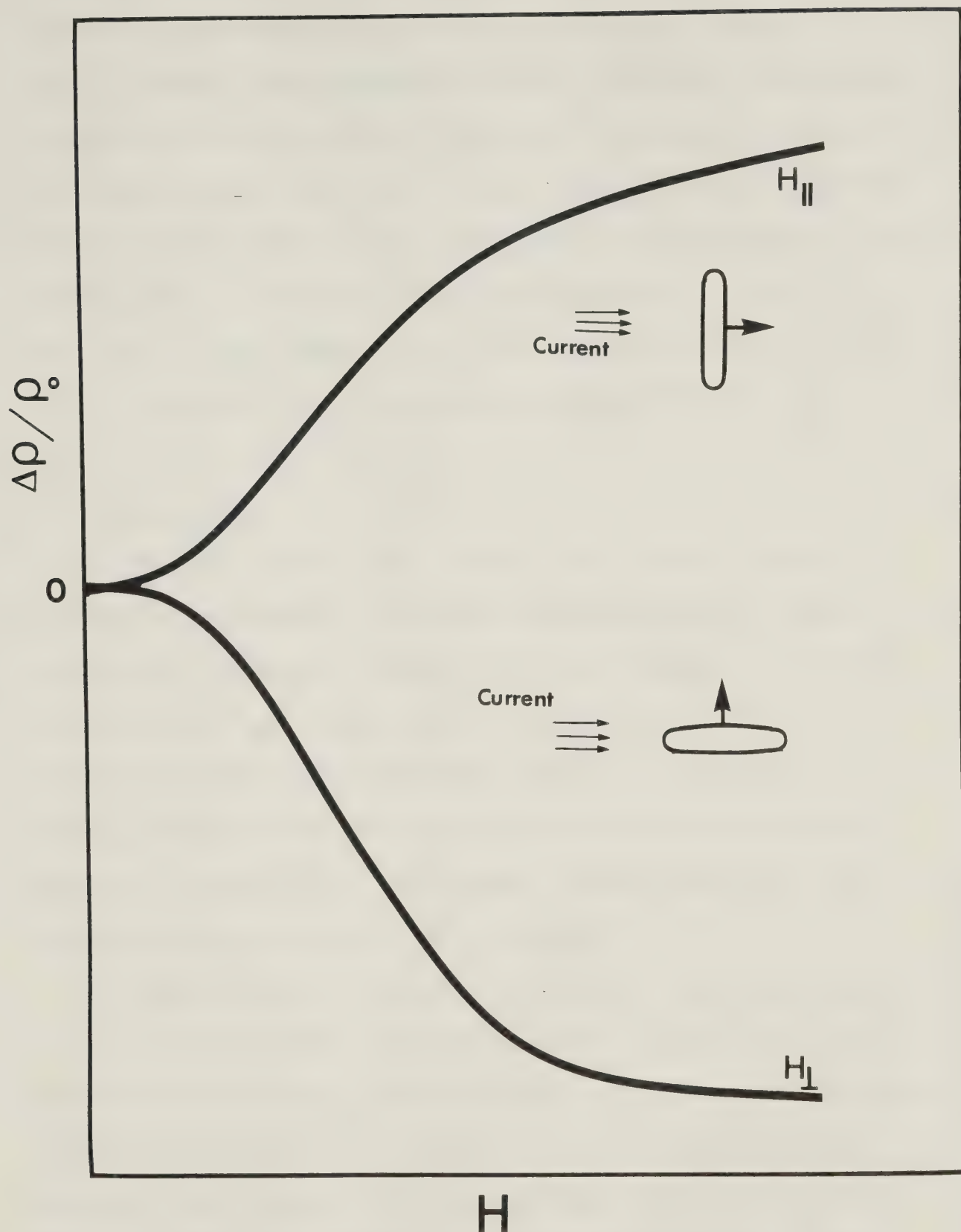


Fig. 2.2 The anisotropy in the magnetoresistance ($\Delta\rho/\rho_0$) as a function of external magnetic field (H).

the orbital angular momentum of the conduction electrons and \vec{J} is the total angular momentum of the f-electron system. The resistivity cross section is different according to whether the quadrupolar axis is parallel or perpendicular to the electrical current, therefore, producing different values for the longitudinal and the transverse magnetoresistances. This mechanism is schematically shown in Fig. 2.2. The sign of the anisotropy $\Delta\rho_A = \Delta\rho_{||} - \Delta\rho_{\perp}$ ($\Delta\rho_{||}$ is the LMR and $\Delta\rho_{\perp}$ is the TMR) depends on the sign of α_J involved in the quadrupolar interaction.

2.5 Spin Glass

A spin glass (Ford, 1982; Hurd, 1982) can be defined as a random, metallic magnetic system characterized by "freezing" of the magnetic moments in random directions below a well defined temperature T_f with no net macroscopic magnetization. For $T \ll T_f$, local or diffuse excitations may exist within the frozen matrix. There has been little theoretical investigation of the transport properties of spin glasses.

The effect of magnetic impurity concentration in a non-magnetic metal can be described as follows. At a very dilute magnetic concentration (i.e. isolated magnetic ions with no direct or indirect magnetic interaction between them) there is the isolated impurity magnetic moment - conduction electron interaction, namely s-f or s-d interaction, expressed as $J \vec{s} \cdot \vec{S}$, where J is the s-f or

s-d coupling constant and \vec{s} and \vec{S} are the spins of the conduction electron and the impurity ion respectively. Such an interaction leads to the well-known Kondo effect for $J < 0$ and the relatively less well-known reverse Kondo effect for $J > 0$, as recently studied by Leike et al (1979) and Tsang et al (1980). Increase in concentration of the magnetic impurity can cause interaction between the magnetic moments by an indirect exchange mechanism of the RKKY type. Although the details of the theoretical formalism are still a matter of active discussion, the interaction of magnetic moments in a spin glass is considered to arise by the RKKY mechanism via the conduction electrons.

Experimental identification of T_f for several spin glass systems has been done by low field susceptibility measurements and Hall-effect studies (Ford, 1982). A cusp-like behaviour is observed in susceptibility data at T_f . Hall-effect measurements by McAlister and Hurd (1976) and McAlister (1978) show a peak in the anomalous Hall coefficient for low fields (e.g. 0.01 T) at T_f .

The electrical resistivity has been found experimentally to vary as $T^{3/2}$ below T_f and sometimes becomes T^2 at the lowest temperatures. A theoretical investigation of the resistivity of spin glasses has been carried out by Rivier and Adkins (1975). They have found the temperature dependence of the resistivity to be $T^{3/2}$ for temperatures below T_f . Here conduction electrons are scattered by

elementary excitations which are of spin diffusive modes. The $T^{3/2}$ behaviour of resistivity has been observed for several 3d-transition metal spin glasses (e.g. AuFe, AuCr, AuMn, CuMn and AgMn, etc., Ford and Mydosh, 1976; Mydosh et al, 1974; Campbell et al, 1982). Recently, Fischer (1979, 1980) have shown that the resistivity can be expressed as $\rho = AT^2 - BT^{5/2}$, where A and B are positive constants. The above expression was derived by taking into account the conservation of the total spin and with the assumption of a spin diffusive mode. The above result for the resistivity of spin glasses is in contrast to the experimentally observed behaviour ($\rho \propto T^{3/2}$) for several spin glasses. This discrepancy has been explained by Fischer (1979, 1980) on the basis of the presence of ferromagnetic clusters which will lead at low temperatures to $\rho \propto T^{3/2}$. At the lowest temperatures the spin waves with a wave length smaller than the cluster size freeze out leading to a T^2 dependence in resistivity, consistent with the experimental results on CuMn, AuMn and AuFe around 1K.

The thermoelectric power (TEP) has been calculated for dilute magnetic alloys by Matho and Béal-Monod (1974) in the interacting pair model. Recently, Fischer (1981) has calculated the TEP of spin glasses on the basis of an s-d exchange model with an additional interaction potential between the magnetic impurities and the conduction electrons which is spin-independent. The TEP of a spin glass was found to have two contributions, namely a "Kondo"

term $S_d^1(T)$ and a "resonance" term $S_d^2(T)$. The "Kondo" term $S_d^1(T)$ reduces to the TEP of a Kondo system for the isolated impurity regime and the "resonance" term $S_d^2(T)$ is of opposite sign and vanishes in the isolated impurity regime. The superposition of these two terms leads to an extremum in the total TEP and for $J < 0$ (J is the exchange interaction coupling constant), i.e. antiferromagnetic coupling, there is a change in sign of the total TEP at a temperature T_0 , which depends on the Kondo temperature (T_K) and on the spin freezing temperature (T_f). For a spin glass system with $J > 0$ (i.e. ferromagnetic coupling), $S_d^1(T)$ reduces to the "reverse" Kondo value for the isolated impurity regime and the sign of the total TEP is not expected to change. However, one expects a peak in the total TEP because of the "resonance" term $S_d^2(T)$. At low temperatures $S_d^2(T)$ has been found to behave as $S_d^2 \propto T$, while at high temperatures $S_d^2 \propto T^{-1}$. For $J < 0$, $S_d^1(T) \propto T^2$ at low temperatures while the dependence is of the form $S_d^1(T) \propto |\ln T|^{-3}$ at high temperatures. A theoretical calculation of $S_d^1(T)$ for $J > 0$ has yet to be done explicitly.

CHAPTER 3

EXPERIMENTAL DETAILS

In order to measure the resistance, the absolute thermoelectric power and the magnetoresistance of metallic rare earth compounds and alloys at liquid helium temperatures, a conventional liquid ^4He cryostat was used. The resistance was measured with the help of a direct-current comparator and galvanometer-amplifier, while the thermoelectric voltage was measured using a potentiometer and the galvanometer-amplifier arrangement. The temperature difference across the sample, created by a small heater, was measured using a calibrated AuFe thermocouple. The resistance measurements in an external magnetic field produced by a superconducting magnet, were done up to a maximum field of 30 KOe.

The following sections describe in some detail the equipment used and the experimental techniques employed in this study.

3.1 The Cryostat

The cryostat used in this study is shown in Fig. 3.1. The main coolant is liquid ^4He in a glass dewar connected to a helium recovery line. There are two brass cans, the inner can contains the sample, thermometers, and the thermocouple. The electrical leads enter through a

Fig. 3.1 The Cryostat and Specimen Holder

- 1 - Outer Can
- 2 - Inner Can
- 3 - } Pumping Tubes
- 4 - }
- 5 - Copper Plate
- 6 - Specimen
- 7 - Phosphor Bronze Spring
- 8 - Thermal Anchoring Post for Leads
- 9 - Heater
- 10 - Thermal Anchoring Post for Leads
- 11 - Germanium Thermometer
- 12 - Indium O-ring

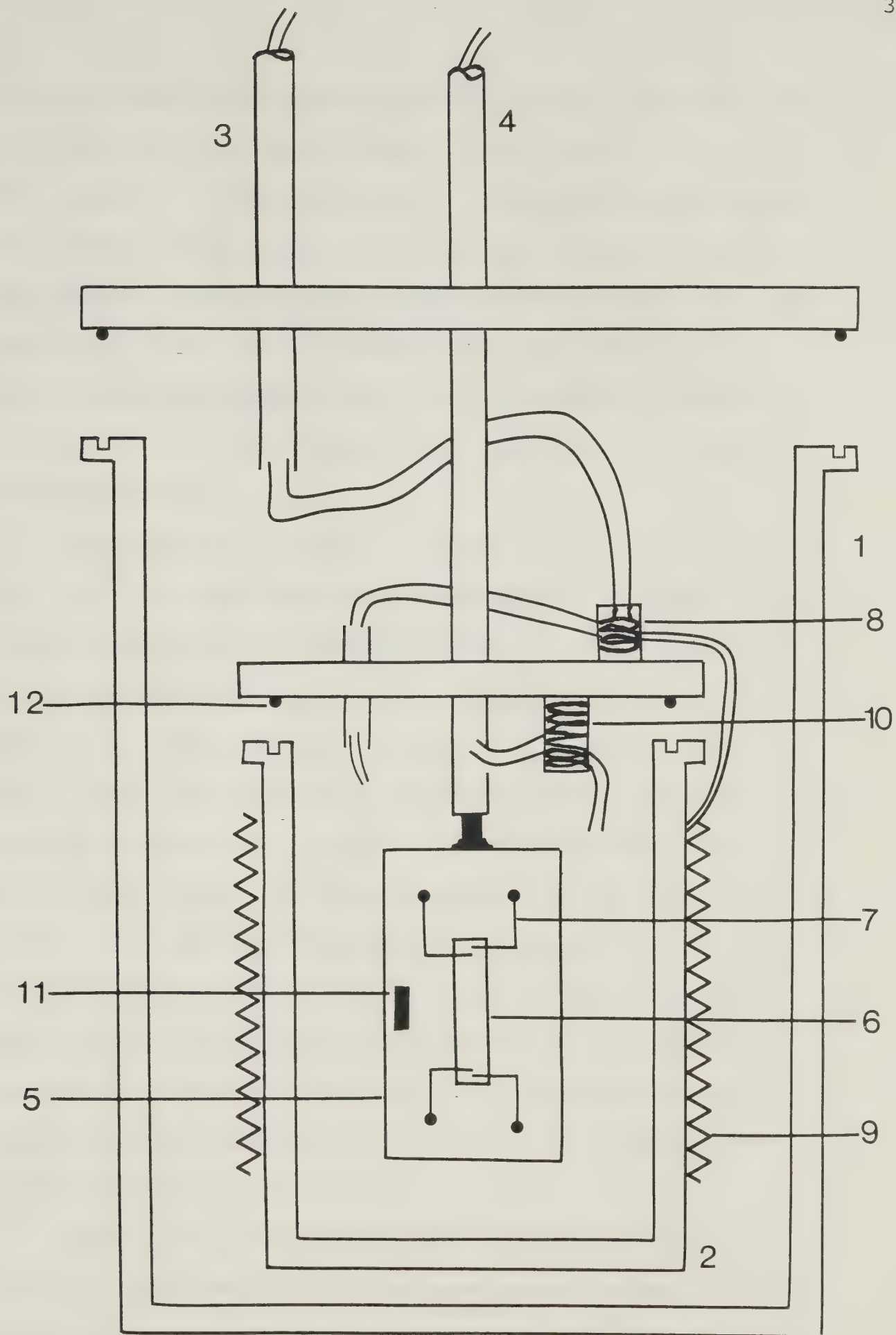


Fig. 3.1

stainless steel tube which is also used to evacuate the can. To raise the temperature of the sample a manganin wire heater of $\sim 100\Omega$ resistance is wrapped on the outer wall of the inner can. The outer can contains a carbon thermometer mounted on the outside of the inner can, and electrical leads to the thermocouple and the heater. These electrical leads enter through another stainless steel tube from room temperature which is also used to evacuate the outer can.

The specimen holder is shown in some detail in Fig. 3.1. The specimen (6) is mounted on a copper plate (5) but electrically insulated from it. The electrical insulation is achieved by a thin layer of Ge varnish which is a good conductor of heat but is electrically insulating. The electrical contacts to the specimen were achieved by pressure contact using phosphor bronze springs held on to the copper plate with the help of nylon screws. The contacts were further improved with a drop of silver paint. The electrical leads were soldered on the phosphor bronze spring and the wires were thermally anchored on a copper post (10). For the temperature measurements a Ge thermometer (11) was glued onto the copper plate using GE varnish.

Each time a new sample was inserted at room temperature, the contact resistance at the pressure contacts was checked with an ordinary ohm meter. Then the electrical leads were soldered onto the phosphor bronze springs.

After the inner can was sealed the heater leads (13) were connected to their appropriate pin site (9), then the inner can was evacuated. Then the sample resistance was measured at room temperature before the outer can was bolted in place and evacuated through tube 3. At this stage some ^4He gas was introduced into the outer and inner cans and the entire sample holder was lowered into a glass dewar.

3.2 Thermometry

A Ge resistance thermometer was used to find the sample temperature in the temperature range from 2K to 40K. The calibration of the Ge thermometer was done using a Chebyshev Polynomial as described in detail by Kapoor (1974). The temperature was measured with an accuracy of 4mK. A calibrated platinum resistance thermometer was used for some high temperature measurements. The resistances of the Ge and the platinum thermometers were measured by a d.c. resistance comparator (Seth, 1969) using a Guildline 9801T precision four terminal variable resistor for the comparison. An auto-feedback temperature controller described by Stackhouse (1977), was used to control the specimen temperature. It was found that up to 30K the temperature could be controlled at a fixed temperature within the accuracy of the Ge thermometer by manually controlling the heater current. Once the heater current was set it took a few minutes at most to stabilize the

temperature for periods of quite long time, sometimes required to take the data.

3.3 Resistance Measurements

The resistance of a specimen (R_x) was measured using a direct current comparator (Guildline Model 9920) bridge. A basic circuit for the resistance measurement is shown in Fig. 3.2. The current through specimen (I_x) is compared with a current through a four terminal standard resistor (R_s) when the voltages across the two resistors are balanced. The ratio I_s/I_x could be read directly from the seven dials on the comparator. When the circuit is balanced then in such a situation,

$$\frac{I_s}{I_x} = \frac{R_x}{R_s} \quad , \quad (3.1)$$

enabling us to find the ratio R_x/R_s to 1 part in 10^7 . The balancing of the circuit (i.e. zeroing of the potential difference across the two resistors, R_x and R_s) was achieved using a Guildline type 5214/9460 photocell galvanometer-amplifier and a Guildline type 9461 galvanometer. This arrangement gave a sensitivity of $\sim 10^{-9}$ V. A standard resistor $R_s = 0.1\Omega$ was used throughout this study, and a constant specimen current $I_x \leq 100$ mA was used to measure the specimen resistance with an uncertainty of 0.01%.

For the magnetoresistance measurements a superconducting magnet was used to obtain magnetic fields up to 30 KOe. It has a critical current at 70A and field factor

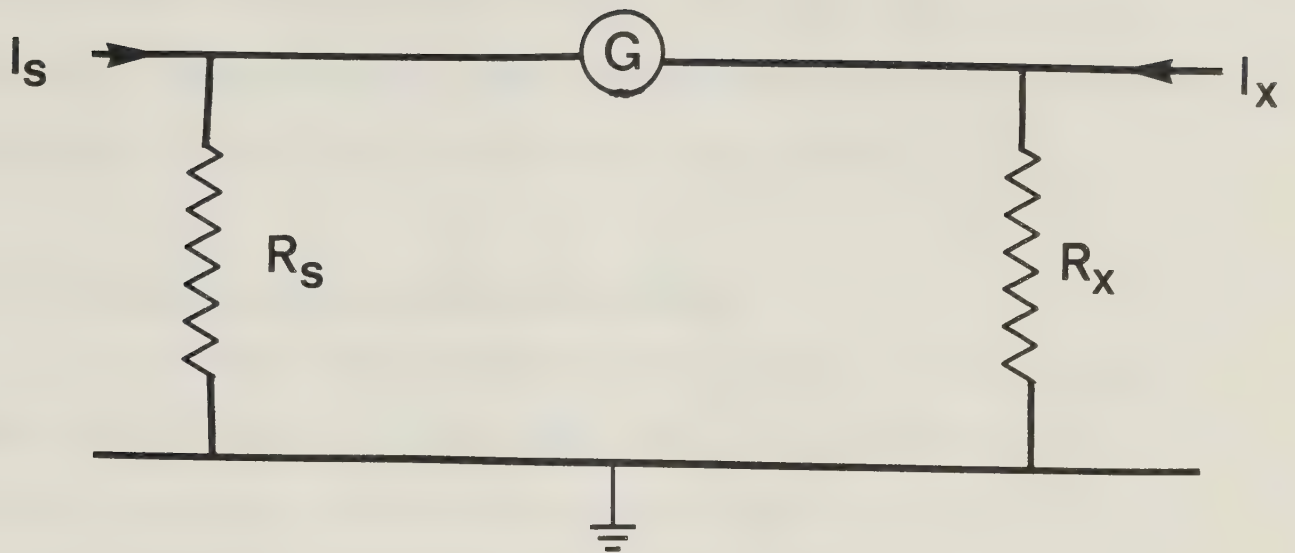


Fig. 3.2 Circuit diagram of direct current comparator bridge. G is the neutral detector.

of 0.473 KOe/A. The current to the magnet was increased or decreased with an automatic field sweep control. The outer can of the sample holder could easily slide into the magnet and the sample was always in the central region of the magnet. To measure the longitudinal and transverse magnetoresistance the direction of sample current is set parallel and perpendicular to the direction of the magnetic field respectively. The temperature was kept constant throughout one run of field from 0 to 30 KOe.

3.4 Thermoelectric Power Measurement

To measure the thermoelectric power a temperature gradient is applied to the specimen with a heater. A simple schematic circuit diagram is shown in Fig. 3.3. It consists of two conductors (A is the specimen and B is leads, insulated copper wires) with two junctions at temperatures T and $T+\Delta T$. Under these conditions a potential difference ΔV_{BA} appears across terminals 1 and 2. The potential difference ΔV_{BA} was measured with a potentiometer (Guildline type 9160) and a galvanometer-amplifier (Guildline type 5214/9460) and a galvanometer (Guildline type 9461). Such an arrangement gives a sensitivity of $\sim 2 \times 10^{-9}$ V. The temperature gradient ΔT was always kept below 3% of the specimen temperature.

The TEP of the circuit can be written as (for $\Delta T \ll T$),

$$S_{BA} = \frac{\Delta V_{BA}}{\Delta T} \quad . \quad (3.2)$$

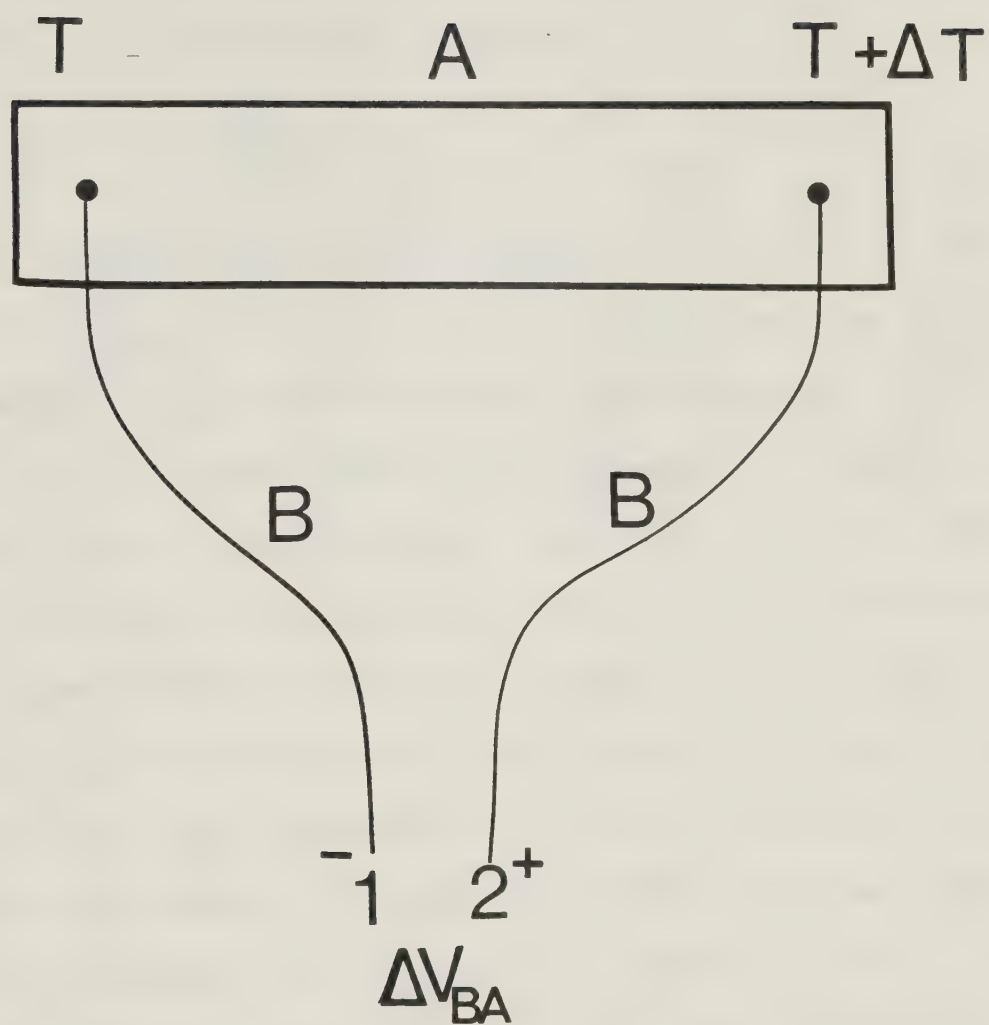


Fig. 3.3 Diagram showing the polarity of the thermoelectric voltage.

If the characteristic TEP of the conductors A and B are S_A and S_B respectively then,

$$S_{BA} = S_B - S_A = \frac{\Delta V_{BA}}{\Delta T} \quad . \quad (3.3)$$

If the polarity of the leads 1 and 2 is as shown in Fig. 3.3 then, by definition, for $\Delta T > 0$

$$S_B - S_A = \frac{\Delta V_{BA}}{\Delta T} > 0 \quad . \quad (3.4)$$

Now, the problem has reduced to finding the TEP of the leads (i.e. S_B). Once S_B is known, the absolute TEP of the specimen (S_A) could be found from equation (3.3).

Since a superconductor has zero TEP, replacing the specimen with a superconductor enables one to find the TEP of the leads directly up to the critical temperature of the superconductor. In this study V_3Ga ($T_c \approx 17K$) was used to find the TEP of the leads below 17K. As a further check and for high temperatures pure Pb (5N purity) wire was used as a sample. The absolute TEP of Pb has been carefully measured and is listed by Roberts (1977). These data were used to find the TEP of the leads above 17K.

3.5 AuFe Thermocouple

In this study AuFe (0.07 at % Fe) - Cu thermocouples were used to find the temperature gradient ΔT across the sample. The most important reason for using such a thermocouple is its high sensitivity at low temperatures. This arises from the anomalous thermoelectric properties caused

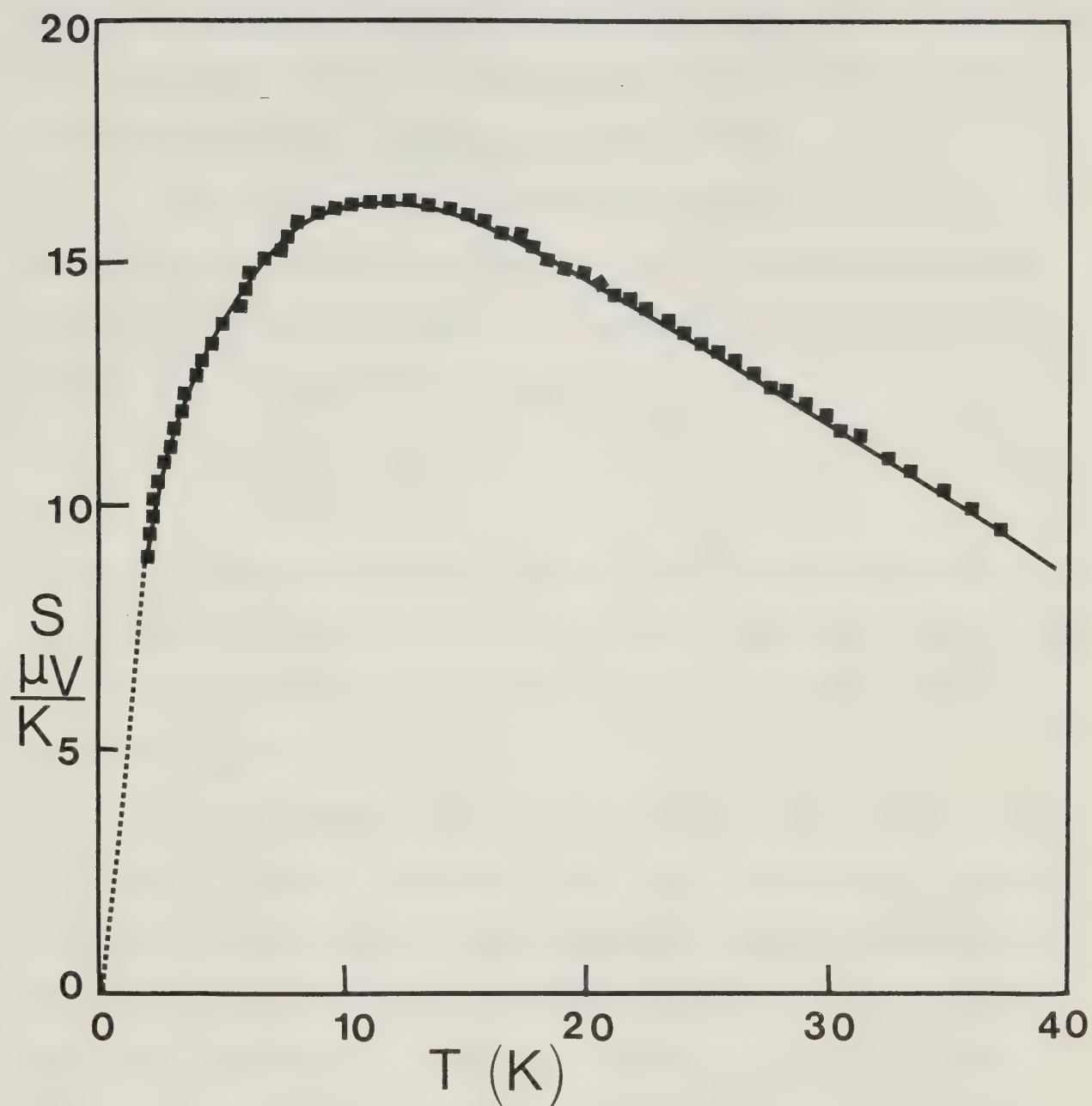


Fig. 3.4 The sensitivity (S) of the AuFe (0.07 at. %) thermocouple as a function of temperature.

by trace amounts of transition elements (in this case Fe) dissolved in noble metals (e.g. Au). Other important reasons for choosing AuFe alloys for thermocouple is the reproducibility of the thermoelectric properties after repeated thermal cycling (Finnemore et al, 1965), behaviour in a magnetic field (Berman et al, 1964), and the effect of heat treatment (Rosenbaum, 1968, 1969).

The thermocouples were calibrated with liquid helium as the reference temperature. The thermoelectric voltage $E(T)$ as a function of temperature for the thermocouple was fitted to a polynomial,

$$E(T) = \sum_{n=1}^L B_n T^n, \quad (3.5)$$

where B_n are coefficients taken from the published results of Spark and Powell (1972) and $L=14$. The sensitivity for the AuFe-Cu thermocouple as a function of temperature is presented in Fig. 3.4.

These thermocouples were made by spot welding AuFe (0.07 at %) wire to Cu-wire and then electrically insulating them with a layer of Ge varnish. The arrangement of the differential thermocouple to measure a temperature gradient ΔT across a sample is shown in Fig. 3.5. The two junctions 1 and 2 were glued on the sample with GE varnish very close to the voltage measuring leads. The thermal gradient was measured in terms of the voltage difference between the copper leads 3 and 4 with the same potentiometer and galvanometer-amplifier arrangement that

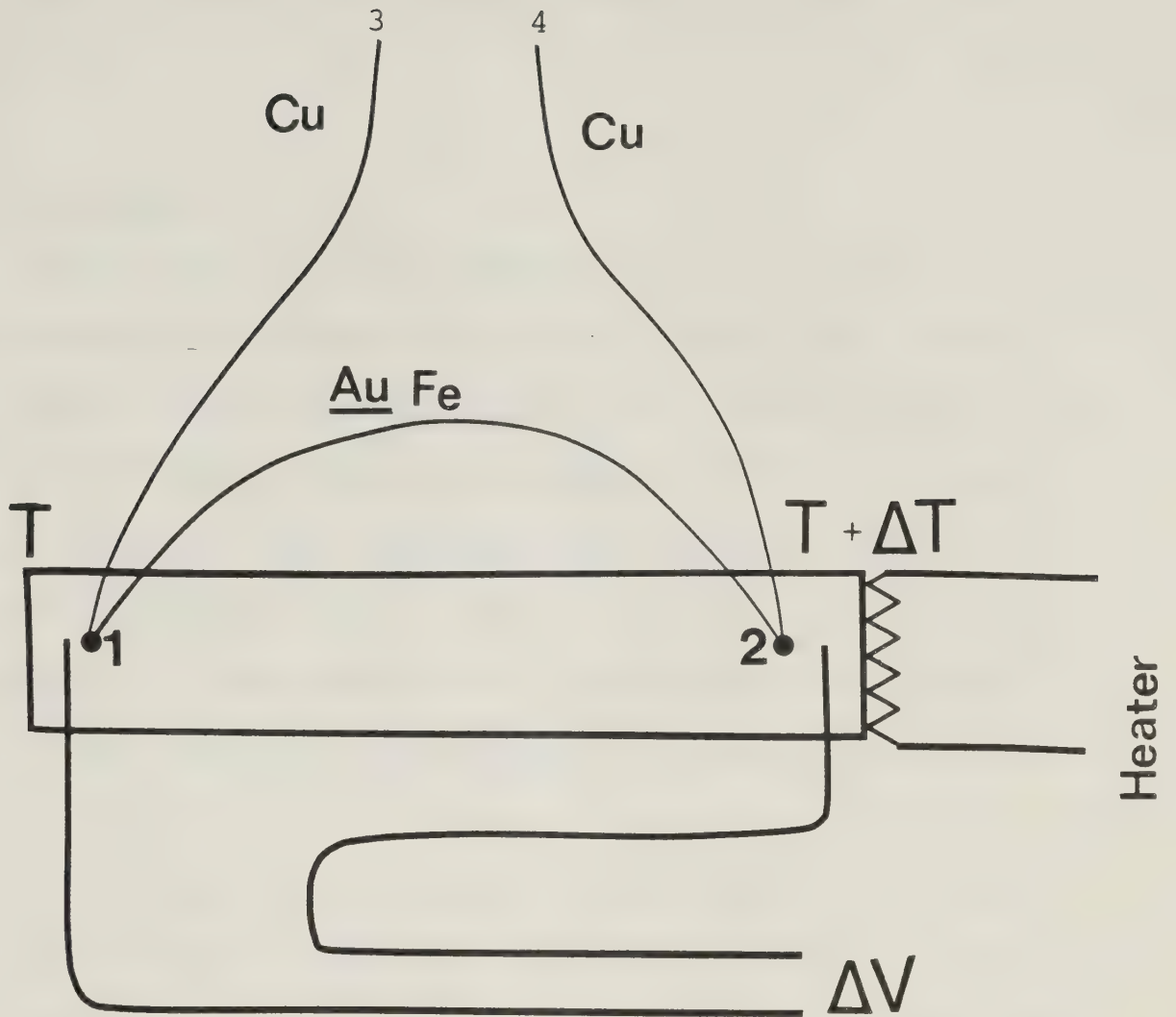


Fig. 3.5 Schematic diagram of the arrangement for measuring the thermoelectric voltage ΔV .

was used to measure the thermoelectric voltage of the sample.

3.6 Specimens

The single crystal specimens of CeB_6 , PrB_6 and NdB_6 were prepared at Tohoku University, Japan, by a floating-zone method and provided to us by Dr. T. Komatsubara. The rest of the samples were polycrystalline and prepared in an arc furnace. The compounds LaB_6 , GdB_6 and DyB_6 were supplied in powder form by Cerac Inc. (Wisconsin) with 99.9% purity. The powder was first compressed into pellet form. These pellets were melted in an argon atmosphere in an arc furnace.

To prepare $[\text{La}_{1-x}\text{Re}_x]\text{B}_6$ alloys (where x is the concentration of $\text{Re} = \text{Gd}$ and Dy) appropriate amounts of LaB_6 and ReB_6 powders were thoroughly mixed and then compressed and arc melted in an argon atmosphere. In the same manner dilute yttrium-rare earth alloys were also prepared. The specimens were cut into rectangular shape from the arc melted buttons using a fine diamond saw. The specimens were etched in dilute nitric acid and washed with alcohol. The annealing of the samples was done in an argon atmosphere at $\sim 800^\circ\text{C}$ for about ~ 8 hours. The typical size of the hexaboride specimens was $2\text{mm} \times 1\text{mm} \times 10\text{mm}$ while the Y-Re alloys were about $2\text{mm} \times 2\text{mm} \times 15\text{mm}$ in size.

CHAPTER 4

REB₆ COMPOUNDS

4.1 Properties of the Compounds

All the REB₆ (RE = La, Ce, Pr, Nd, Gd, and Dy) compounds, we have studied, order antiferromagnetically at low temperatures except, of course, for non-magnetic LaB₆. Néel temperatures (T_N) found from our resistivity data are given in Table 4.1 along with the other values from the literature. The crystal structure of REB₆ is of CsCl type with RE ions at Cs sites and the Cl sites occupied by a small octahedron of B atoms (Fig. 4.1). The lattice constants, taken from Gschneider (1961), are given in Table 4.1. As discussed in Chapter 2, in the case of rare earth magnetic ions the magnetic f-electrons are well screened by the outer electrons. The magnetic moment is localized on the rare earth ions. These localized magnetic moments of free ions are retained in solids containing rare earth ions. It can be seen from Table 4.1 that the magnetic moments of the rare earth ions in REB₆ are very close to their free ionic value. In such magnetic systems it is believed that the magnetic moments interact with each other indirectly via conduction electron (RKKY interaction). The magnetic ordering temperature in a mean field model is found to be:

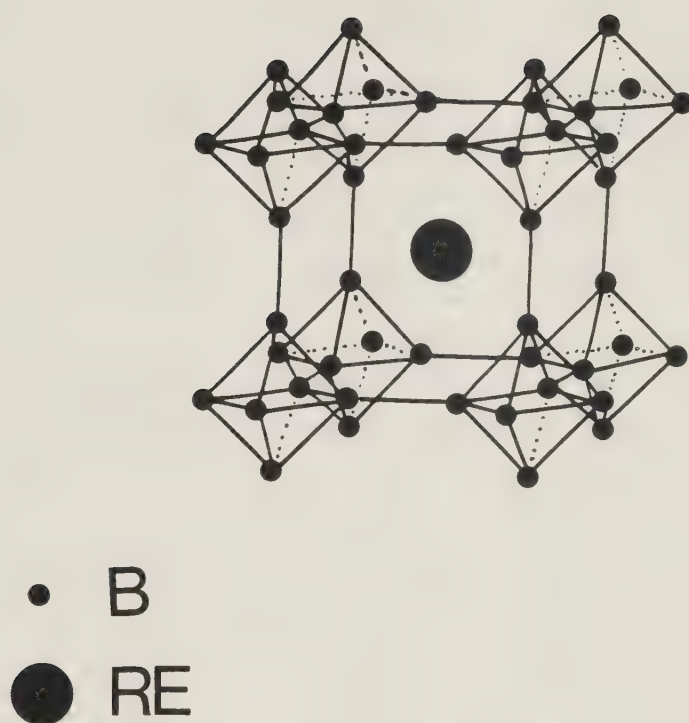


Fig. 4.1 Structure of rare earth hexaborides (REB_6).

Table 4.1 Crystallographic and magnetic data for REB_6 compounds.

REB_6	Lattice constant (\AA)	T_N (K)	θ_P (K)	μ_{eff} (μ_B)	μ_{cal} (μ_B)
LaB_6	4.154	-	-	-	-
CeB_6	4.139	2.4	-76	2.49	2.54
PrB_6	4.130	6.99	-68	3.59	3.58
NdB_6	4.125	7.74	-42	3.54	3.62
GdB_6	4.111	15.2K	-55	8.01	7.94
DyB_6	4.098	20.3K	-21	10.63	10.63

$$T_0 = J(g_J - 1)^2 \frac{J(J+1)}{3}, \quad (4.1)$$

where J and J are the exchange constant and the total angular momentum of the magnetic ion. The magnetic transition temperature (T_0) is expected to be proportional to $(g_J - 1)^2 J(J+1)$, sometimes called de Gennes factor (G), in a series of isostructural metallic rare earth compounds. In such a series J is not expected to vary much. Fig. 4.2 shows the experimental Néel temperature for rare earth hexaborides as well as the Néel temperatures calculated from the de Gennes rule (eqn. (4.1)) by first finding J for GdB_6 ($T_N = 15.15\text{K}$) from eqn. (4.1). The deviation from the de Gennes rule is quite evident. These deviations are usually attributed to the crystalline electric field.

The asymptotic Curie-Weiss temperature in the RKKY approximation is given by (de Gennes, 1962)

$$\theta_p = -\frac{3Z^2\Gamma^2}{4k_B E_f} (g-1)^2 J(J+1) \sum_{i \neq j} F(2K_f R_{ij}), \quad (4.2)$$

$F(x) = (x \cos x - \sin x)/x^4$, where Γ is the s-f exchange integral. In the above expression E_f and K_f represent the Fermi energy and Fermi wave vector of the conduction electrons, K_B is the Boltzmann's constant, and Z is the average number of conduction electrons per atom. The summation extends over all distances R_{ij} between localized moments. For the isostructural compounds REB_6 in which RE atoms have the same valency one has within the free electron model,

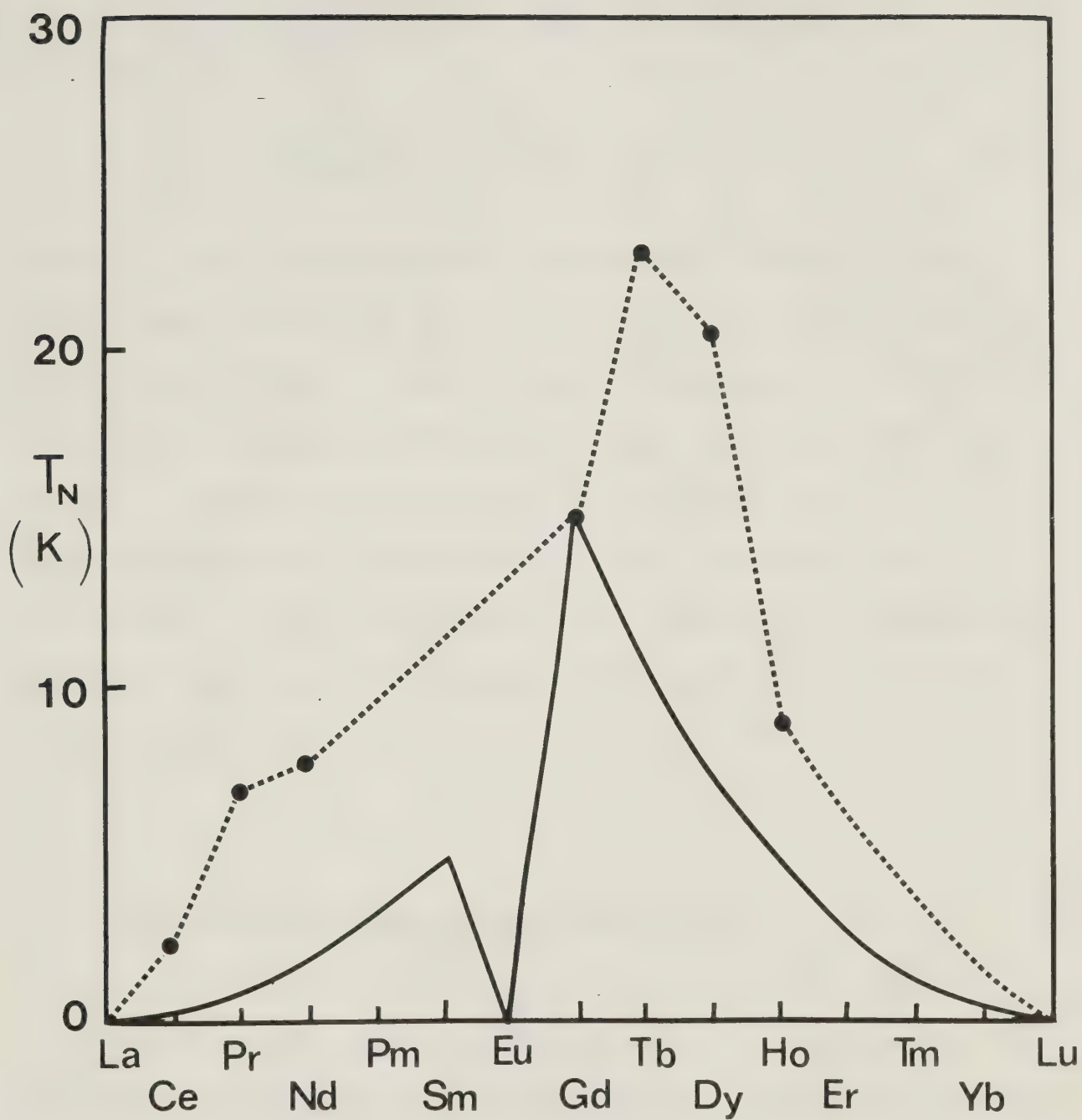


Fig. 4.2 Observed Néel temperatures (T_N) of REB_6 (dashed line), with corresponding predictions of the de Gennes rule (solid line).

$$\theta_p = A \Gamma^2 (g-1)^2 J(J+1) , \quad (4.3)$$

where A is the same constant for all these compounds. To compare the values of the s-f exchange integral Γ_R of different REB_6 compounds we can normalize Γ_R^2 with respect to Γ_{Gd}^2 and we have

$$\frac{\Gamma_R^2}{\Gamma_{\text{Gd}}^2} = \frac{\theta_p(\text{REB}_6)}{\theta_p(\text{GdB}_6)} \times \frac{\frac{7}{2} \times \frac{9}{2}}{(g-1)^2 J(J+1)} , \quad (4.4)$$

where θ_p are experimentally determined values for REB_6 taken from Paderno et al (1967). Fig. 4.3 shows that Γ_R^2 variation in REB_6 is very large and decreases by more than two orders of magnitude from the light to heavy REB_6 compounds. Such a large variation in Γ_R^2 for light rare earth hexaborides (particularly CeB_6) might be due to difference in the strength of the interaction responsible for the coupling of the magnetic moments at low and high temperatures (Lee and Bell, 1972; Nickerson and White, 1969).

4.2 Experimental Results and Discussion

Resistivity, thermoelectric power (TEP) and magnetoresistance (MR) of REB_6 (RE = La, Ce, Pr, Nd, Gd and Dy) have been measured at low temperatures. The experimental results and the discussion of the results is presented in the following two sub-sections. We have separated CeB_6 from the rest of the antiferromagnetic REB_6 compounds because of the anomalous behaviour of CeB_6 .

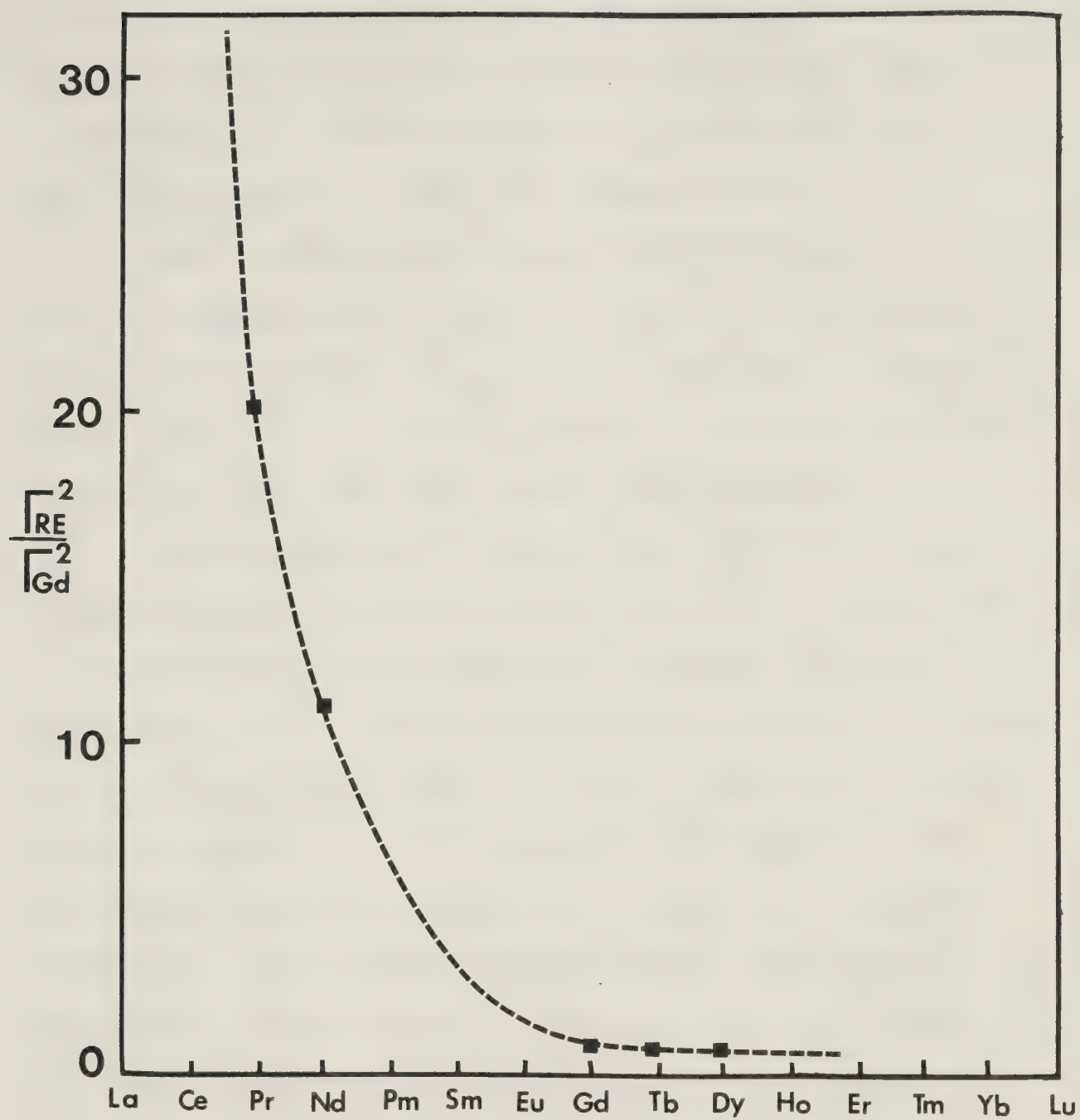


Fig. 4.3 Dependence on atomic number of the ratio $(\Gamma_{\text{RE}}/\Gamma_{\text{Gd}})^2$ for REB_6 compounds.

4.2.1 CeB₆

The resistance data for CeB₆ from 1.8K to room temperature is shown in Fig. 4.4. A minimum is found at ~150K. The resistivity decreases with increasing temperature above a maximum of 3.5K. Above 4K the resistivity is proportional to $\log T$ as shown in Fig. 4.4. There is a rapid drop in resistance below $T_N = 2.4K$ which is due to the transition to the antiferromagnetic phase.

The thermoelectric power (TEP) of CeB₆ as a function of temperature is shown in Fig. 4.5. A giant peak of 265 $\mu V/K$ in the TEP at $T_{\max} = 10K$ is observed. There is a small peak at $T \approx 4.3K$ and a change in slope at 2.4K associated with T_N . The TEP becomes negative below 2.2K.

It is possible to define three phases in CeB₆ (Kasuya et al, 1981). The phase III is for $T < T_2$, where $T_2 = 2.4K$ is the antiferromagnetic ordering temperature. This phase is found to be magnetically anisotropic according to Kasuya et al (1981). Phase II exists in the temperature range $T_2 < T < T_1$, where T_1 corresponds to the maximum in the resistivity data. This phase is nearly isotropic. And finally, phase I, which is completely isotropic, exists above T_1 . The resistivity in phase I has been interpreted by Kasuya et al (1981) using the Suhl-Nagaoka formula (Daybell, 1973), which was derived for dilute (or single impurity) Kondo systems. The resistivity below 4K cannot be explained by the formulation for dilute or single impurity Kondo systems.

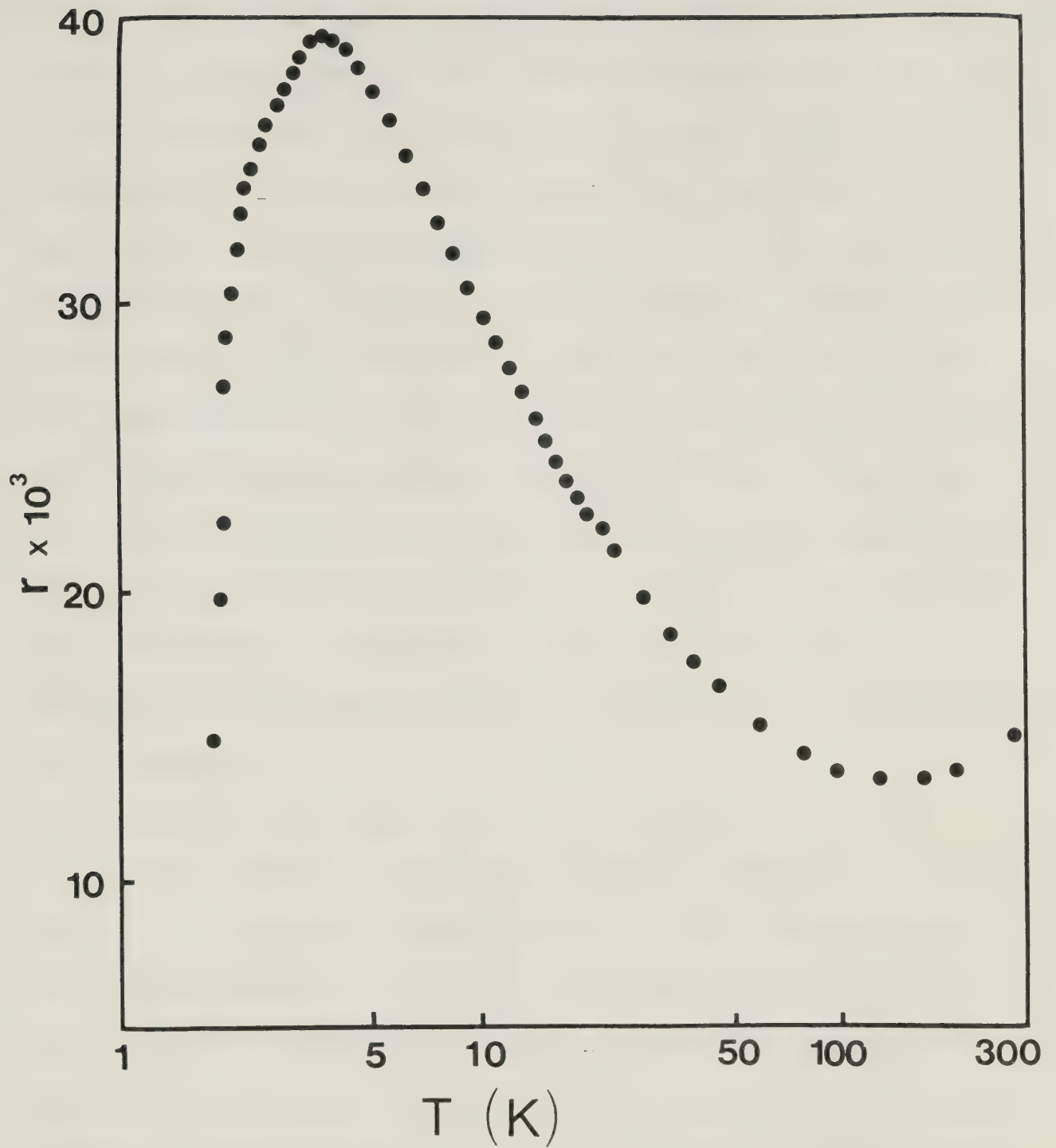


Fig. 4.4 Electrical resistance (r) of CeB_6 as a function of $\log T$ (T = temperature).

Recently, there have been some theoretical investigations taking into account the so-called "Kondo lattice" model. The term "Kondo lattice" was coined by Doniach (1977). Jullien et al (1977) have suggested that the need of the theoretical investigation of concentrated Kondo compounds or "Kondo lattice" beyond the isolated impurities arises due to the competing nature of electron-local spin interaction in these systems. For the 'normal' rare earth systems, the 4f level is far below the Fermi level and these materials have an integral number of 4f electrons with a well defined magnetic moment. In the "anomalous" rare earth systems the 4f level is close to the Fermi level, and a large resonant scattering can occur in these systems. This scattering is believed to be responsible for the Kondo effect that appears in many rare earth alloys and in some compounds.

Lacroix and Cyrot (1979) transformed the Kondo interaction using the idea of Yoshimori and Sakurai (1970) into a fictitious s-f hybridization. This hybridization gives a resonance of width T_K (Kondo temperature) at the Fermi level. The above authors considered a system of conduction electrons interacting with periodically arranged magnetic ions described by an Anderson Hamiltonian. Such a hamiltonian has been shown by Schrieffer and Wolff (1966) to be equivalent to the s-f hamiltonian. The hamiltonian with s-f hybridization is given by

$$\begin{aligned}
H = & \sum_{K\sigma} \left(\epsilon_K + \frac{g}{4} \right) c_{K\sigma}^\dagger c_{K\sigma} + \sum_{i\sigma} \left(E_0 + \frac{Jn}{4} \right) d_{i\sigma}^\dagger d_{i\sigma} \\
& + \frac{g}{2} \sum_i x_i (d_{i\uparrow}^\dagger c_{i\uparrow} + c_{i\downarrow}^\dagger d_{i\downarrow}) + \frac{g}{2} \sum_i y_i (d_{i\downarrow}^\dagger c_{i\downarrow} + c_{i\uparrow}^\dagger d_{i\uparrow}),
\end{aligned}
\tag{4.5}$$

where c_K^\dagger, d_i^\dagger and ϵ_K, E_0 are the creation operators and energies of an s-electron of wave vector K and an f-electron on site i respectively. J is the usual s-f coupling constant, n is the number of conduction electrons per atom (knowing that there is one impurity for each site), x_i and y_i represent the fictitious s-f hybridization. These are considered as order parameters and their average values are reduced to zero above a temperature T_K^* . As soon as $x \neq 0$ (assuming $x=y$) a gap is opened in the electron density of states around the energy of the impurity level.

In the high temperature limit the Kondo lattice system can be treated as a collection of incoherent impurities as the interaction between the rare earth ions becomes negligible. Taking into account thermal fluctuations of x , Lavagna et al (1982) have found that the high temperature resistivity decreases logarithmically as found in CeB_6 (Fig. 4.4). At the low temperatures coherence develops between the impurities and the system can be considered as a "Kondo lattice". According to Lavagna et al (1982), the spatial fluctuations (from site to site) of the s-f hybridization are responsible for the electron

scattering. The low temperature resistivity of a Kondo lattice, according to Lavagna et al (1982), has a maximum at

$$T_M = 0.367 T_K (1-n)^{1/3} . \quad (4.6)$$

From the Hall measurements by Kasuya et al (1981), we know that $n = 0.9$ for CeB_6 at low temperatures. The value of T_K found from eqn. (4.6) is 20.5K. This value of Kondo temperature is twice the Kondo temperature found from the position of the peak in the TEP of CeB_6 (Fig. 4.5). In the resistivity calculation by Lavagna et al (1982) the effect of magnetic ordering at low temperatures has not been taken into account. However, this "Kondo lattice" model calculation gives the qualitative behaviour of resistivity as observed in the case of CeB_6 . The resistivity increases with temperature, has a maximum at $T_1 = 3.5\text{K}$ and above 4K it decreases as $\log T$ as the incoherent Kondo scattering dominates.

Based on the same model Lavagna et al (1982a) calculated the TEP of a "Kondo lattice" system. According to them at lowest temperatures the TEP is positive for $n < 1$ and increases with temperature, has a maximum at a temperature above T_1 . The TEP can be written as approximately

$$S(T) = S_0 / [1 + (T/T_1)^2] , \quad (4.7)$$

where

$$S_0 = -(2\pi^2 k_B / 3e) \left[\frac{3}{4} \pi (1-n) \right]^{-2/3} (T/T_K) .$$

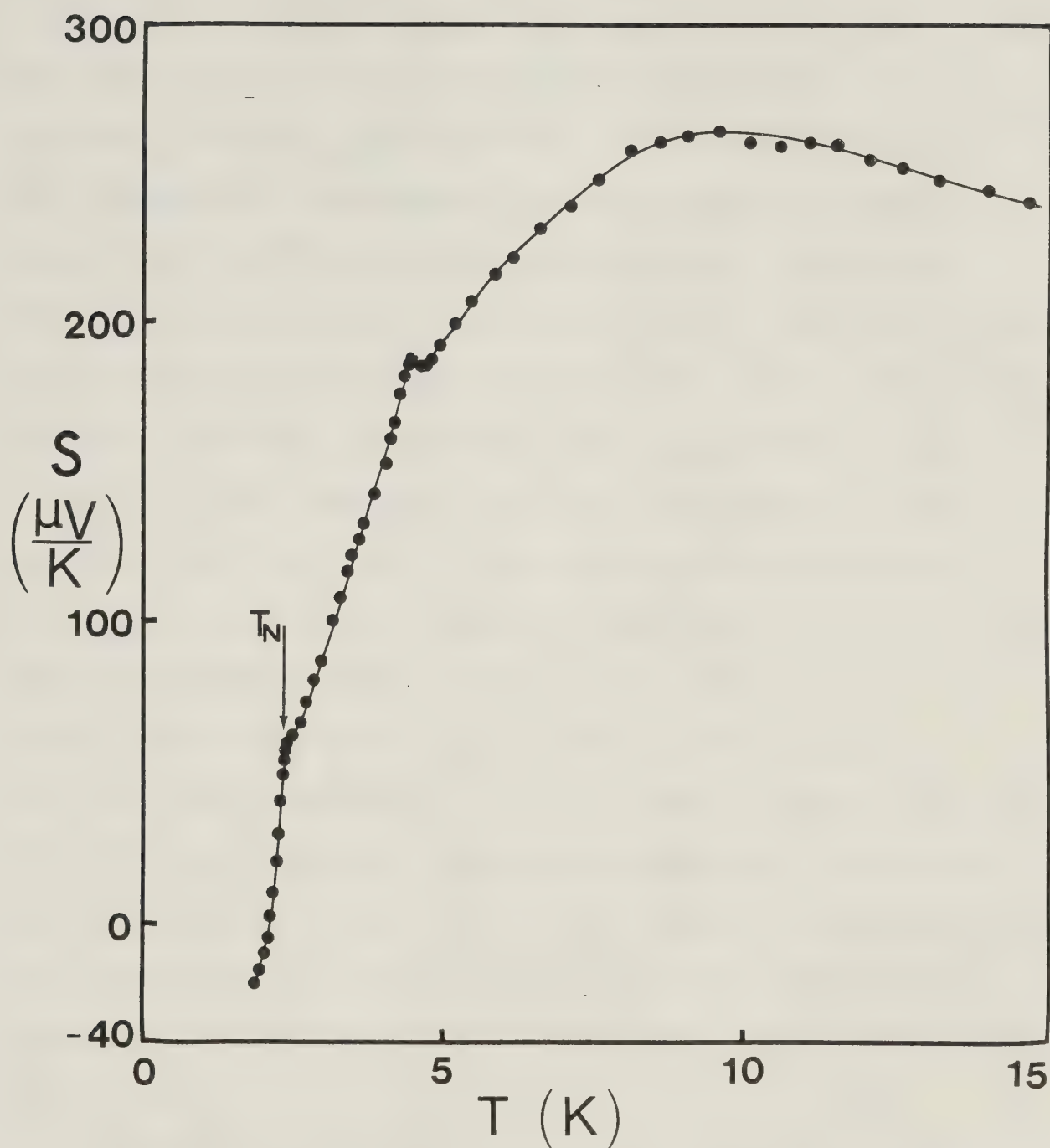


Fig. 4.5 The absolute thermoelectric power (S) of CeB_6 as a function of temperature (T).

The giant positive value in the TEP is expected because of the factor $(1-n)^{-2/3}$ in S_0 . For $n=0.9$ and $T_1=3.5\text{K}$ from the resistivity data of CeB_6 , we find

$$S_0 = 725 \text{ } \mu\text{V/K} \quad \text{at} \quad 10\text{K}.$$

The Kondo lattice model calculation again qualitatively explains the giant values of the TEP data and a qualitative temperature dependence can be understood without taking into account the magnetic ordering. Therefore, one can conclude that even if there is no detailed theoretical understanding of the behaviour of 'dense Kondo' CeB_6 , the 'Kondo lattice' model does give a qualitative understanding of the transport properties exhibited by CeB_6 . Recently there has been a longitudinal MR measurement by Sato et al (1983) at a constant temperature of 0.6K in the antiferromagnetic phase of CeB_6 (i.e. phase III). Their results show that for $T < T_N$ the MR is positive and increases with increasing field and goes through a maximum at a critical field H_C , the antiferromagnetic to paramagnetic transition field. For $H > H_C$, the MR decreases with increasing field. This is consistent with the behaviour expected for an antiferromagnetic metal (Yamada and Takada, 1973, 1973a).

We have done the MR measurements in the phase I (i.e. $T > 3.5\text{K}$) of CeB_6 up to a field of 30 KOe and in the temperature range from 4.2K to 20K. The isothermal longitudinal MR and transverse MR at 4.2K, 10K and 20K are

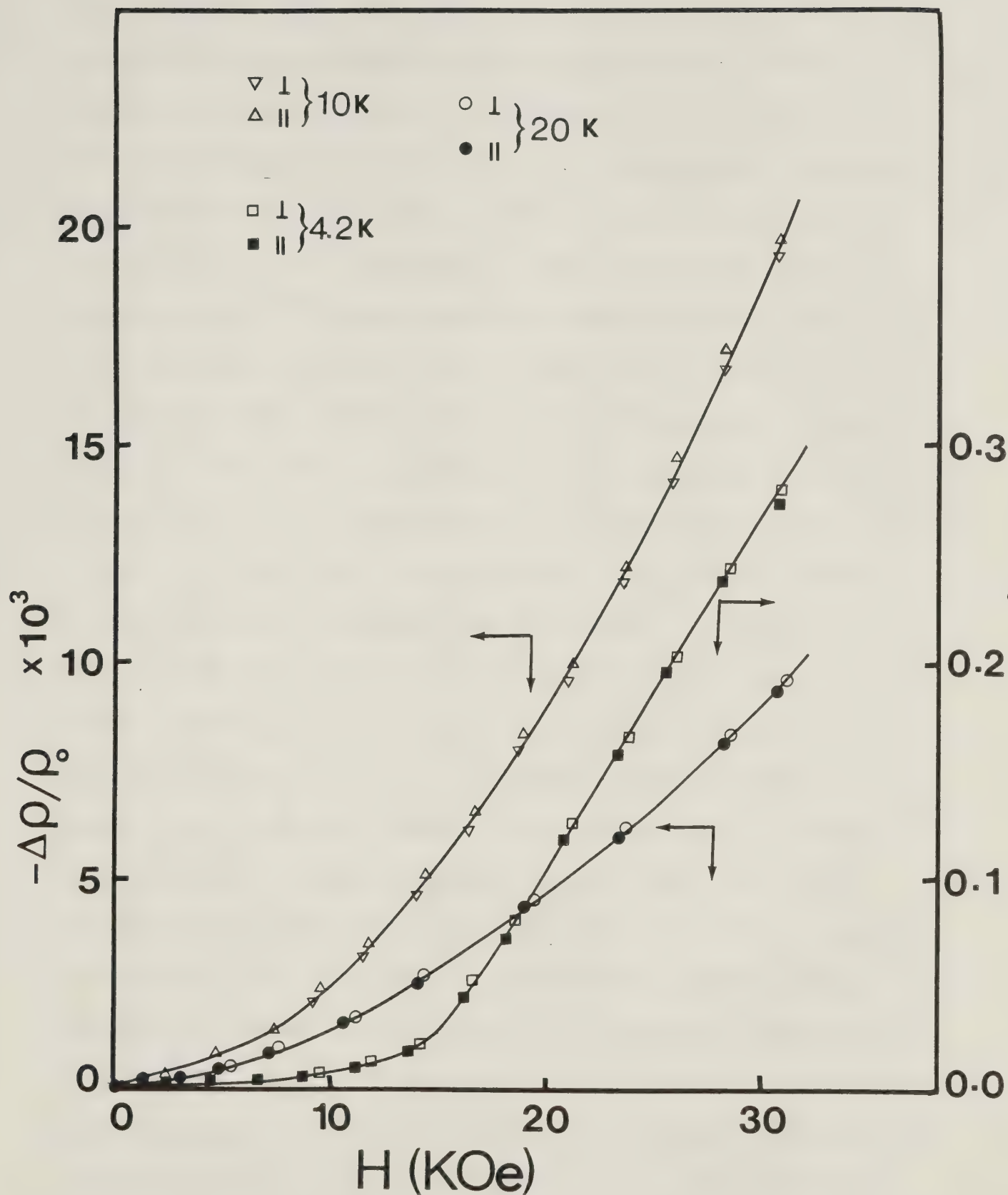


Fig. 4.6 The magnetoresistance ($\Delta\rho/\rho_0$) of CeB_6 as a function of external magnetic field (H) at various temperatures. Symbol \parallel and \perp means longitudinal and transverse magnetoresistance respectively.

shown in Fig. 4.6. The MR are negative and decrease with increasing field (H). We observe that there is very little anisotropy in the MR in phase I, that is, the longitudinal and transverse MR are the same. This is consistent with the results of Kasuya et al (1981), as they have suggested that phase I is completely isotropic. We find from the MR data at 10K and 20K that the MR is proportional to H^2 as shown in Fig. 4.7. The 4.2K isotherm shows a H^2 dependence only below 16 KOe; above that field the MR is linear in H . From Fig. 4.6 and Fig. 4.7 we observe that there is some kind of transition from one phase to the other at 16KOe for 4.2K isotherm. This is consistent with the phase diagram obtained by Kasuya et al (1981). At 4.2K as H is increased from zero to above ~16KOe the phase changes from the phase I to phase II. From our MR data it is found that the MR varies as H^2 in phase I while it has a linear H dependence in phase II, and the critical field H_c of transition from phase I to phase II at 4.2K is ~16KOe. The negative MR in phase I and phase II is quite consistent with the theoretical results for an antiferromagnetic metal for $T > T_N$ (Yamada and Takada, 1973, 1973a). As mentioned earlier, CeB_6 can be treated as a collection of incoherent impurities in phase I. Hence for $T > 4\text{K}$ the MR in phase I is expected to be similar to the dilute magnetic alloys. The negative magnetoresistance appears because of the suppression of fluctuations of the localized spins by an external magnetic

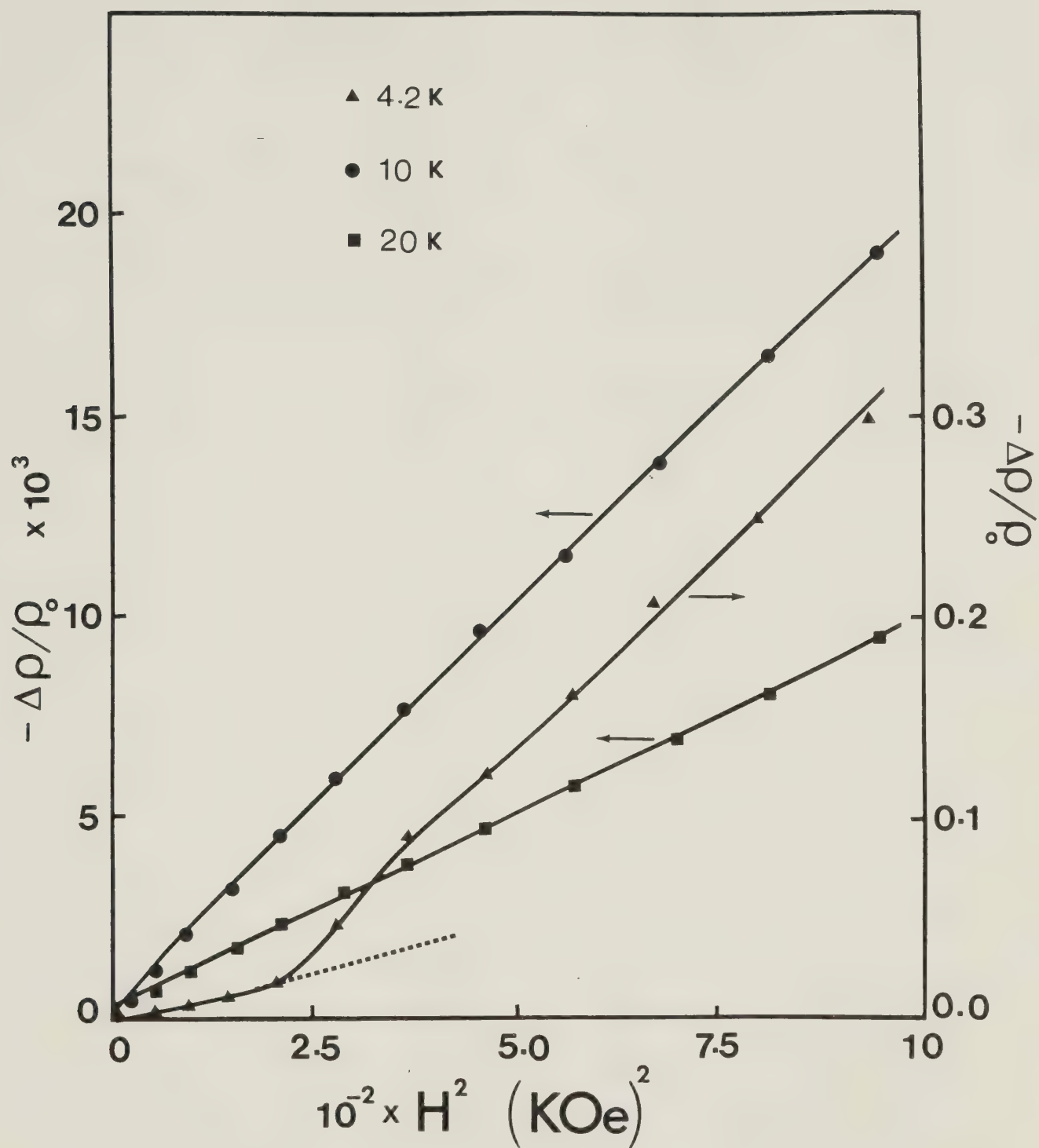


Fig. 4.7 The magnetoresistance ($\Delta\rho/\rho_0$) of CeB₆ as a function of H^2 at various temperatures.

Table 4.2. CeB_6 values of parameter A in phase I for CeB_6 .

$A (\text{KOe})^{-2}$	$A \times T (\text{K}/\text{KOe}^2)$	$T (\text{K})$
-8.9×10^{-5}	-3.7×10^{-4}	4.2
-19.2×10^{-6}	-1.9×10^{-4}	10
-9.0×10^{-6}	-1.8×10^{-4}	20

field. Such negative MR are observed in ferromagnetic and paramagnetic phases and also in dilute magnetic alloys (Yamada and Takada, 1973; Béal-Monod and Weiner, 1968).

As mentioned earlier, the MR in phase I can be expressed as

$$\frac{\Delta\rho}{\rho_0} = \frac{\rho(H,T) - \rho(H=0,T)}{\rho(H=0,T)} = A(T) H^2 \quad . \quad (4.8)$$

The values of the parameter A for temperatures in phase I are given in Table 4.2. We find that A has an inverse temperature dependence with some discrepancy at 4.2K due to phase change from phase I to phase II.

4.2.2 Antiferromagnetic REB₆ (RE = Pr, Nd, Gd and Dy)

The residual resistance ratios (RRR), the ratios of the resistivities at 293K to those at 4.2K, are given in Table 4.3 for the REB₆ compounds. In this section we present an experimental study of resistivity, thermoelectric power (TEP) and magnetoresistance of antiferromagnetic hexaborides (REB₆, RE = Pr, Nd, Gd and Dy) along with non-magnetic LaB₆.

4.2.2a Resistivity

The resistance ratio $r = R_x / R_s$ (R_x = sample resistance and $R_s = 0.1\Omega$, standard resistance) is measured directly with the d.c. comparator as discussed in Chapter 3. In this presentation, r is reported rather than the sample resistivity because of the geometrical uncertainty with

Table 4.3 Residual resistivity ratio (RRR) for REB_6 compounds.

Sample	RRR = $\rho(293\text{K})/\rho(4.2\text{K})$	$\rho(293\text{K}) \mu\Omega\text{-cm}$
LaB_6	16	9
PrB_6	18	15
NdB_6	16	14.6
GdB_6	8	31
DyB_6	9	40

irregular and small specimens.

The resistivity of non-magnetic LaB_6 does not change significantly below 30K as shown in Fig. 4.8. A similar result has been found by Kasuya et al (1981). The phonon resistivity is expected to be negligible in iso-structural REB_6 below 30K.

The resistance data for PrB_6 , NdB_6 , GdB_6 and DyB_6 are presented in Fig. 4.8 and Fig. 4.9. The common features of the resistance (r) data are a rapid increase in r with temperature T below T_N , a change in slope of r at T_N and a slow increase in r which is linear in T above T_N . The Néel temperatures (T_N) are given in Table 4.1. In the case of PrB_6 we observe a thermal hysteresis in the r vs T curve at $\sim 4\text{K}$, as shown clearly in the insert of Fig. 4.8. According to the neutron diffraction studies on PrB_6 by McCarthy et al (1980), below $\sim 6.9\text{K}$ there is an incommensurate antiferromagnetic phase with magnetic lattice vector $Q = (0.23, 0.23, 0.5) 2\pi/a_0$ while a commensurate phase with $Q = (0.25, 0.25, 0.5) 2\pi/a_0$ is seen to coexist with the incommensurate phase at 4.2K . At lower temperatures only the commensurate phase exists. The hysteresis in r vs T data at 4K is associated with the low temperature phase transition. At $T < 3.8\text{K}$ only the commensurate phase exists. The extrapolation of resistance data (Fig. 4.8) in both phases show that the resistivity is smaller in the commensurate phase than in the incommensurate phase. This is quite consistent because the commensurate phase is

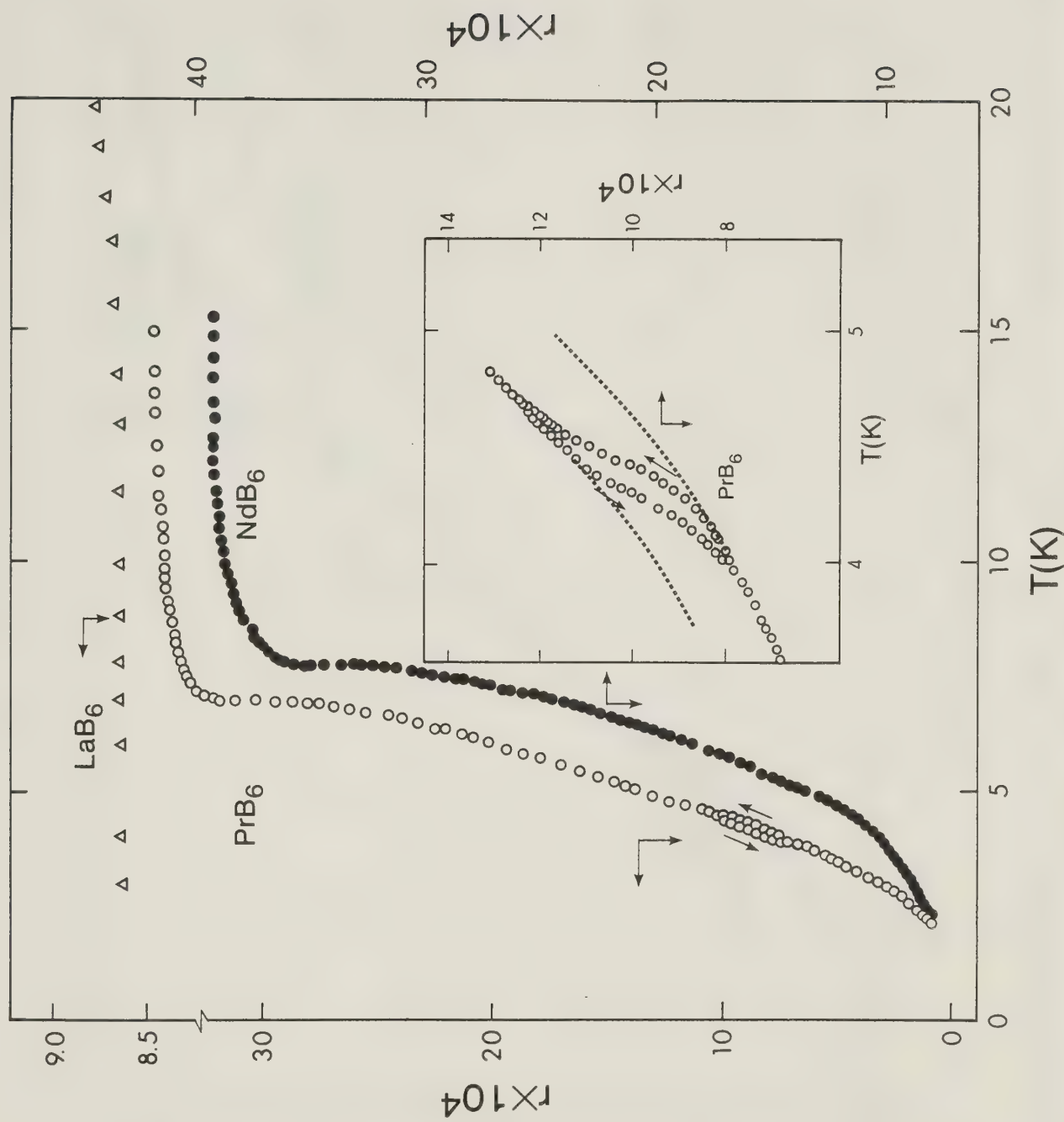


Fig. 4.8 Resistance ratio $r = R_x/R_g$, where R_x is specimen resistance and $R_g = 0.1\Omega$, as a function of temperature (T) for LaB_6 , PrB_6 and NdB_6 . The insert is a magnified curve for r of PrB_6 in the temperature range 3 - 5K.

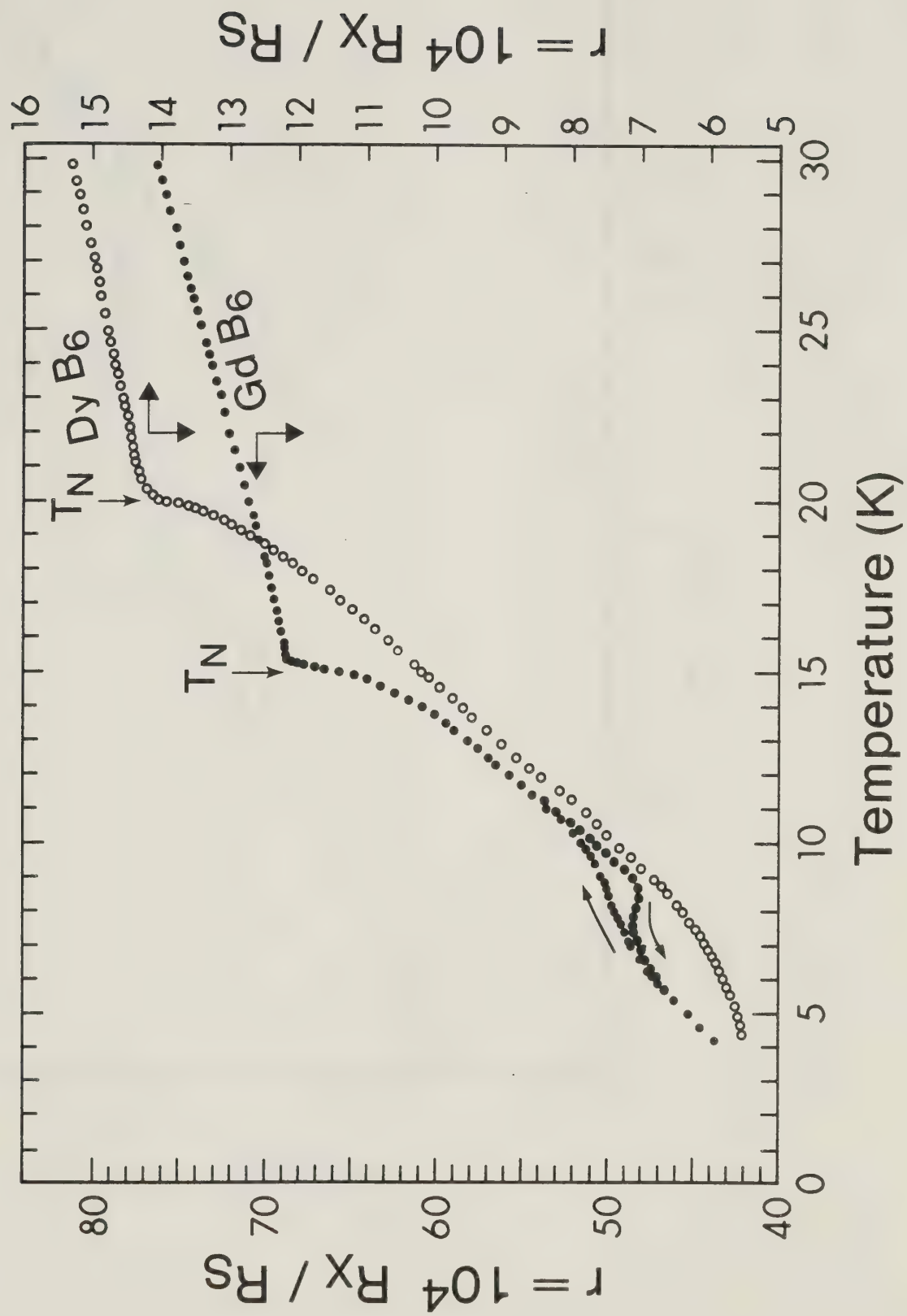


Fig. 4.9 Resistance (r) of GdB₆ and DyB₆ as a function of temperature (T).

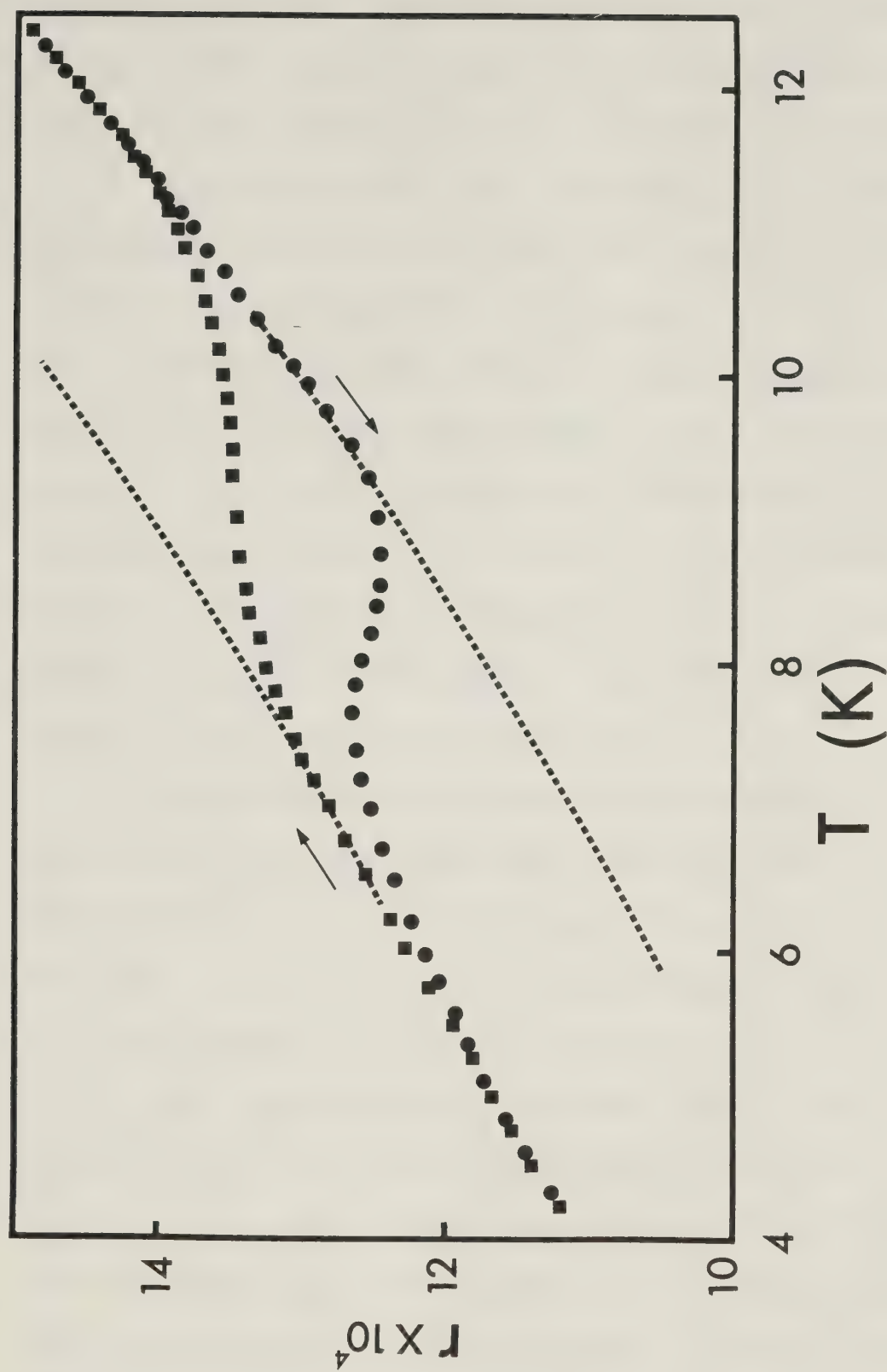


Fig. 4.10 Resistance (r) of GdB₆ in the temperature range 4.2 - 12K showing a thermal hysteresis.

relatively a more ordered phase than the incommensurate phase. The neutron diffraction data shows only a commensurate phase for NdB_6 below T_N (McCarthy and Thompson, 1980).

The resistivity data for GdB_6 (Fig. 4.9) reveals hysteresis at about 7K. This hysteresis is associated with a second phase transition (Nozaki et al, 1980). The magnetic structure is not known in GdB_6 . However, the extrapolation of the resistance data in Fig. 4.10 shows that phase II has greater resistivity than phase I. This suggests that phase I is relatively more ordered than phase II. A neutron diffraction study could reveal whether phase II is an incommensurate magnetic phase. The resistance of DyB_6 shows only one phase up to T_N .

To interpret the temperature dependence of the resistivity of REB_6 compounds, we shall first discuss the resistivity at the lowest temperatures, then the resistivity due to electron-spin wave scattering and finally the critical resistivity in the vicinity of T_N .

The resistivity of the REB_6 ($\text{RE} = \text{Pr}, \text{Nd}, \text{Gd}$ and Dy) compounds at the lowest temperatures varies as T^2 as shown in Fig. 4.11. The temperature range of T^2 dependence for each compound is given in Table 4.4. Kasuya et al (1981) have also observed a T^2 dependence of resistivity for "dense Kondo" CeB_6 at $T \ll T_N$ ($T_N \approx 2.4\text{K}$). A similar T^2 dependence of resistivity below 0.3K has been found for CeAl_3 which is also a "dense Kondo" material. Mott (1974) and Andres et al (1975) have interpreted this T^2 dependence

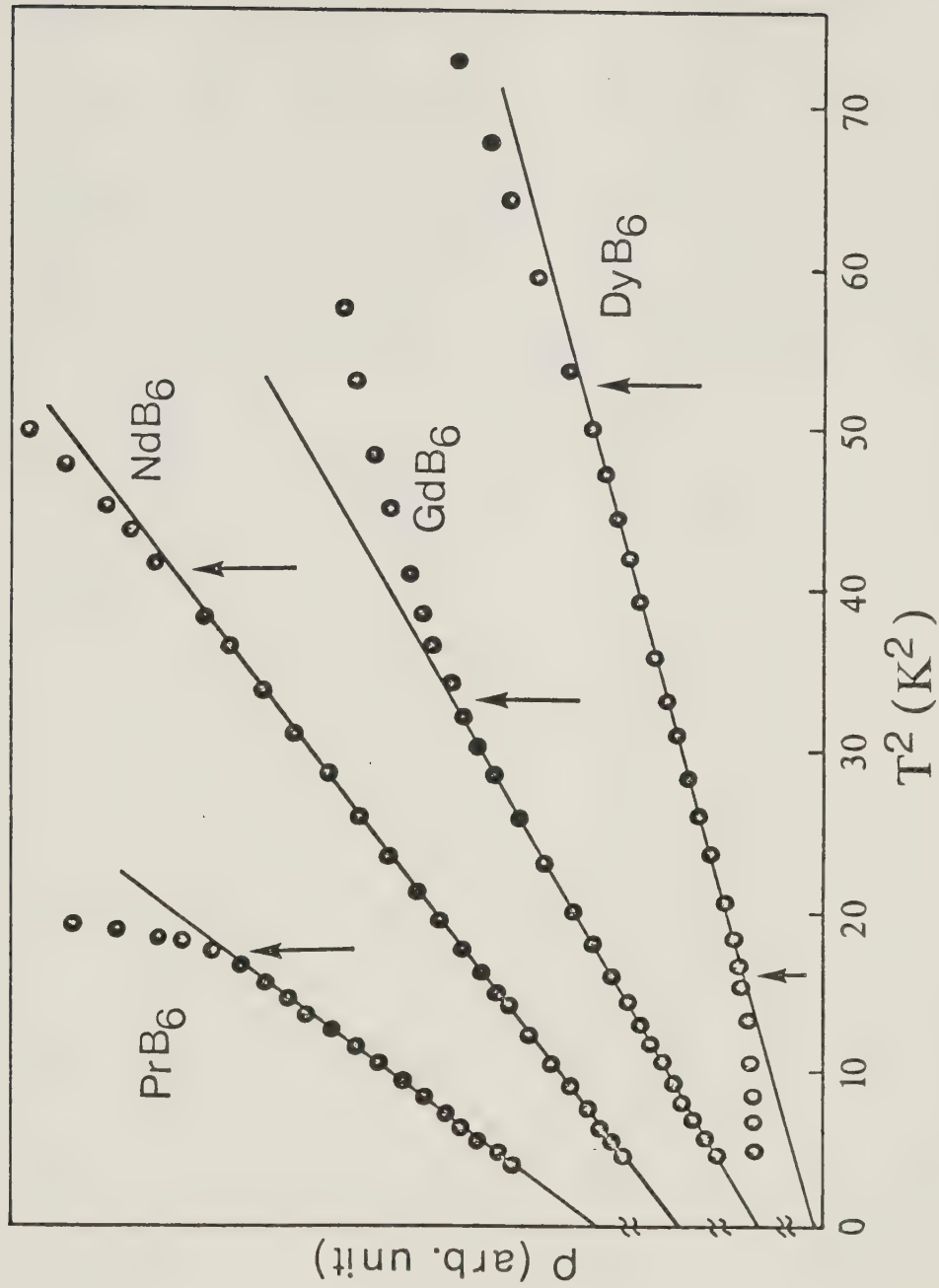


Fig. 4.11 Electrical resistivities of PrB₆, NdB₆, GdB₆ and DyB₆ plotted against T^2 . The arrows indicate the range of T^2 dependence for each compound.

Table 4.4 Temperature range of T^2 and T^4 or T^3 dependences for REB_6 compounds.

Sample	T^2 range	T^4 or T^3 range
PrB_6	$T \leq 4.2\text{K}$	$5.1\text{K} \leq T \leq 6.8\text{K}$
NdB_6	$T \leq 5.8\text{K}$	$5.9\text{K} \leq T \leq 7.6\text{K}$
GdB_6	$T \leq 5.7\text{K}$	$6.7\text{K} \leq T \leq 14.4\text{K}$
DyB_6	$3.8\text{K} \leq T \leq 7.3\text{K}$	$12\text{K} \leq T \leq 19.5\text{K}$

as an interband scattering effect between the conduction electrons and the band of collective states.

The phonon scattering, which as we have remarked earlier is negligible in LaB_6 below 30K, is expected to be the same in the other isostructural hexaborides. At the same time recent de Haas-van Alphen studies of some REB_6 (RE = La, Ce, Pr and Nd) by van Deursen et al (1982), show that the 4f-electrons have only minor influence on the geometry of the Fermi surface but the dispersion of the bands near the Fermi energy is very much dependent on the filling of the 4f band, which is evident from the high values of effective mass. The large masses are attributed to the interaction between the conduction electrons and the partially filled 4f-electron states.

The T^2 resistivity variation appears only in those REB_6 with some occupied 4f-electron states and not in LaB_6 . Neither do all the REB_6 compounds that show the T^2 resistance show a Kondo effect. On the other hand, electron scattering of the Baber type (Baber, 1937; Mott, 1974) in which the low mass conduction electrons are scattered into large mass states should be significant in each of the compounds containing a rare earth with a partially filled f-band, just as it is in the transition metals (Dugdale, 1977). This scattering is proportional to the square of the density of empty large mass states, which in turn is proportional to the square of the electronic specific heat, $C_{el} = \gamma T$. The resistivity, $\rho = AT^2$, shown in Fig. 4.11 should

then be related to the specific heat. The specific heat has been measured for PrB_6 (Lee et al, 1970; McCarthy et al, 1980) and both sets of data yield an approximate value of $\gamma = 280 \text{ mJ mol}^{-1} \text{ K}^{-2}$. From our data for PrB_6 $A = 3.8 \times 10^{-8} \Omega \text{ cm K}^{-2}$. Thus, in these units $A/\gamma^2 = 0.5 \times 10^{-12}$ which is very close to the value 0.3×10^{-12} quoted by Dugdale (1977) for the Pd, Pt and Ni groups of transition metals. Other transition metals have similar values for A/γ^2 and from these comparisons it would appear that the importance of electron-electron scattering in rare earth hexaborides is similar to that in the transition metals. From these observations of the T^2 dependence of ρ we conclude that this behaviour is not a characteristic property of "dense Kondo" Ce compounds but rather is common to all the magnetic rare earth hexaborides.

A T^4 dependence of resistance is observed for PrB_6 and NdB_6 and a T^3 dependence is found for GdB_6 and DyB_6 just below their respective Nèel temperatures as shown in Fig. 4.12 and Fig. 4.13. The temperature regime of the T^4 or T^3 dependence is given in Table 4.4. According to Rivier and Mensah (1977) the resistivity (ρ) of an anti-ferromagnetic material due to electron-spin wave scattering can be written as

$$\rho_{\text{metal}} \sim T^4$$

and

$$\rho_{\text{alloy}} \sim T^3$$

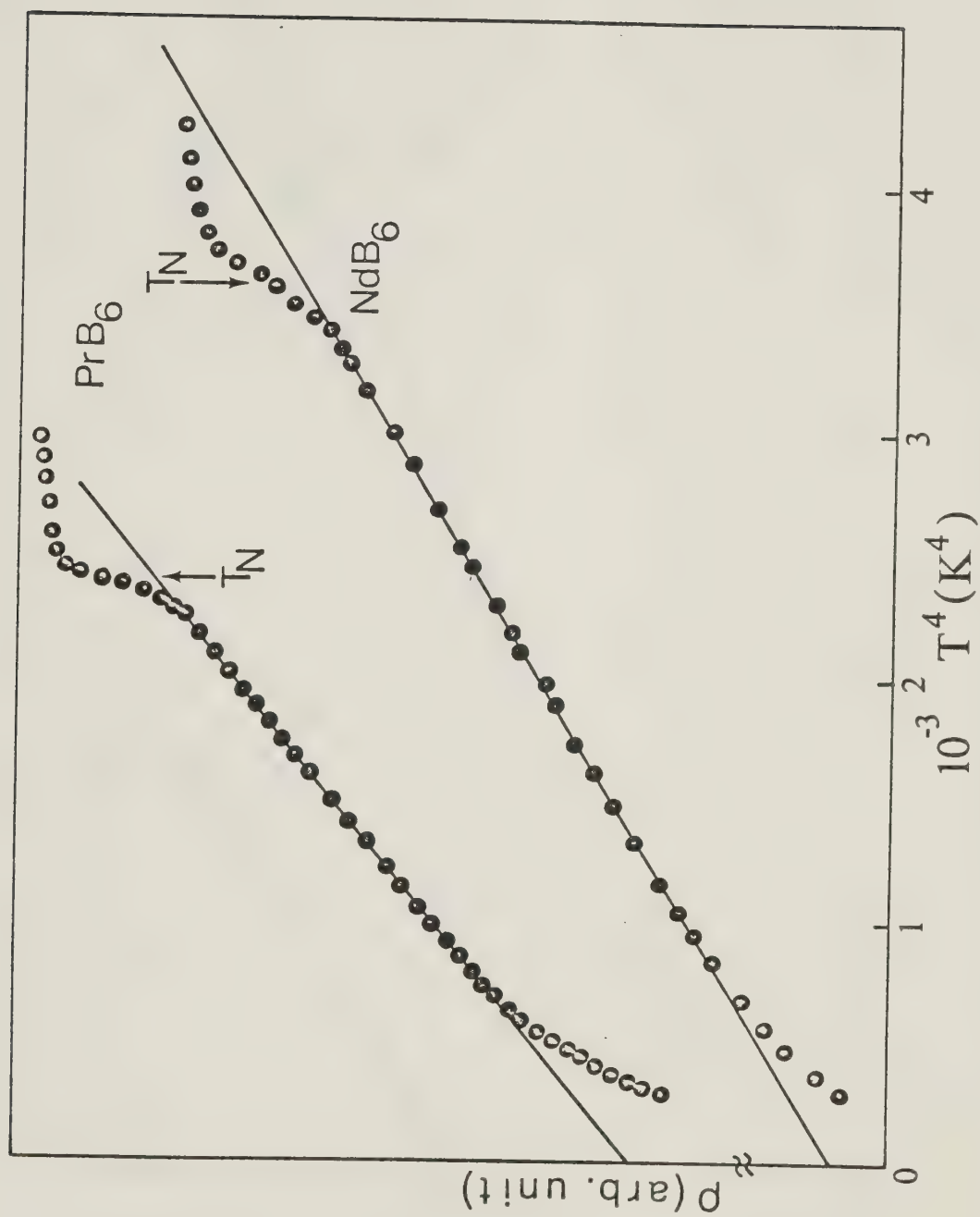


Fig. 4.12 Electrical resistivities of PrB₆ and NdB₆ plotted against T^4 .

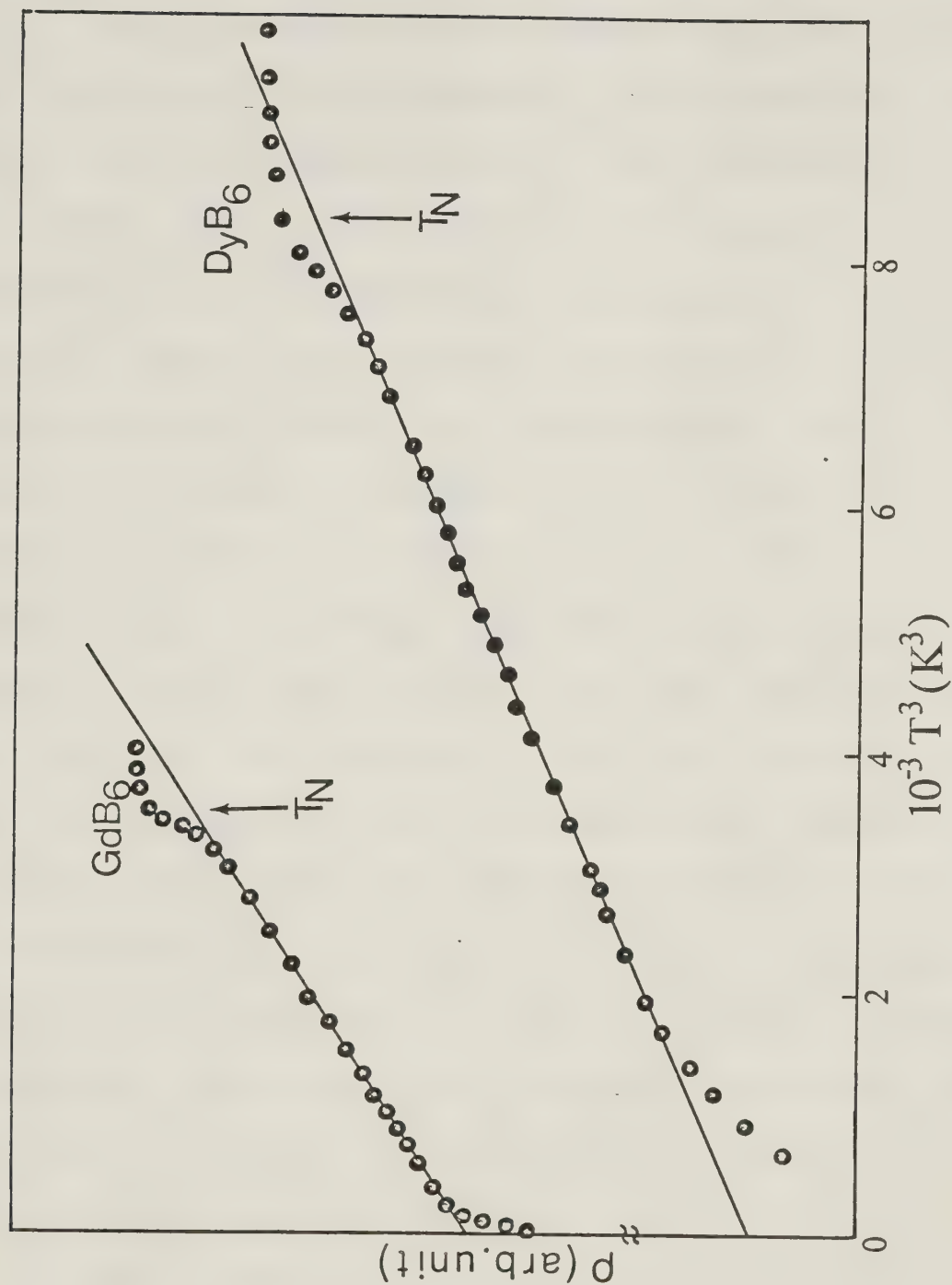


Fig. 4.13 Electrical resistivities of GdB_6 and DyB_6 plotted against T^3 .

as discussed in Chapter 2. It is therefore believed that the observed T^4 dependence for PrB_6 and NdB_6 and T^3 dependence for GdB_6 and DyB_6 is due to conduction electron-spin wave scattering.

To study the critical resistivity, the resistivity in the vicinity of the magnetic phase transition of the REB_6 , a detailed measurement of the resistance is done around T_N . Any reasonable fitting of the critical resistivity in the narrow temperature range where it is visible near T_N needs a very accurate measurement of resistance. It was possible to measure the resistance ratio $r = R_x/R_s$ with an accuracy of one parts in 10^7 as discussed in Chapter 3. Some of the advantages of studying the critical resistivity of the REB_6 compounds are as follows: (i) These compounds have cubic crystal structures and the resistivity is expected to be isotropic, hence the critical exponents can be obtained even with polycrystalline samples. (ii) The ordering temperatures of these hexaborides are below 25K a convenient range for precise control of the temperature and accurate measurements. (iii) All other temperature dependent contributions to resistivity are small for temperatures below 30K as evident from the resistivity data of isostructural non-magnetic LaB_6 .

The resistance (r) in the vicinity of T_N along with its temperature derivative (r') is shown in Figs. 4.14, 4.15, 4.16 and 4.17 for PrB_6 , NdB_6 , GdB_6 and DyB_6 respectively. We observe a divergence in r' at T_N as expected from the

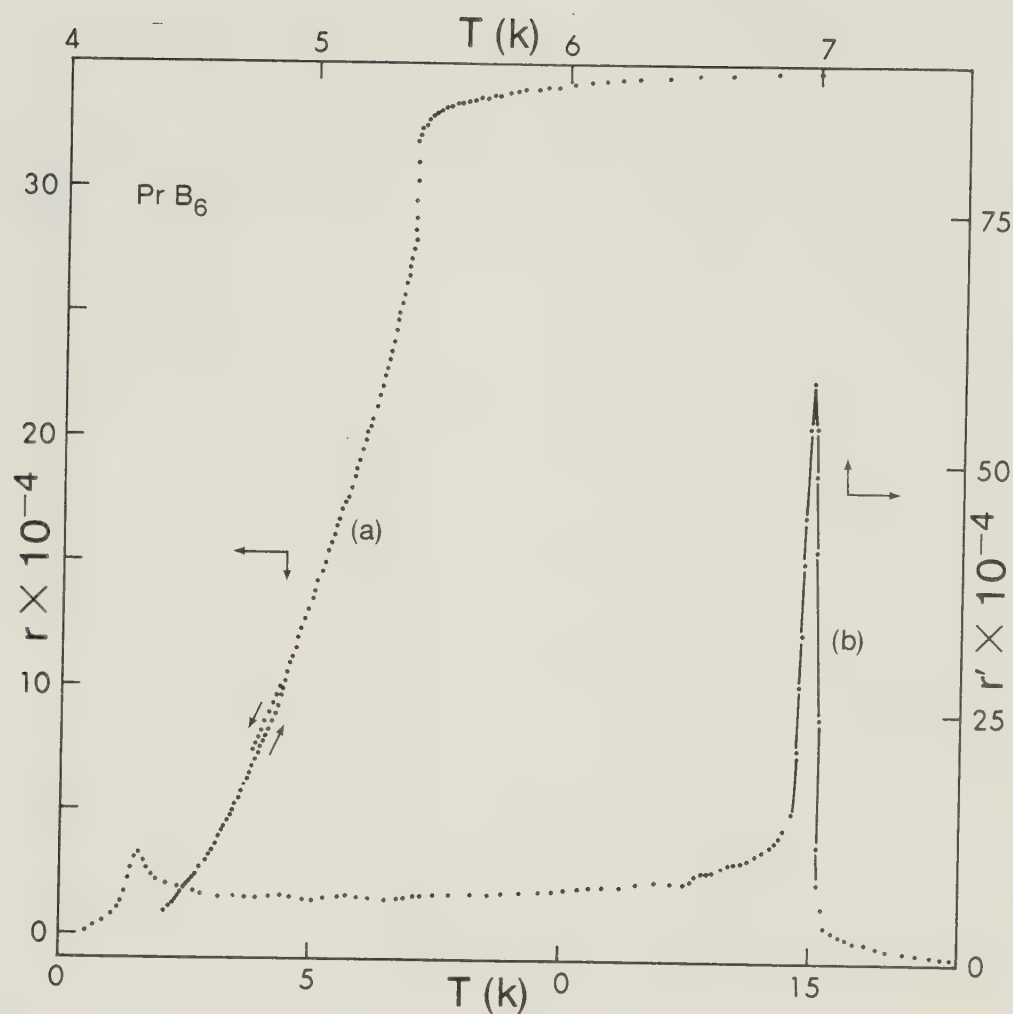


Fig.4.14(a). Variation of normalized resistance $r = R_x/R_s$, where R_x is sample resistance and $R_s=0.1\Omega$ (standard resistance), as a function of temperature T in PrB_6 .

Fig.4.14(b). The temperature derivative of the resistance $r'(T)$ showing a maximum at the Néel temperature ($T_N=6.99\text{K}$) and a smaller peak at $\sim 4.2\text{K}$ corresponding to the second phase.

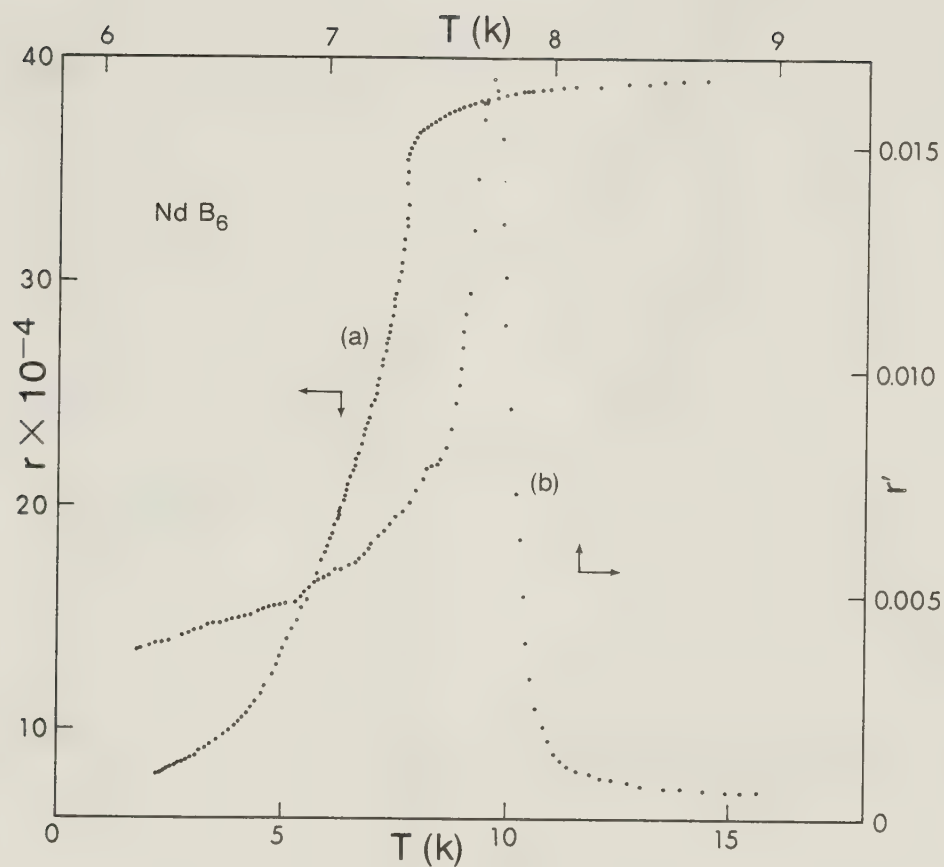


Fig.4.15(a). The resistance (r) data for NdB_6 as a function of temperature.

Fig.4.15(b). The temperature derivative of the resistance r' as a function of T , showing a sharp peak at the Néel temperature ($T_N = 7.74\text{K}$) of NdB_6 .

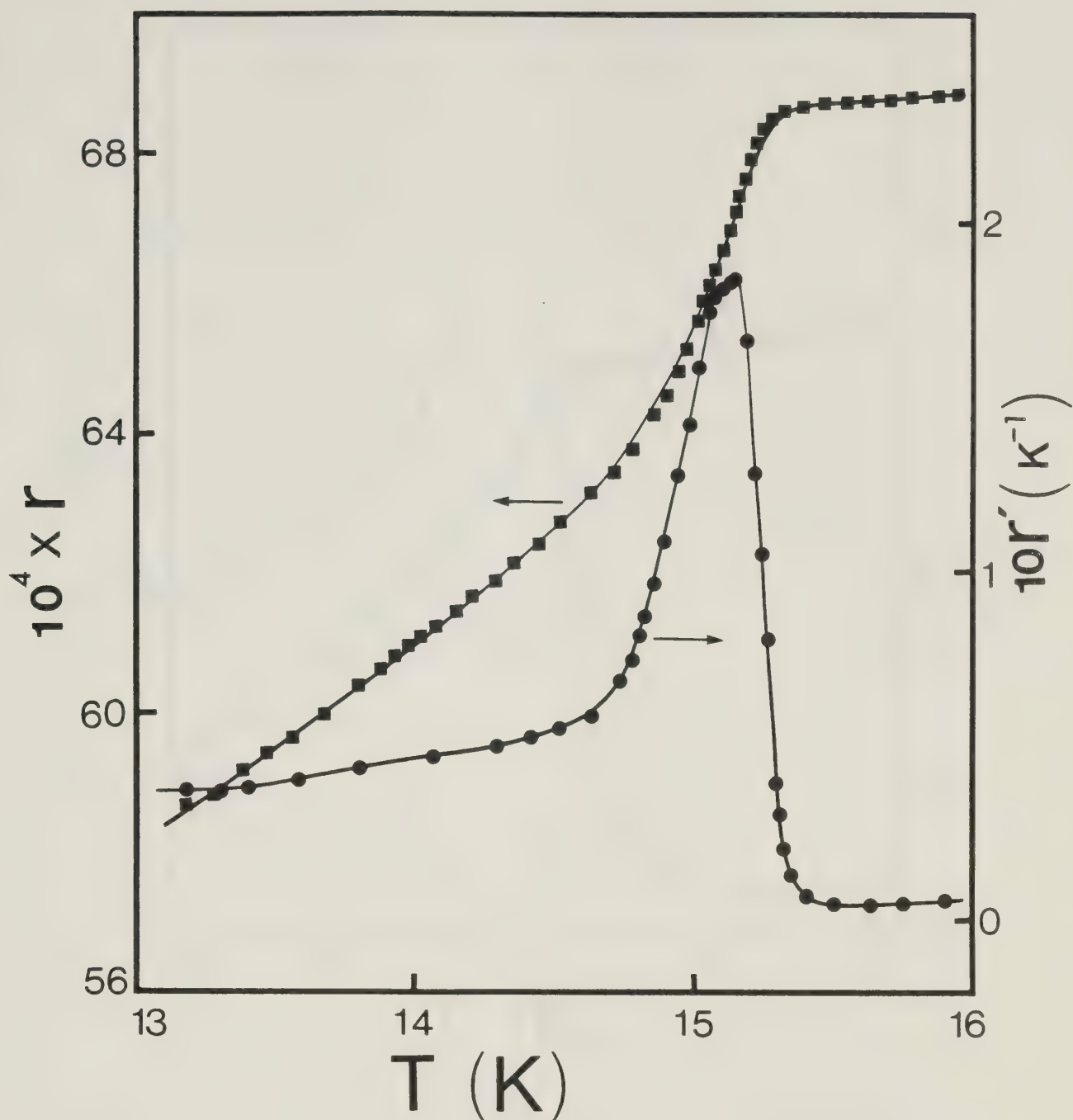


Fig. 4.16 The resistance (r) and its temperature derivative (r') as a function of temperature (T) for GdB_6 in the neighbourhood of T_N .

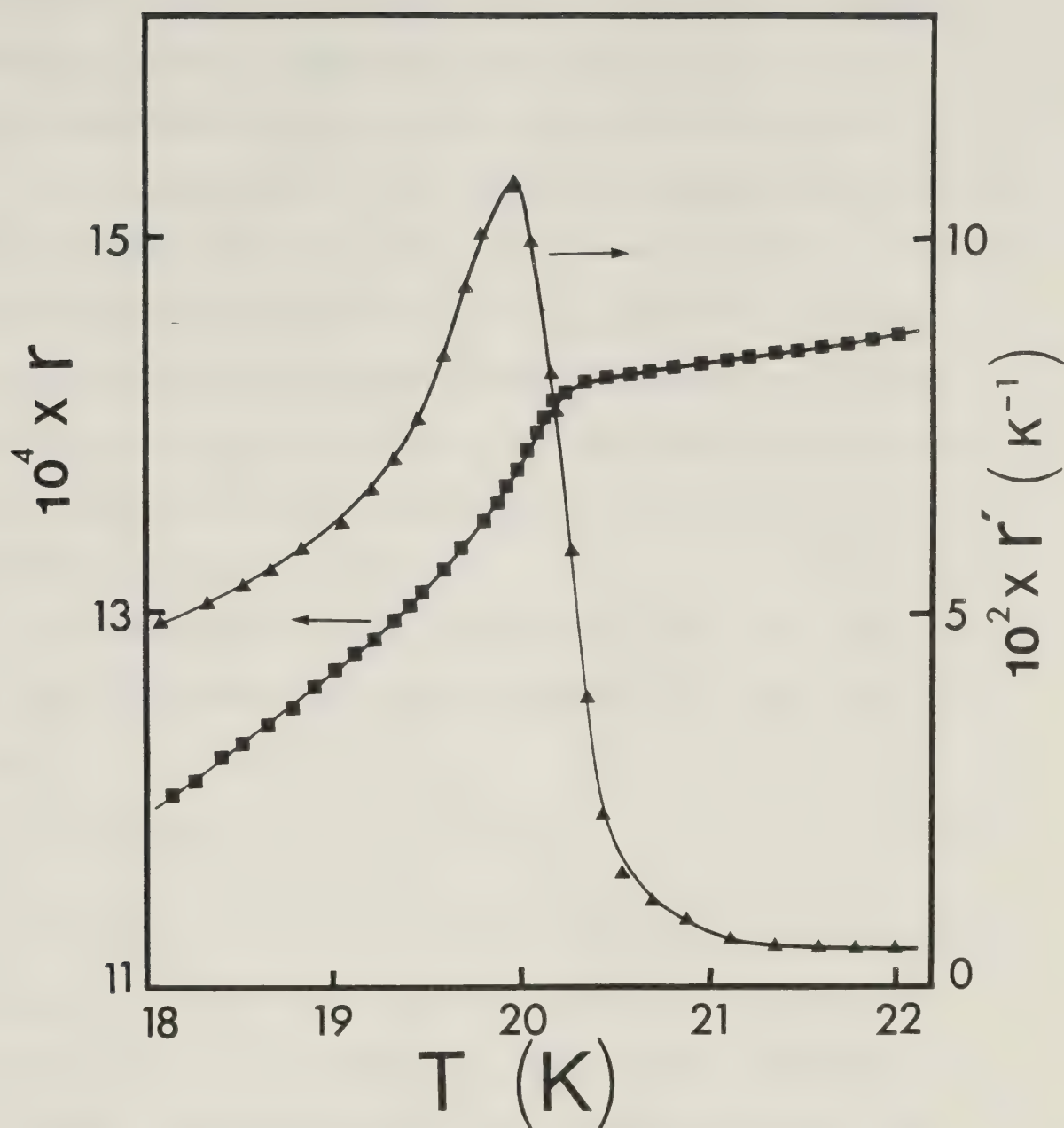


Fig. 4.17 The resistance (r) and its temperature derivative (r') as a function of Temperature (T) for DyB_6 in the vicinity of T_N .

theoretical prediction discussed in Chapter 2. The anti-ferromagnetic REB_6 compounds are classified as type II antiferromagnets because of the positive divergence in r' .

The derivative r' was obtained by numerically differentiating the measured value of r . To do this a group of adjacent data points were fitted to a quadratic equation and then the first derivative was calculated at the midpoint. By sliding the curve along the experimental data, it was possible to obtain the values of r' for the entire temperature range of interest.

The analysis of the experimental data was carried out using the expression for the resistance r in the vicinity of T_N :

$$r = r_0 + B_{\pm}|t| + A_{\pm}|t|^{1-\alpha_{\pm}}, \quad (4.9)$$

where subscript + or - is used for the reduced temperature $t > 0$ or $t < 0$. The first term in the above equation is due to regular spin scattering, the second term represents a small linear contribution due to phonon scattering and finally the last term is the contribution due to the critical scattering. Recent theoretical calculations have shown that the critical exponent $\alpha_+ = \alpha_- = \alpha$ (Malmström and Geldart, 1982; and Balberg and Maman, 1979).

There are some difficulties to be aware of in analyzing the experimental data to extract a reliable value of the critical exponent. These are, (i) changes in the spin scattering from the critical region to the classical

spin fluctuation region are gradual and an inaccurate value of the critical exponent may be deduced by choosing too large a range of t . This arises from an uncertainty in the temperature range over which the theoretical expression can be used; (ii) an accurate expression for phonon resistivity in magnetic metals is not available and (iii) the values of the critical exponents calculated by various theoretical models differ only by small amounts, hence it is difficult to provide experimental verification of one. In spite of the above difficulties a careful analysis of the data can give us valuable information. The criteria for a satisfactory fit to the data were that it must yield a random distribution of residuals as a function of the reduced temperature and that the root mean square error is of the order of the estimated experimental error. To reduce the correlation among the parameters, T_N was treated as a fixed parameter in the regression procedure. The value of T_N was first estimated by taking it to be the temperature at which r' has a maximum. A small deviation in T_N from the maximum in r' is possible due to crystal imperfections and strains as well as by the numerical method used in extracting r' from the experimental data. Hence T_N found from the maximum in r' was changed in small steps in search of a better fit to the data.

The resistance data for $T < T_N$ as well as for $T > T_N$ were analyzed using eqn. (4.9). The values of T_N and α are given in Table 4.5 for PrB_6 , NdB_6 , GdB_6 and DyB_6 .

Table 4.5 Experimentally determined values of the critical exponent (α) for REB_6 antiferromagnets.

REB_6	$T_N (\text{K})$	α
PrB_6	6.99	-0.019
NdB_6	7.74	-0.017
GdB_6	15.14	-0.36
DyB_6	20.32	-0.16

The values for GdB_6 and DyB_6 are taken from the work of Singh and Woods (1981).

According to theoretical calculations the values of α for $d=3$ and $n=1,2,3,4$ and 6 are $0.125, -0.02, -0.11, -0.17$ and -0.38 (or -0.27) respectively (Bak and Mukamel, 1976; Leguillon and Zinn-Justin, 1980; and Malmström and Geldart, 1980). For PrB_6 and NdB_6 the values of α are very close to the theoretical value -0.02 for $d=3$ and $n=2$. The value of α for DyB_6 suggests it to be equivalent to a system with $d=3$ and $n=4$, while for GdB_6 the critical exponent corresponds to $d=3$ and $n=6$.

4.2.2b Thermoelectric power

The absolute thermoelectric power (TEP) of REB_6 compounds as a function of temperature is shown in Fig. 4.18 and Fig. 4.19. The main features of the TEP data of REB_6 are as follows: (i) a minimum in the TEP (S_{\min}) is observed near the lowest temperatures for all the REB_6 measured, (ii) at higher temperatures the TEP of non-magnetic LaB_6 is linear in T and positive, while for REB_6 ($\text{RE}=\text{Pr}, \text{Nd}, \text{Gd}$ and Dy) the TEP is linear in T above T_N but with a negative slope and at higher temperatures the TEP is negative, (iii) at T_N we observe a rapid increase in the TEP for $\text{PrB}_6, \text{NdB}_6$ and GdB_6 , while for DyB_6 there is a gradual change in the slope of S just above T_N , (iv) for PrB_6 there is a small peak at $\sim 3.5\text{K}$ associated with the low-temperature commensurate phase while the low-temperature phase of GdB_6 is

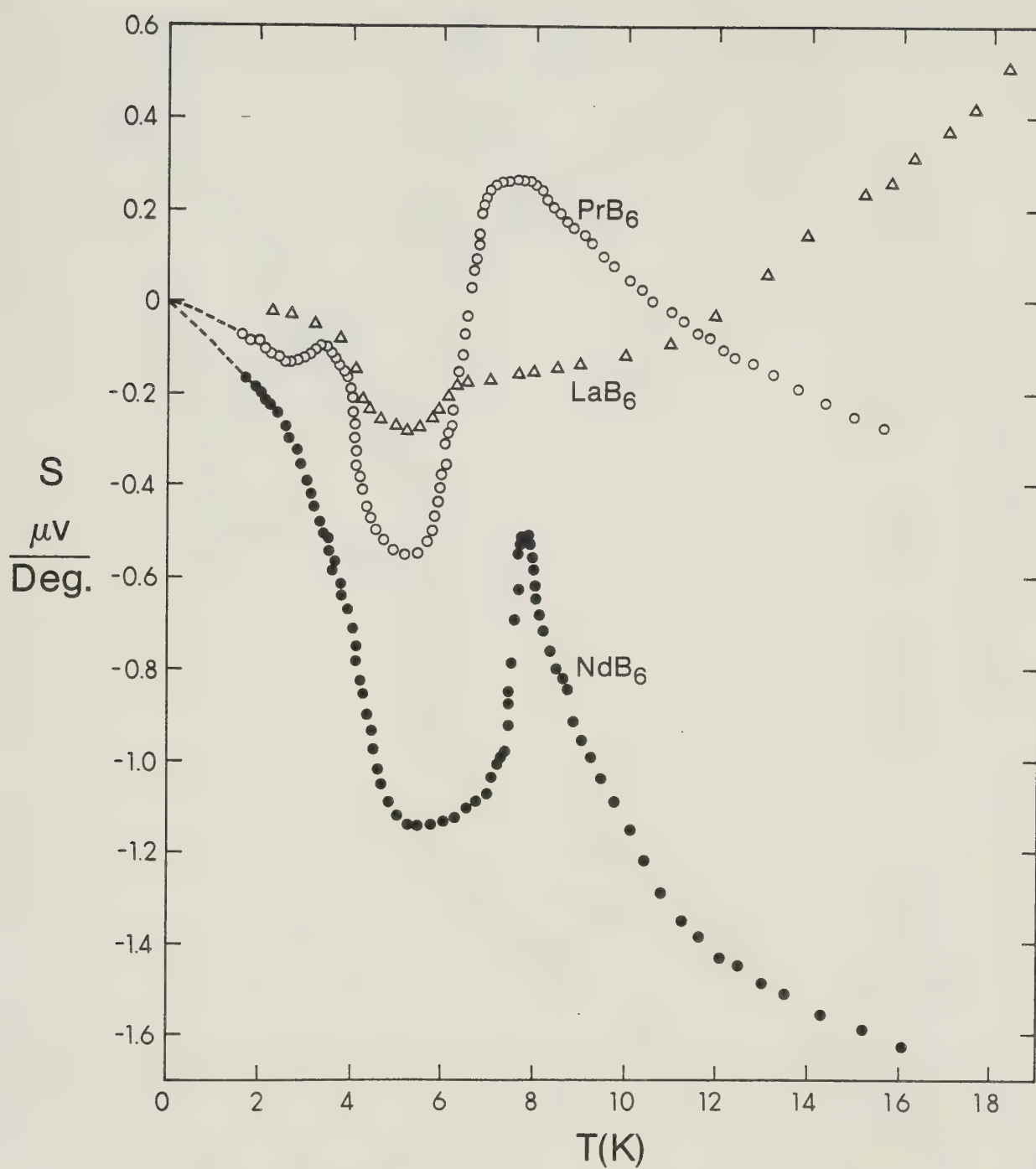


Fig. 4.18 Absolute thermoelectric power (S) of LaB_6 , PrB_6 and NdB_6 as a function of temperature (T).

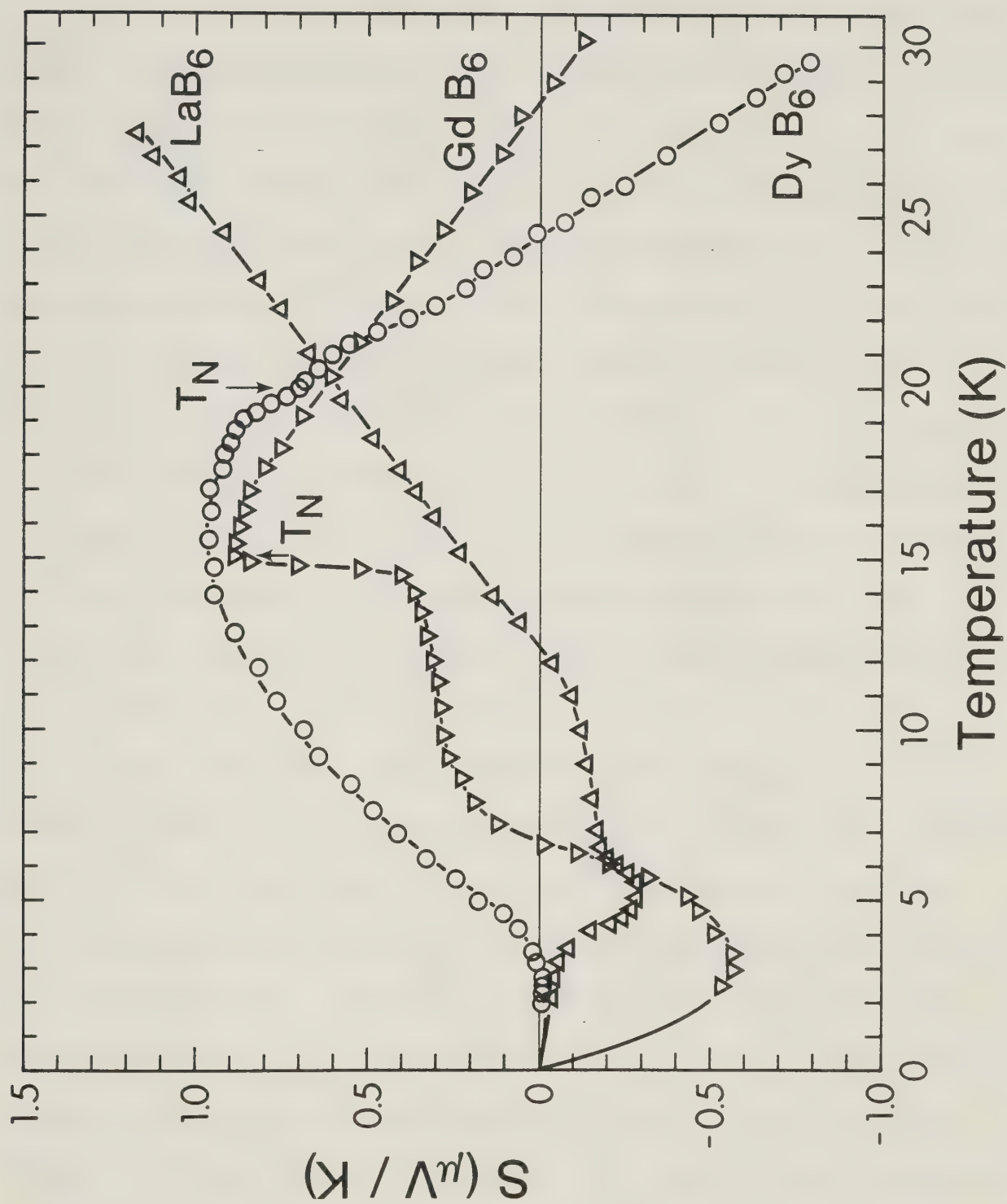


Fig. 4.19 Absolute thermoelectric power (S) of LaB_6 , GdB_6 and DyB_6 as a function of temperature (T).

evidenced by a shoulder in S at $\sim 7\text{K}$ and (v) a broad maximum in S is found for DyB_6 at $\sim 16\text{K}$. The values of S_{\min} and the temperature at which they occur are given in Table 4.6.

We will first discuss the TEP data of non-magnetic LaB_6 . The non-linearity in the TEP below $\sim 10\text{K}$ is thought to be mainly due to phonon drag contribution (S_g) because at low temperatures the linear electron-diffusion term is expected to be very small. Three contributions to the TEP are schematically shown in Fig.4.20, where S_{gN} is the phonon drag contribution due to normal electron-phonon scattering and S_{gU} is due to Umklapp electron-phonon processes and S_e is the electron-diffusion term. At higher temperatures S_g becomes linear in T . These three contributions can qualitatively produce a minimum at lower temperatures and a linear TEP behaviour at higher T as shown schematically in Fig. 4.20.

We note that REB_6 compounds are isostructural and specific heat measurements by Lee, et al (1970) and Westrum, et al (1966) have been interpreted in terms of the non-magnetic lattice specific heat being the same for each at low temperatures. In the case of antiferromagnetic REB_6 compounds for $T < T_N$, in addition to S_g and S_e contributions there is possibly another contribution S_m due to magnon drag. As mentioned in Chapter 2, S_m has the same temperature dependence as S_g . Hence it is believed that the shift in T_{\min} and change in S_{\min} for different REB_6 is due to this additional magnetic contribution S_m to the non-

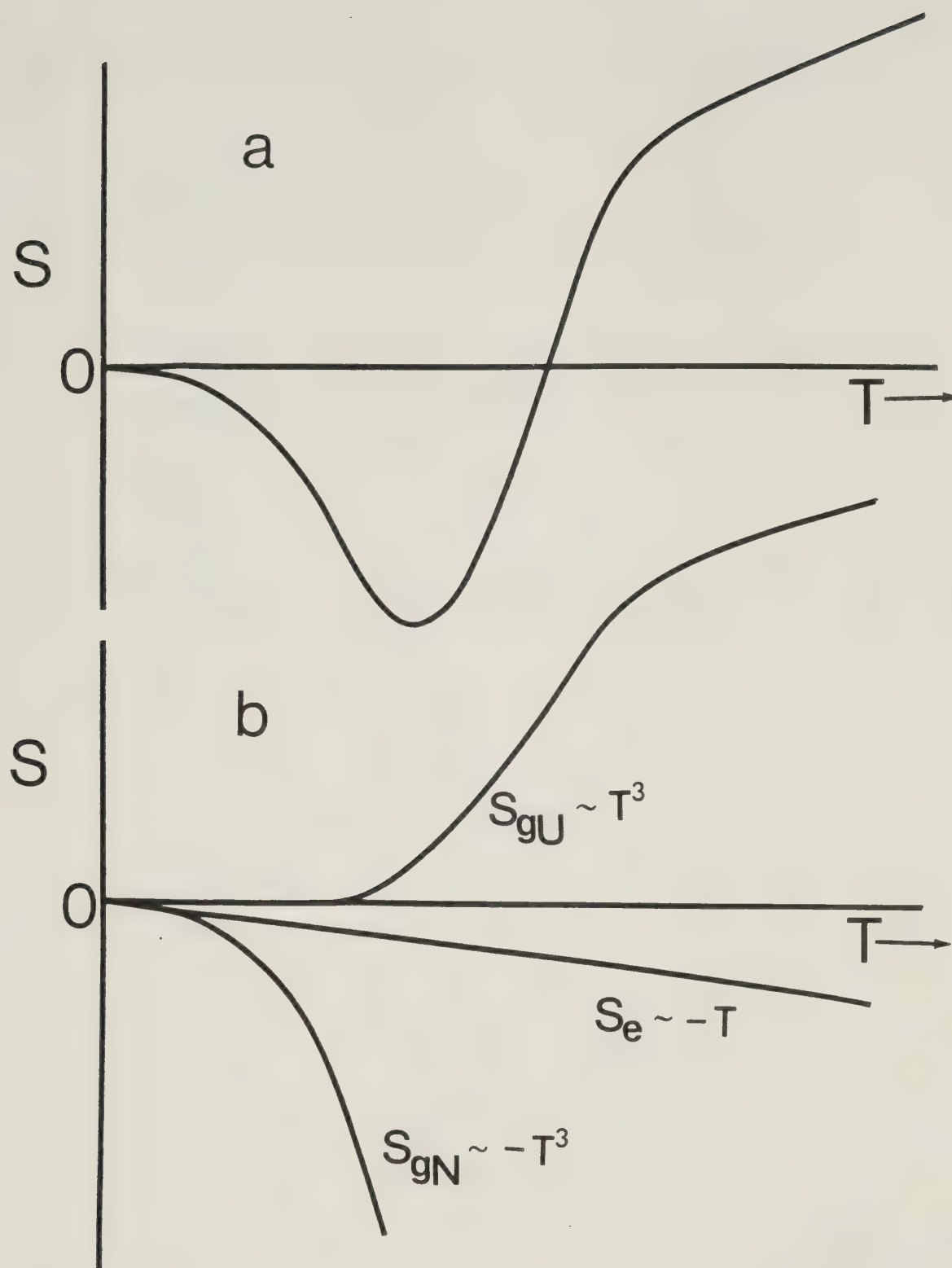


Fig. 4.20 a) Schematic diagram of the resultant thermoelectric power (S) as a function of T .
 b) Schematic diagram of the individual thermoelectric power contributions (S_e , S_{gN} and S_{gU}) as a function of T .

Table 4.6 Values of S_{\min} and T_{\min} of REB_6 compounds.

Sample	$S_{\min} (\mu\text{V/K})$	$T_{\min} (\text{K})$
LaB_6	-0.28	5.5
PrB_6	-0.55	5.7
NdB_6	-1.15	5.9
GdB_6	-0.58	3.1
DyB_6	-0.02	2.5

magnetic contribution $S_g + S_e$. Because of similar temperature dependences it is difficult to isolate each individual contribution.

The broad maximum in the TEP of DyB_6 at $\sim 16\text{K}$ is possibly due to the crystalline-field effects. In the case of a crystal-field split ground state there is an effect on the TEP due to variation in the thermal population of the different crystal-field levels (Peschel and Fulde, 1970; and Sierro et al, 1975). Umlauf et al (1973) have demonstrated that these effects show up in the TEP but not necessarily in the resistivity. Takayama and Fulde (1975) have shown that for two singlet levels separated by an energy Δ the TEP has a maximum at $T \approx \Delta/2$. According to them the broadness of the maximum is due to interaction between the magnetic ions via the conduction electrons. We suspect that the broad peak at $\sim 16\text{K}$ in DyB_6 is due to crystal-field effects.

The TEP contribution due to the random magnetic moments of RE ions in REB_6 compounds for $T \gg T_N$ is called the spin-disorder TEP (S_{spd}). Because of lack of any theoretical calculation of S_{spd} one is forced to estimate S_{spd} from a phenomenological approach. As discussed in Chapter 2, one can write,

$$S_{\text{spd}} = (S^{\text{m}} - S^{\text{nm}}) \frac{\rho}{\rho_{\text{spd}}} , \quad (4.10)$$

where in our case S^{m} is the TEP of magnetic REB_6 ($\text{RE} = \text{Pr}, \text{Nd}, \text{Gd}$ and Dy) and S^{nm} is the TEP of LaB_6 . The ratio

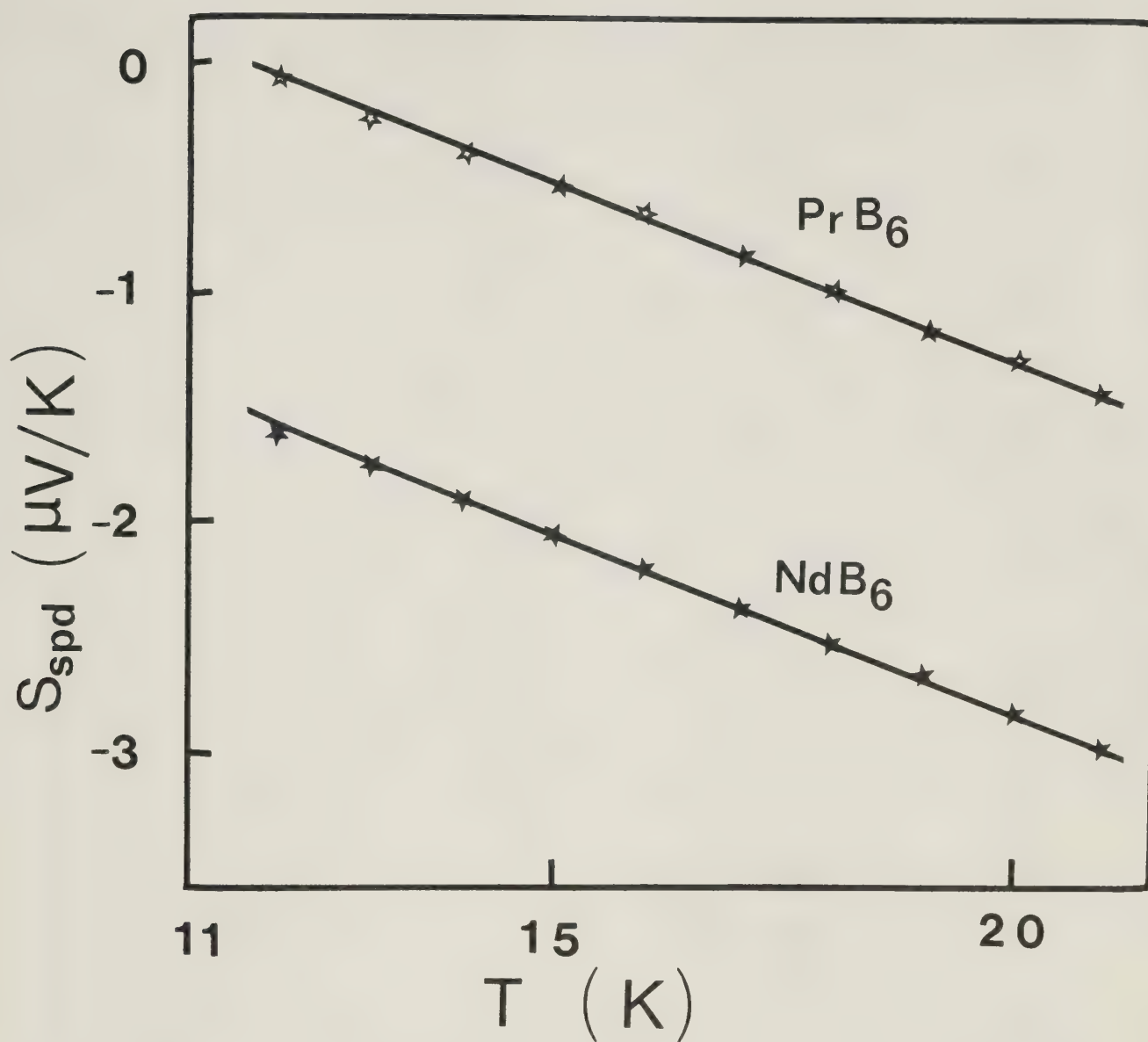


Fig. 4.21 The spin disorder thermoelectric power (S_{spd}) of PrB_6 and NdB_6 as a function of T .

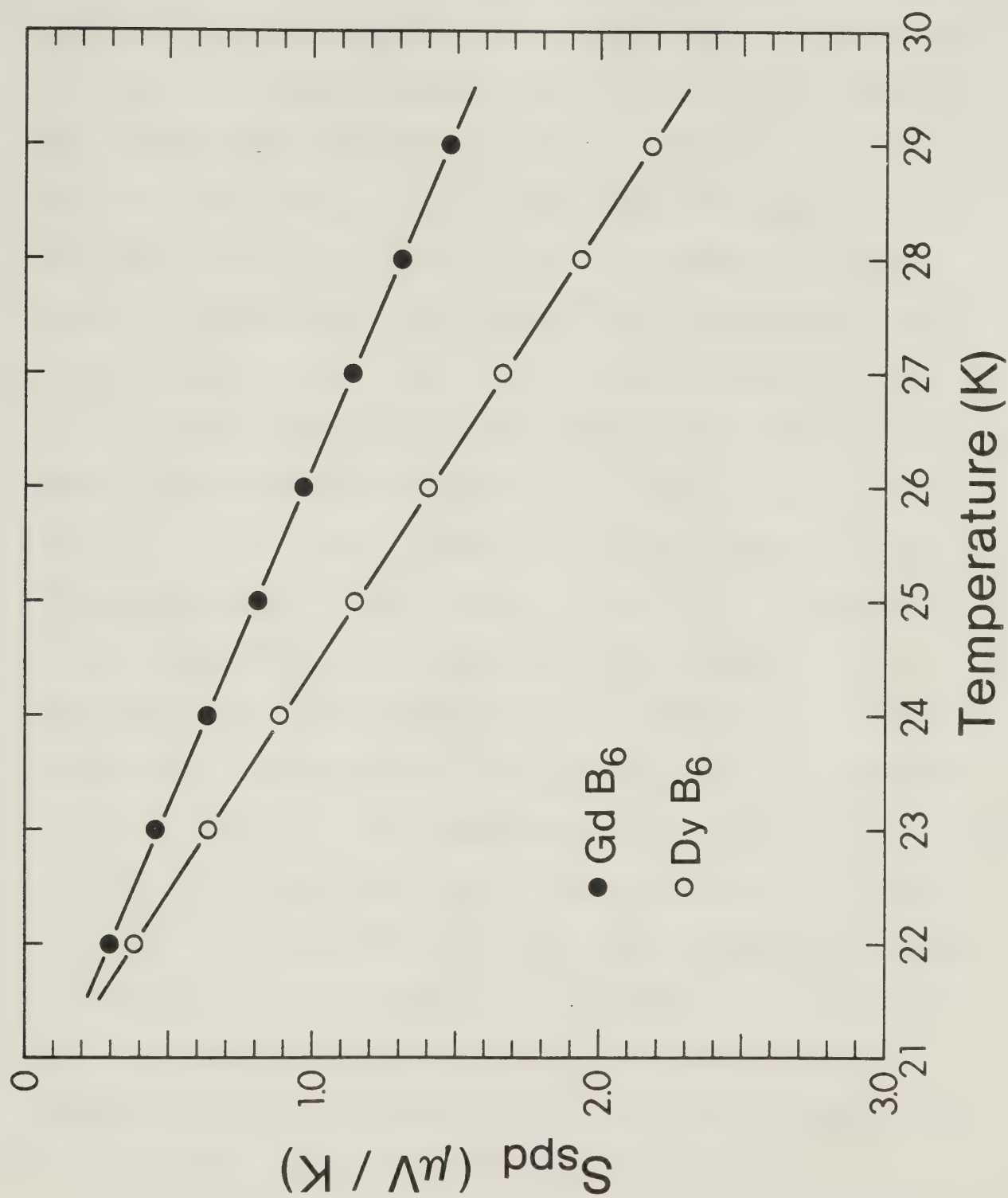


Fig. 4.22 The spin disorder thermoelectric power (S_{spd}) of Gd B_6 and Dy B_6 as a function of T .

ρ/ρ_{spd} is equal to R_x/R_{spd} where R_x is the sample resistance at temperature T and $R_{\text{spd}} = R(T_N) - R_0$. Here $R(T_N)$ is the resistance at T_N and R_0 is the residual resistance found by extrapolating the resistance data to zero temperature. The estimated S_{spd} as a function of temperature for antiferromagnetic REB_6 is shown in Fig. 4.21 and Fig. 4.22 for $T > T_N$. It is clear that the S_{spd} is negative and linear in T for all four hexaborides. This result is consistent with the earlier findings of Gratz and Zuckermann (1982) for GdAl_2 , GdNi and GdCu_2 .

The TEP shows the phase transition from antiferromagnetic to paramagnetic phase as a sharp increase in S near T_N . In the case of DyB_6 this phase transition is not as sharp because of the masking effect of the anomalous TEP due to crystal-field effects. According to the theoretical investigations cited in Chapter 2, the TEP in the critical regime should show a divergence in $dS/dT = S'$ at T_N as in dr/dT . The temperature derivative of S in the vicinity of T_N was obtained by first fitting the experimental data to a smooth curve and then finding the slope of the smooth curve around T_N . In Figs. 4.23, 4.24 and 4.25 we have shown $r' = dr/dT$ and $S' = dS/dT$ in the neighbourhood of T_N for PrB_6 , NdB_6 and GdB_6 respectively. We do observe a peak in S' at T_N as in r' .

To test that the S' and r' are directly proportional and have the same critical behaviour (Ausloos, 1977a, 1978; and Helman and Balberg, 1978), we have plotted S' vs r'

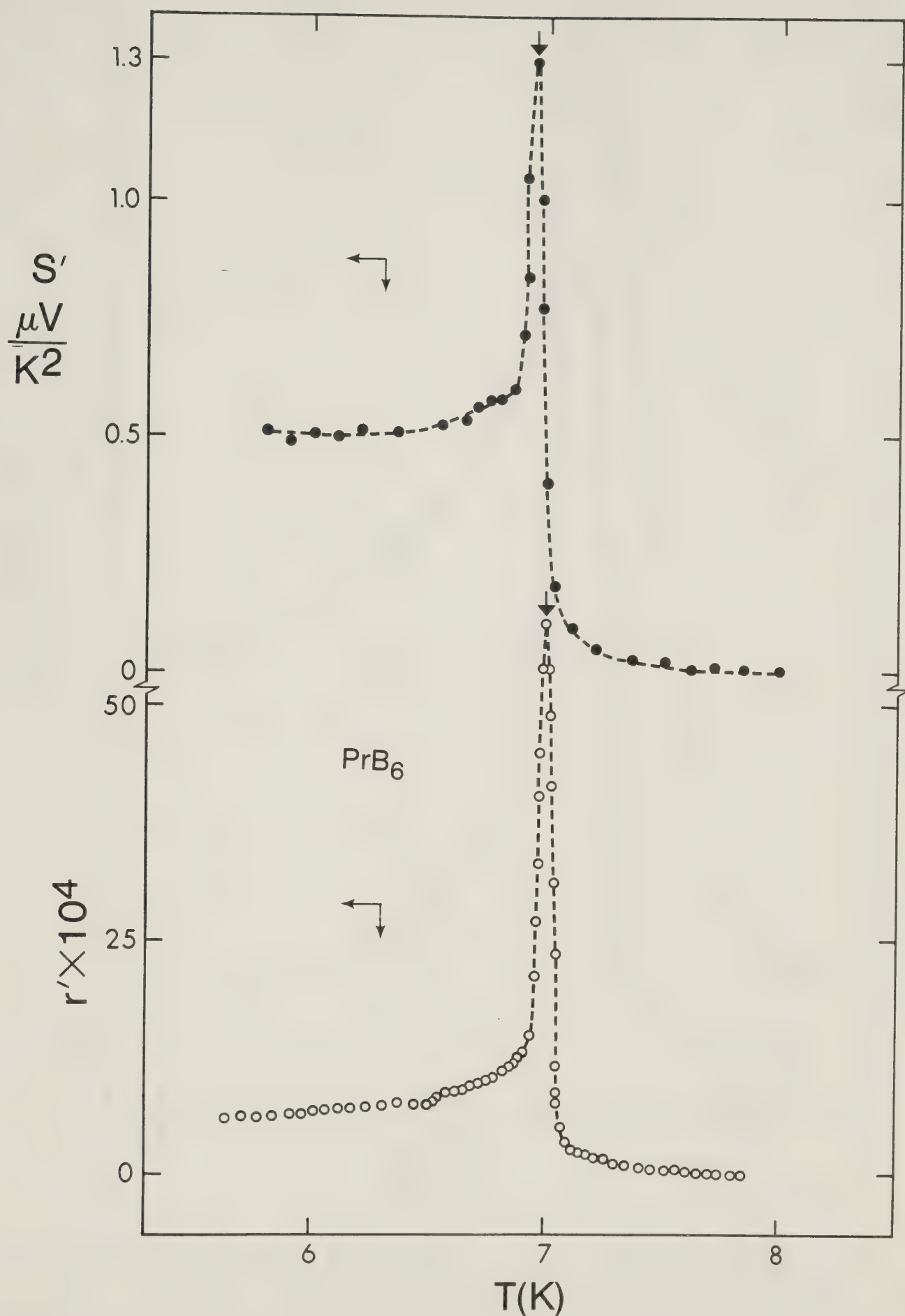


Fig. 4.23 The temperature derivative of the resistance (r') and the thermoelectric power (S') as a function of T for PrB_6 in the vicinity of T_N .

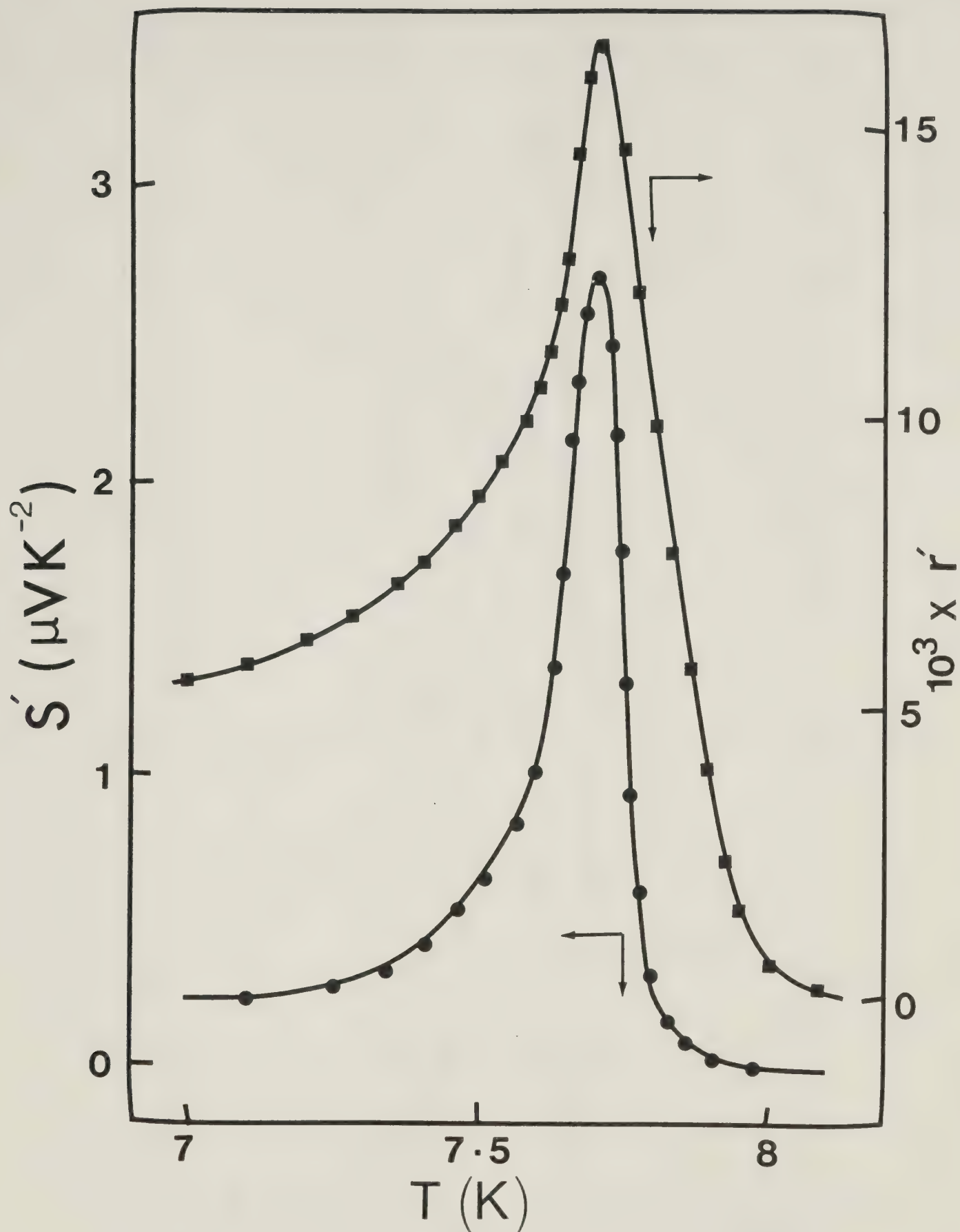


Fig. 4.24 The temperature derivative of the resistance (r') and the thermoelectric power (S') as a function of T for NdB_6 in the vicinity of T_N .

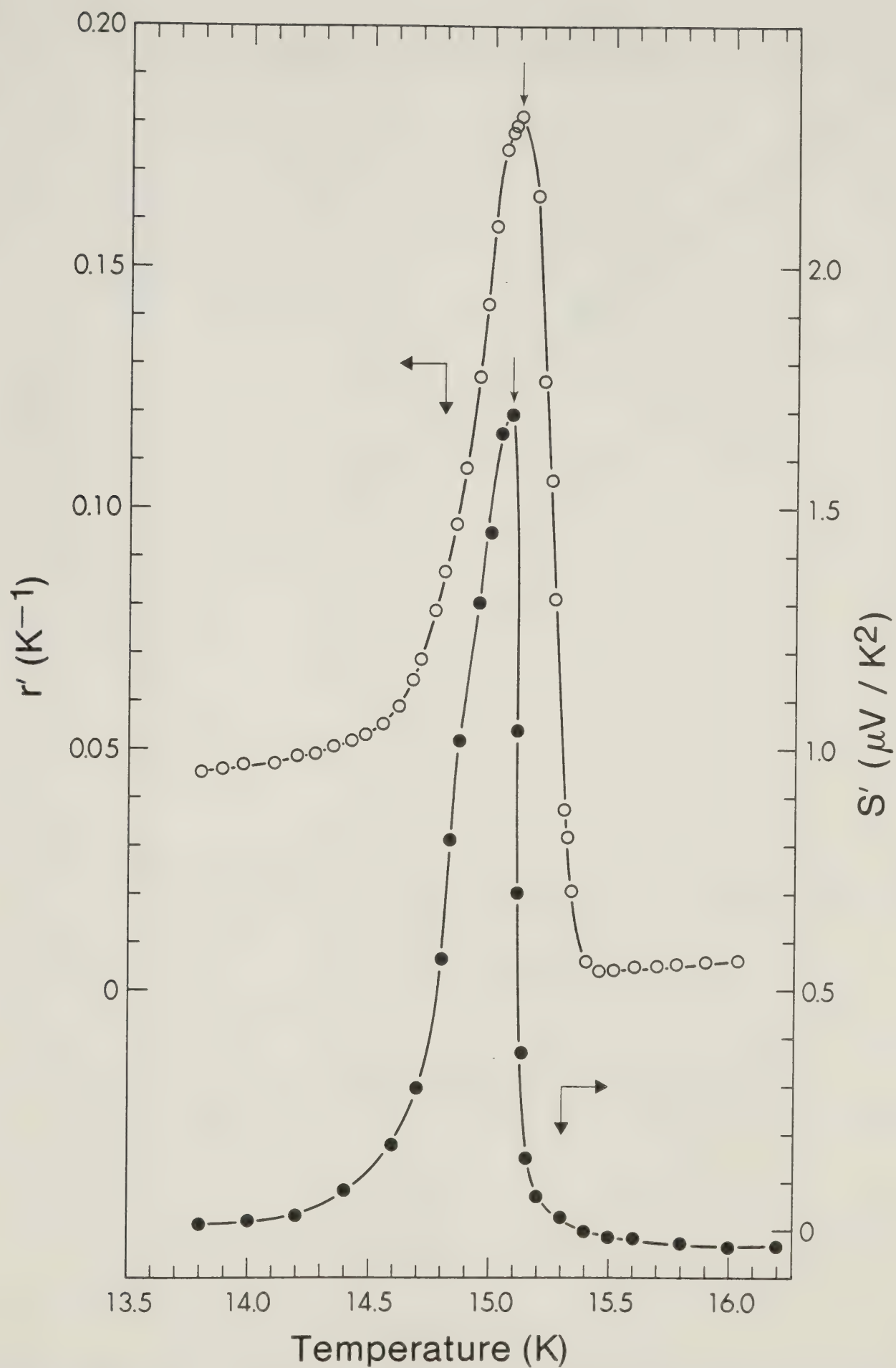


Fig. 4.25 The temperature derivative of the resistance (r') and the thermoelectric power (S') as a function of T for GdB_6 in the vicinity of T_N .

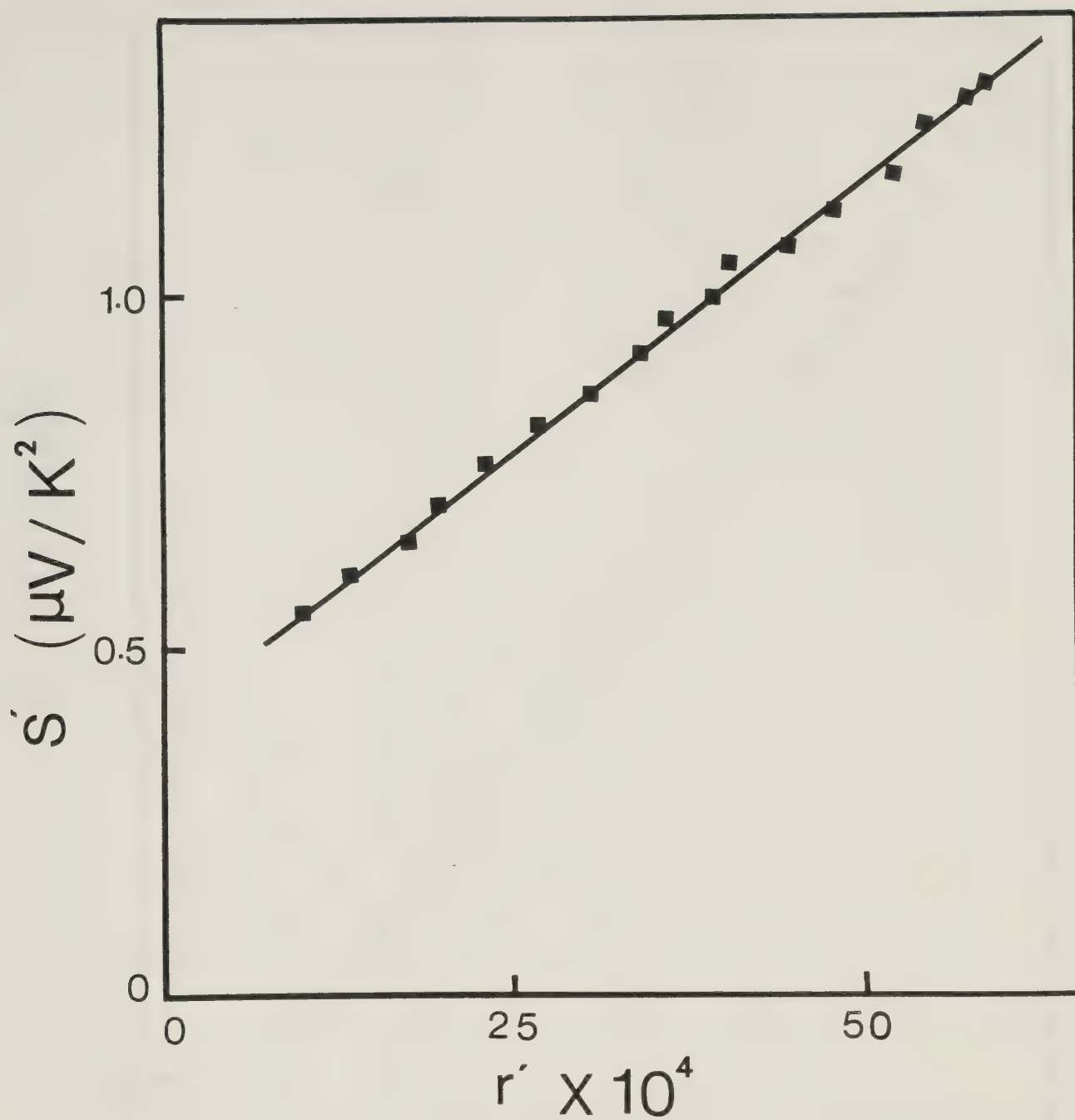


Fig. 4.26 In the vicinity of T_N , experiment shows a linear relation between $S' = dS/dT$ and $r' = dr/dT$ for PrB_6 .

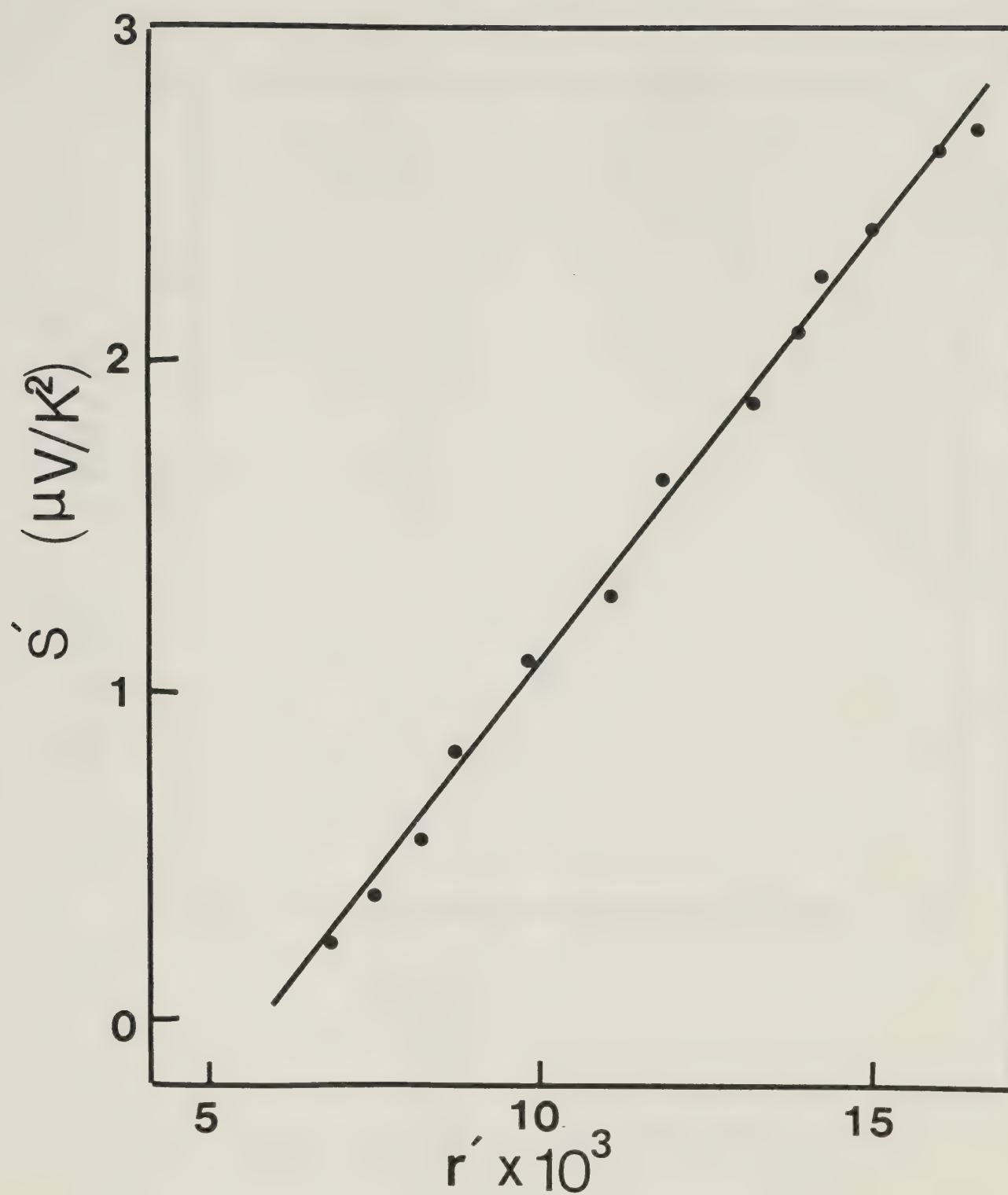


Fig. 4.27 In the vicinity of T_N , experiment shows a linear relation between $S' = dS/dT$ and $r' = dr/dT$ for NdB_6 .

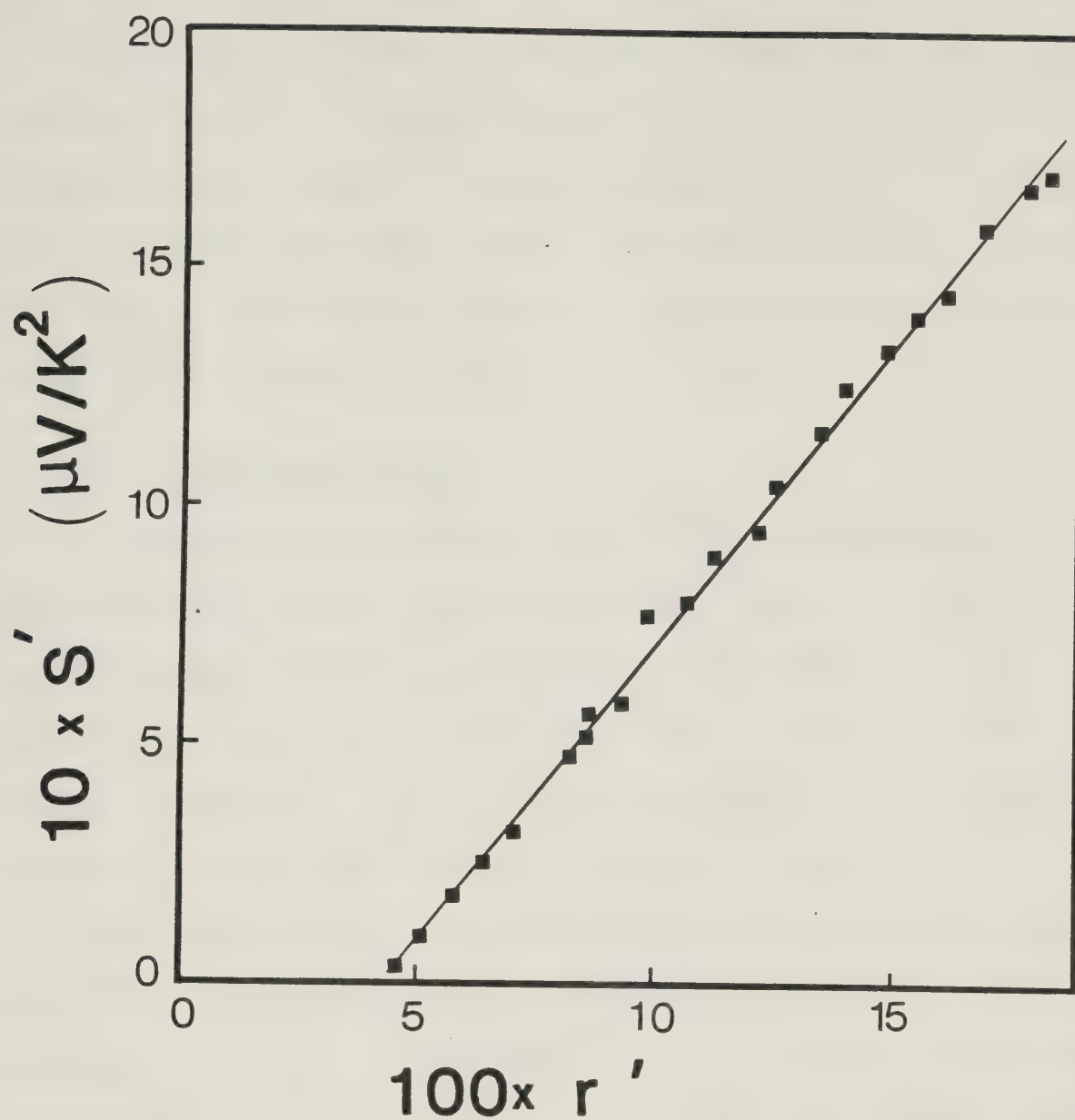


Fig. 4.28 In the vicinity of T_N , experiment shows a linear relation between $S' = dS/dT$ and $r' = dr/dT$ for GdB_6 .

(Figs. 4.26-4.28) for temperatures very close to T_N and we find that for antiferromagnetic REB_6 compounds r' and S' are linearly related as has been found for some ferromagnetic metals. We have found that the temperature dependence of r' and S' are the same which is in complete agreement with the theoretical prediction that all transport coefficients should have the same temperature dependence in the vicinity of T_N .

4.2.2c Magnetoresistance

The magnetoresistance (MR) of antiferromagnetic REB_6 compounds shows very interesting results. The isothermal longitudinal magnetoresistances (LMR) for PrB_6 , NdB_6 , GdB_6 and DyB_6 are shown in Figs. 4.29-4.32. The common features of the MR data of antiferromagnetic REB_6 compounds are as follows: (i) The MR is positive and increases with increasing external field (H) for $T < T_N$, (ii) the MR decreases with increasing temperature at a constant field for $T < T_N$, and (iii) at T_N the MR drops very rapidly and for $T > T_N$ changes very much more slowly. The temperature dependence of the MR for constant fields (H) is shown in Figs. 4.33-4.36. Similar temperature dependence of the MR of the antiferromagnetic compound, $GdRh_{1.07}Sn_{4.21}$, has been observed by Ali et al (1984).

In the absence of a theory for the antiferromagnetic metals with rare earth ions, a quantitative comparison with theory is not possible, but the ideas of Yamada and

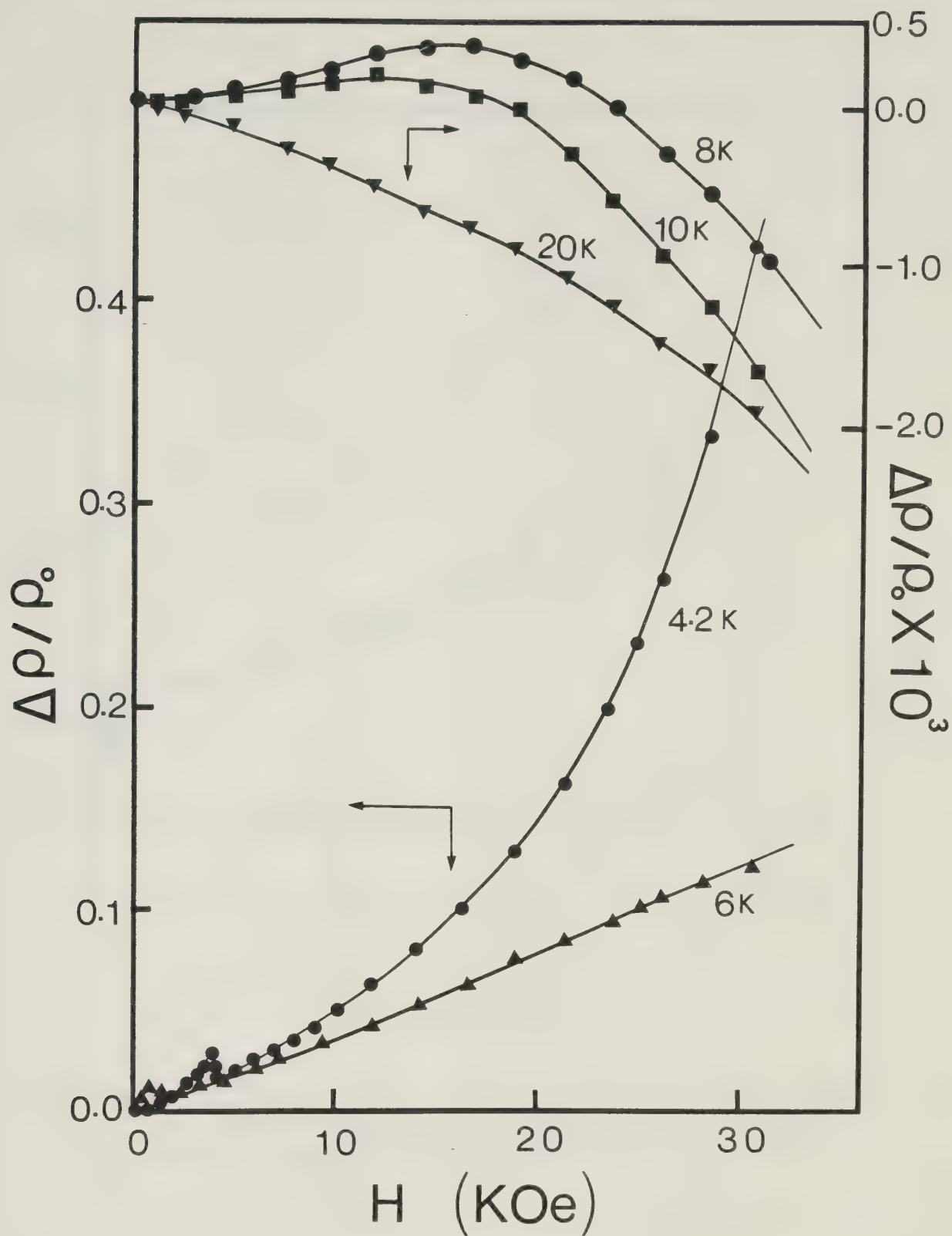


Fig. 4.29 The longitudinal isothermal magnetoresistance ($\Delta\rho/\rho_0$) as a function of external field (H) at various temperatures for PrB_6 .

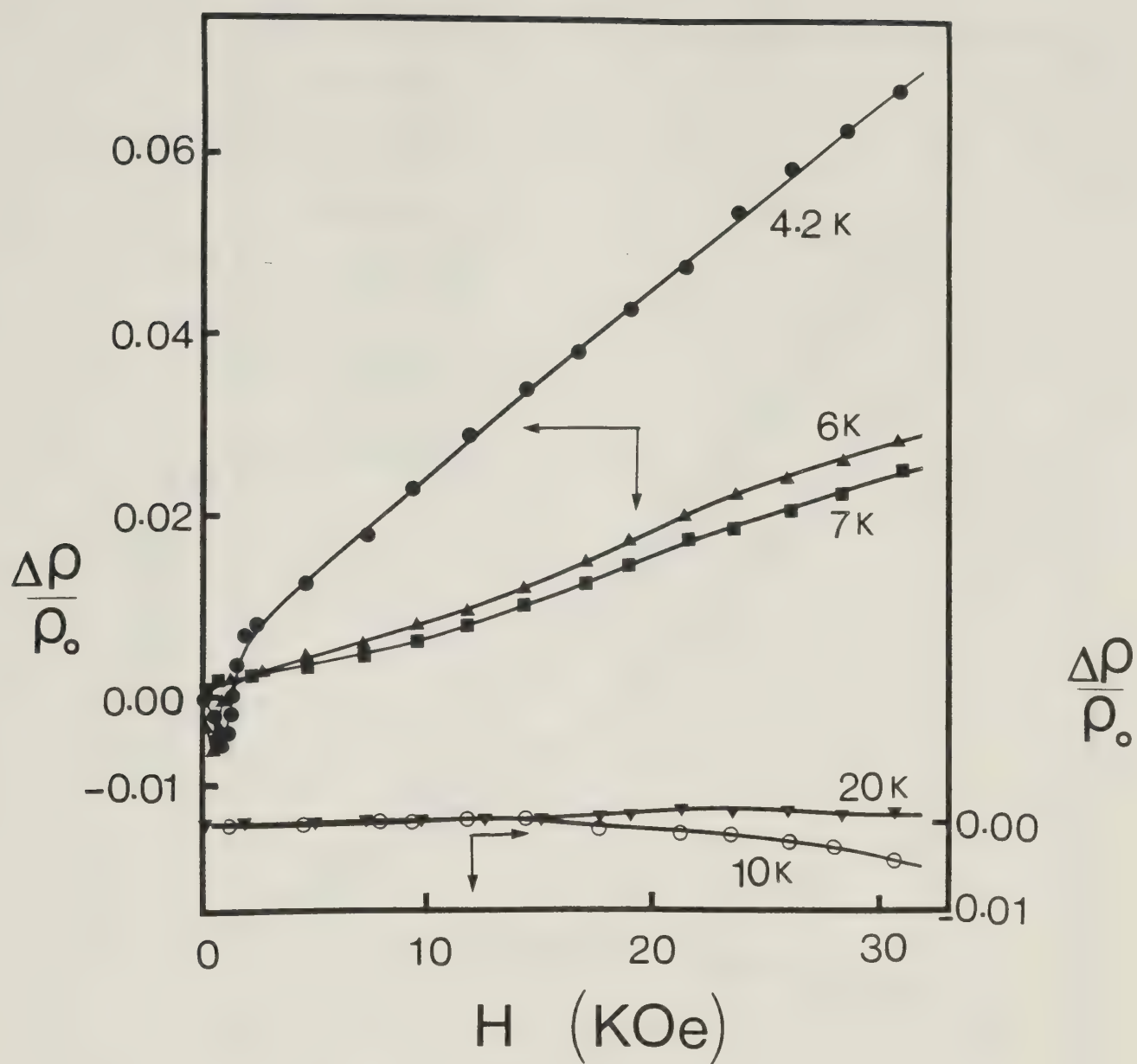


Fig. 4.30 The longitudinal isothermal magnetoresistance ($\Delta\rho/\rho_0$) as a function of external field (H) at various temperatures for NdB_6 .

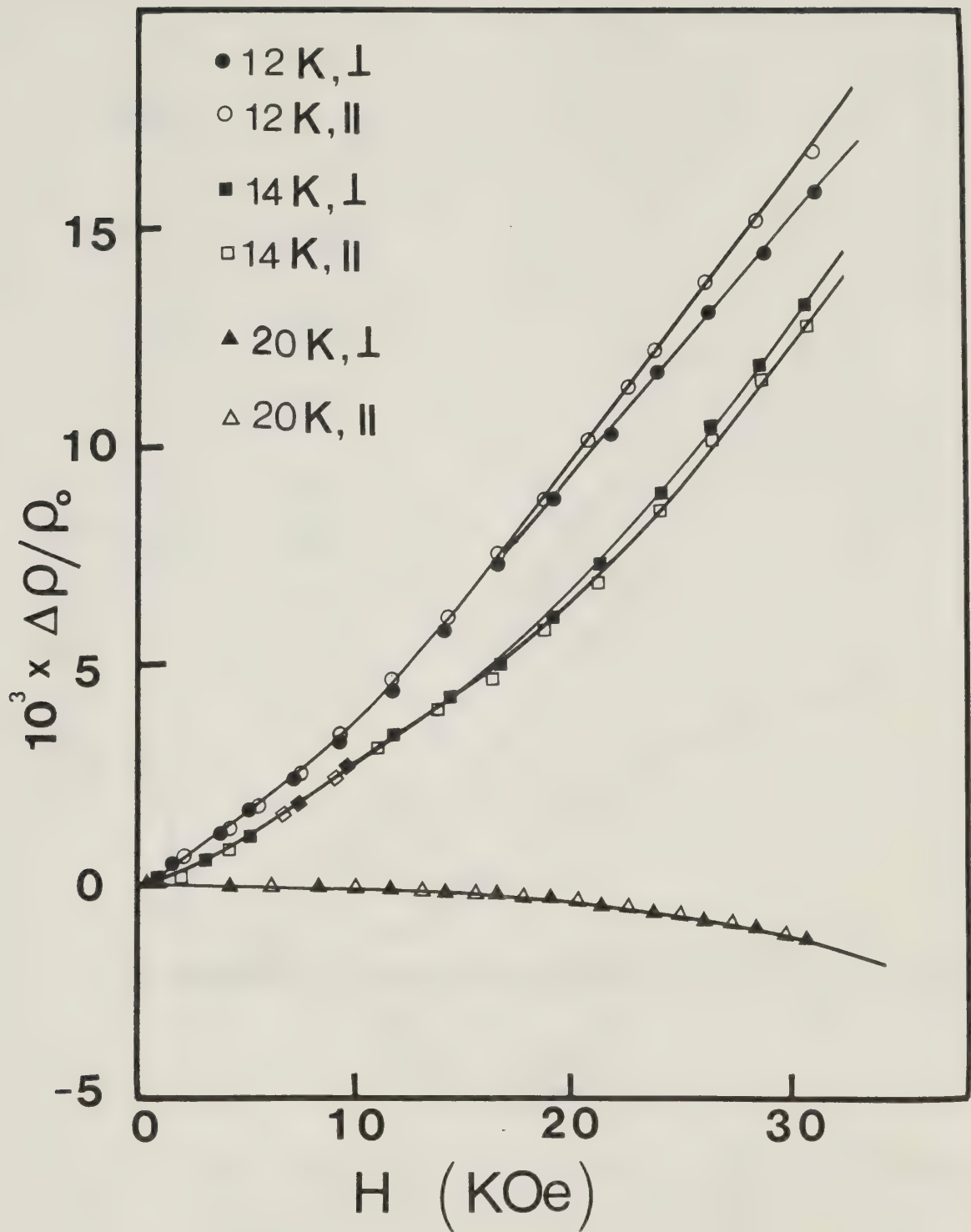


Fig. 4.31 The longitudinal isothermal magnetoresistance ($\Delta\rho/\rho_0$) as a function of external field (H) for various temperatures for GdB_6 .

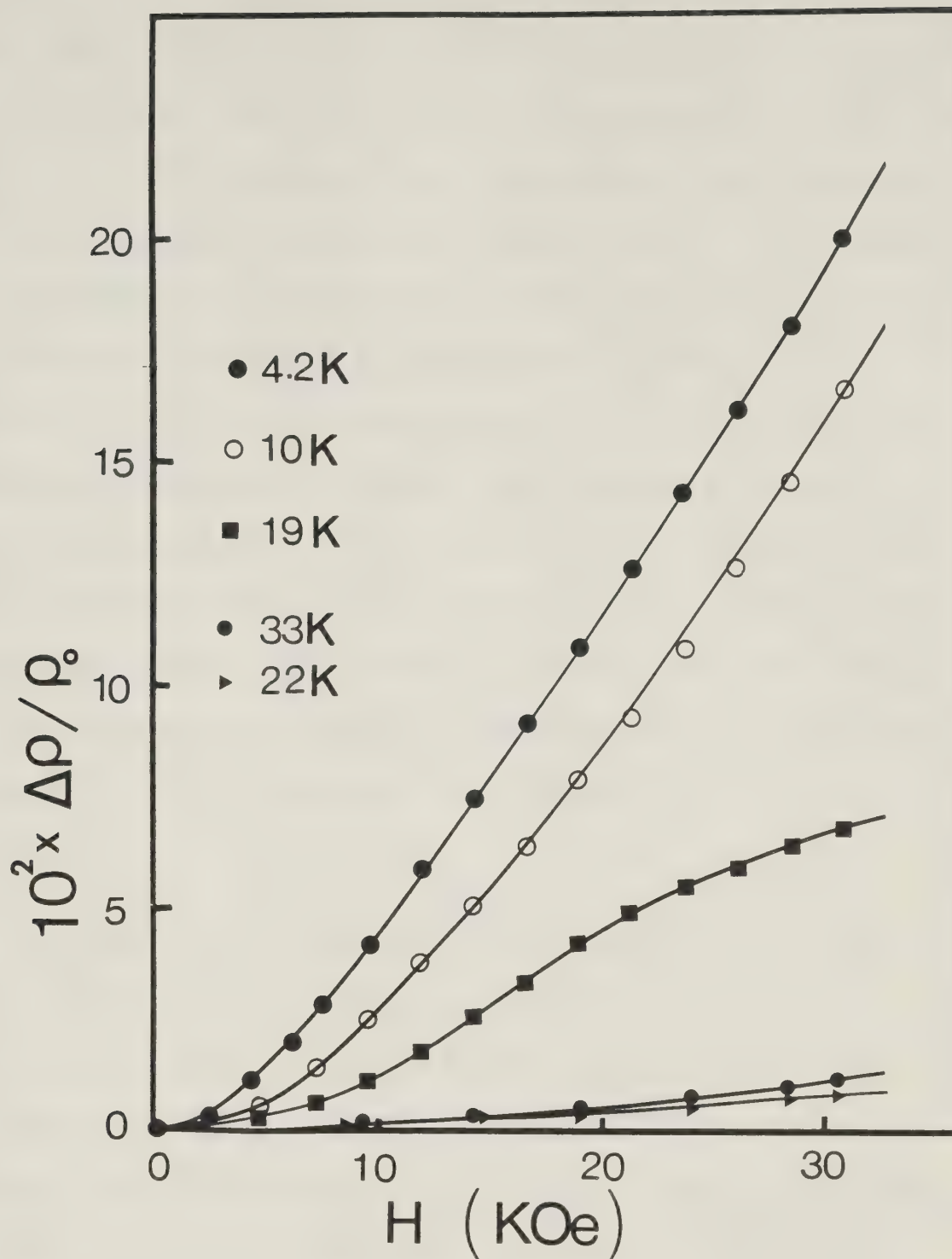


Fig. 4.32 The longitudinal isothermal magnetoresistance ($\Delta\rho/\rho_0$) as a function of external field (H) at various temperatures for DyB_6 .

Takada (1973, 1973a) may be used to qualitatively account for the MR data. The MR of the antiferromagnetic REB_6 metals for $T < T_N$ increases with increasing field because of a field-induced increase in the spin fluctuations, which is in contrast to a suppression of the spin fluctuations in an external field for a ferromagnetic metal. The decrease in the MR with increasing T for $T < T_N$ is due to the relative suppression of the spin fluctuations in a magnetic field, that is, in a fixed field ρ changes less for a given temperature change than it does in zero field for the same temperature change. The MR field and temperature dependences and details of the experimental data are discussed for each hexaboride as follows.

PrB_6

The MR data in Fig. 4.29 for single crystal PrB_6 shows a peak at $H_{c1} = 4\text{KOe}$ and 1KOe for $T = 4.2\text{K}$ and 6K respectively. This peak is thought to be due to a spin flop transition (H_{c1}) which decreases with increasing temperature. The polycrystalline samples of PrB_6 do not show this peak. At $T > T_N$ the MR becomes negative at higher field as would be expected for paramagnetic metals due to field-induced alignment of the magnetic moments. The temperature dependence of the MR shown in Fig. 4.33 is found to be T^{-2} for temperature $T < T_N$. It was possible to fit the experimental data to the expression

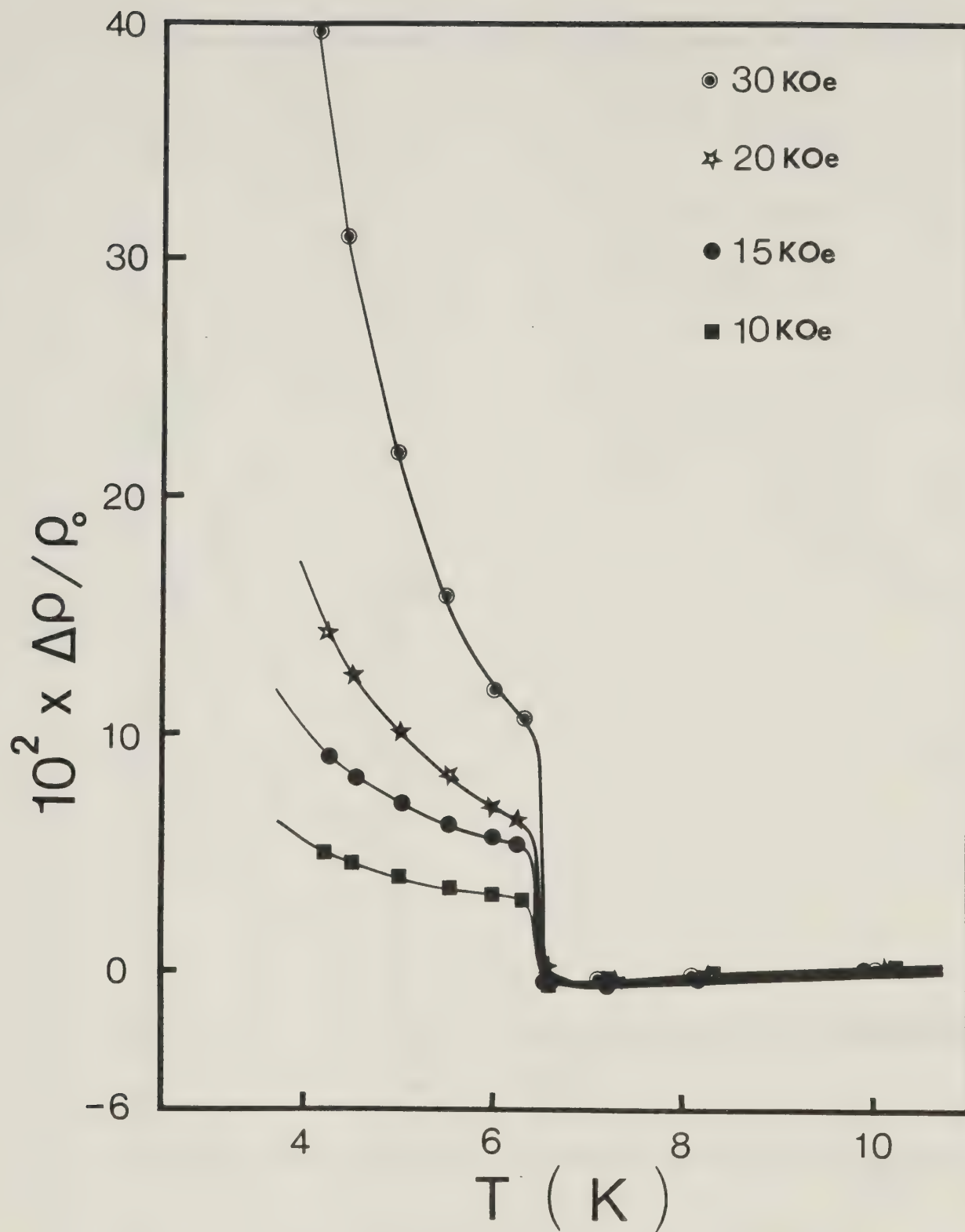


Fig. 4.33 The longitudinal isofield magnetoresistance ($\Delta\rho/\rho_0$) as a function of temperature (T) at various fields for PrB_6 .

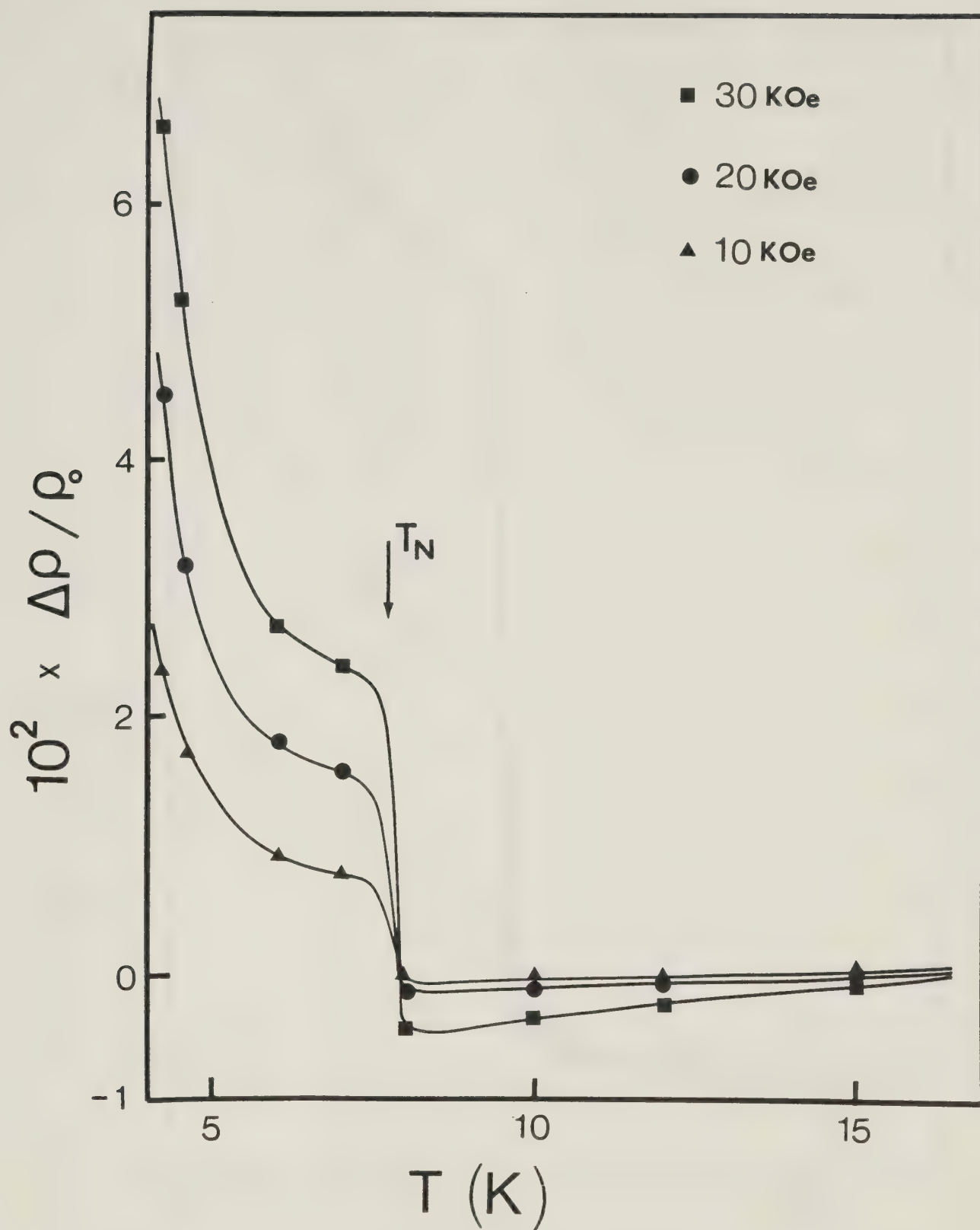


Fig. 4.34 The longitudinal isofield magnetoresistance ($\Delta\rho/\rho_0$) as a function of temperature (T) at various fields for NdB_6 .

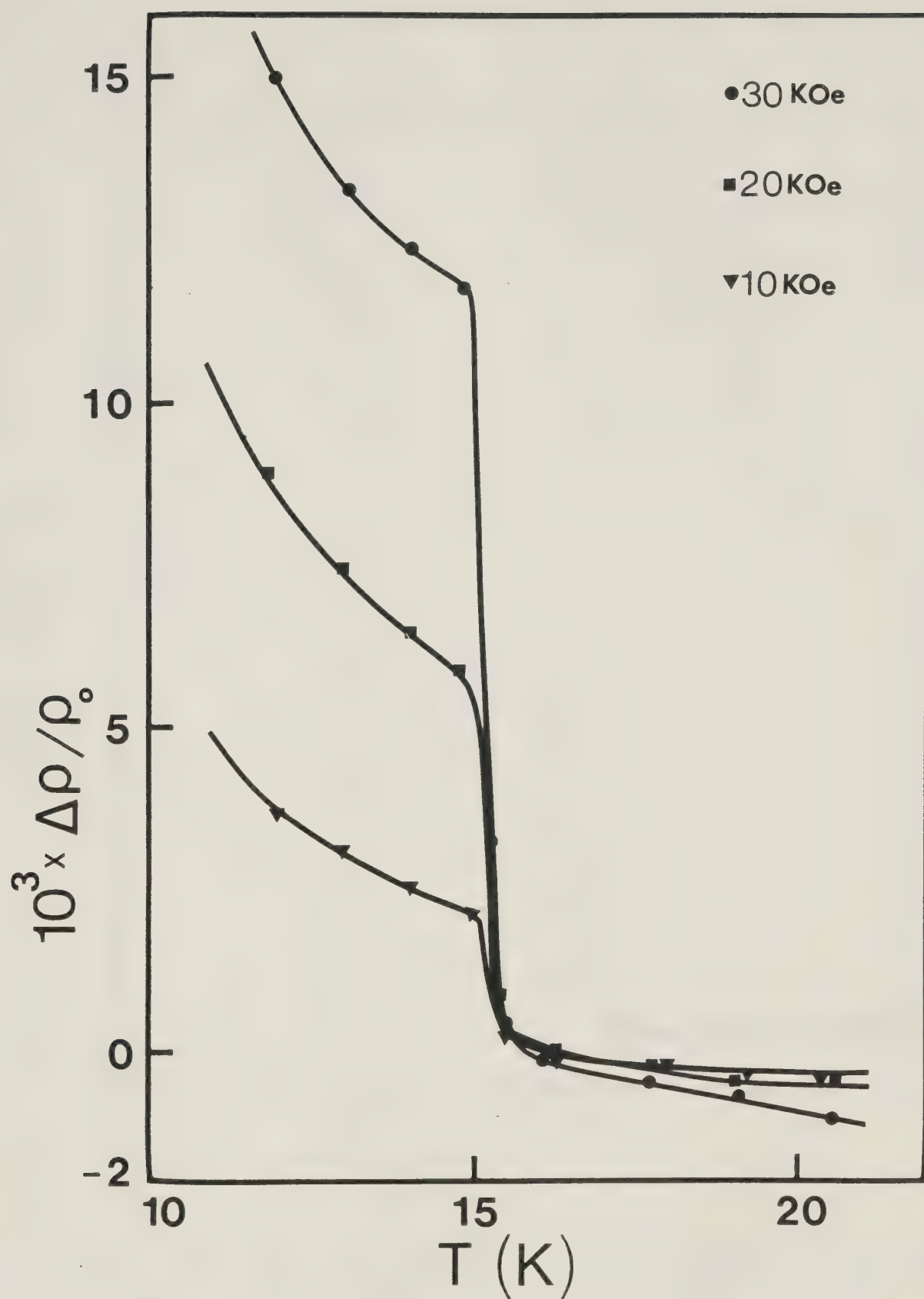


Fig. 4.35 The longitudinal isofield magnetoresistance ($\Delta\rho/\rho_0$) as a function of temperature (T) at various fields for GdB_6 .

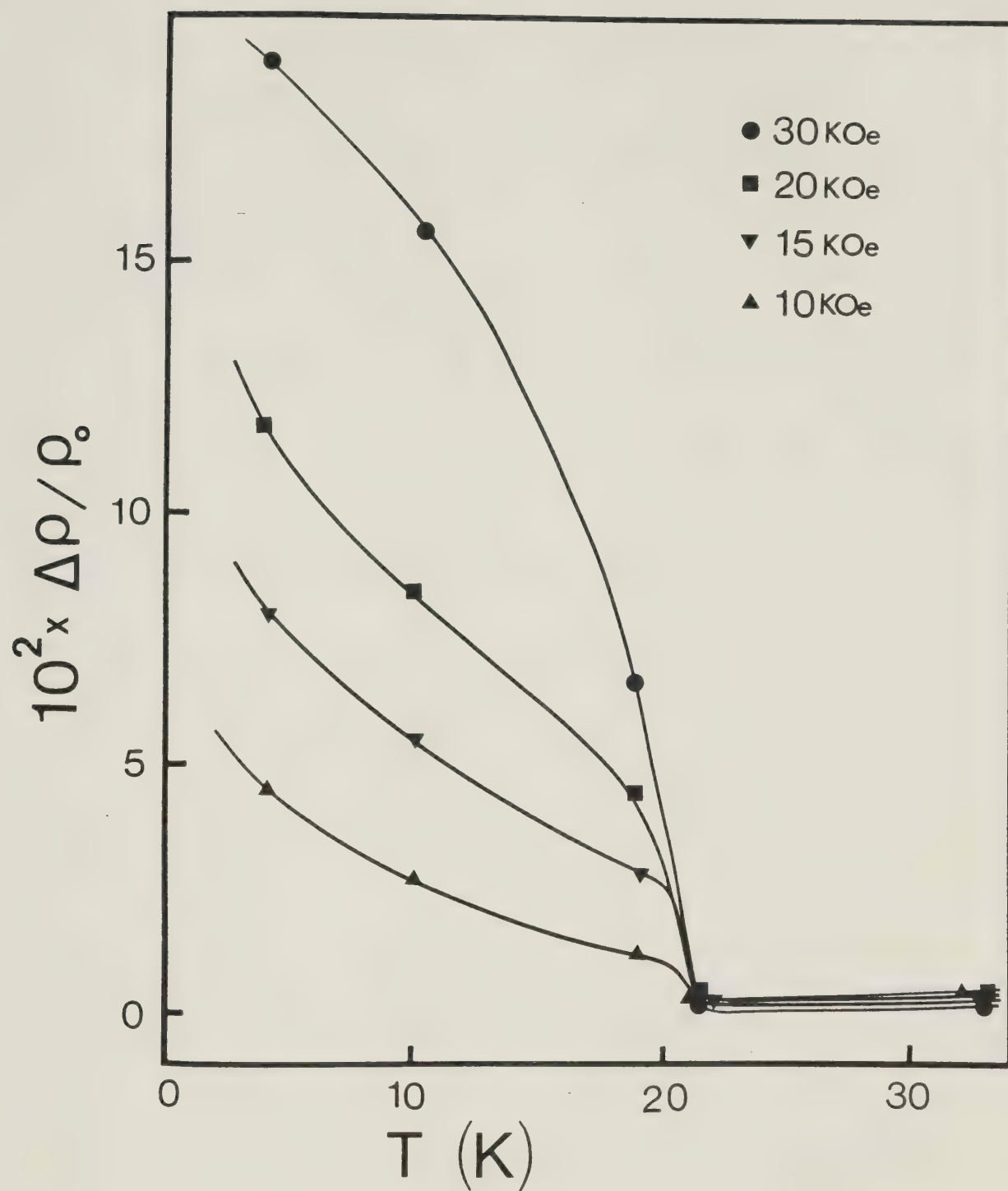


Fig. 4.36 The longitudinal isofield magnetoresistance ($\Delta\rho/\rho_0$) as a function of temperature (T) at various fields for DyB_6 .

Table 4.7 Experimental value of the parameter A for PrB_6 for various fields.

$H(\text{KOe})$	$A(\text{K}^2)$	A/H^2
10	6.2	6.2×10^{-3}
15	2.45	6.0×10^{-3}
20	2.63	6.1×10^{-3}
25	4.63	7.4×10^{-3}
30	9.0	10×10^{-3}

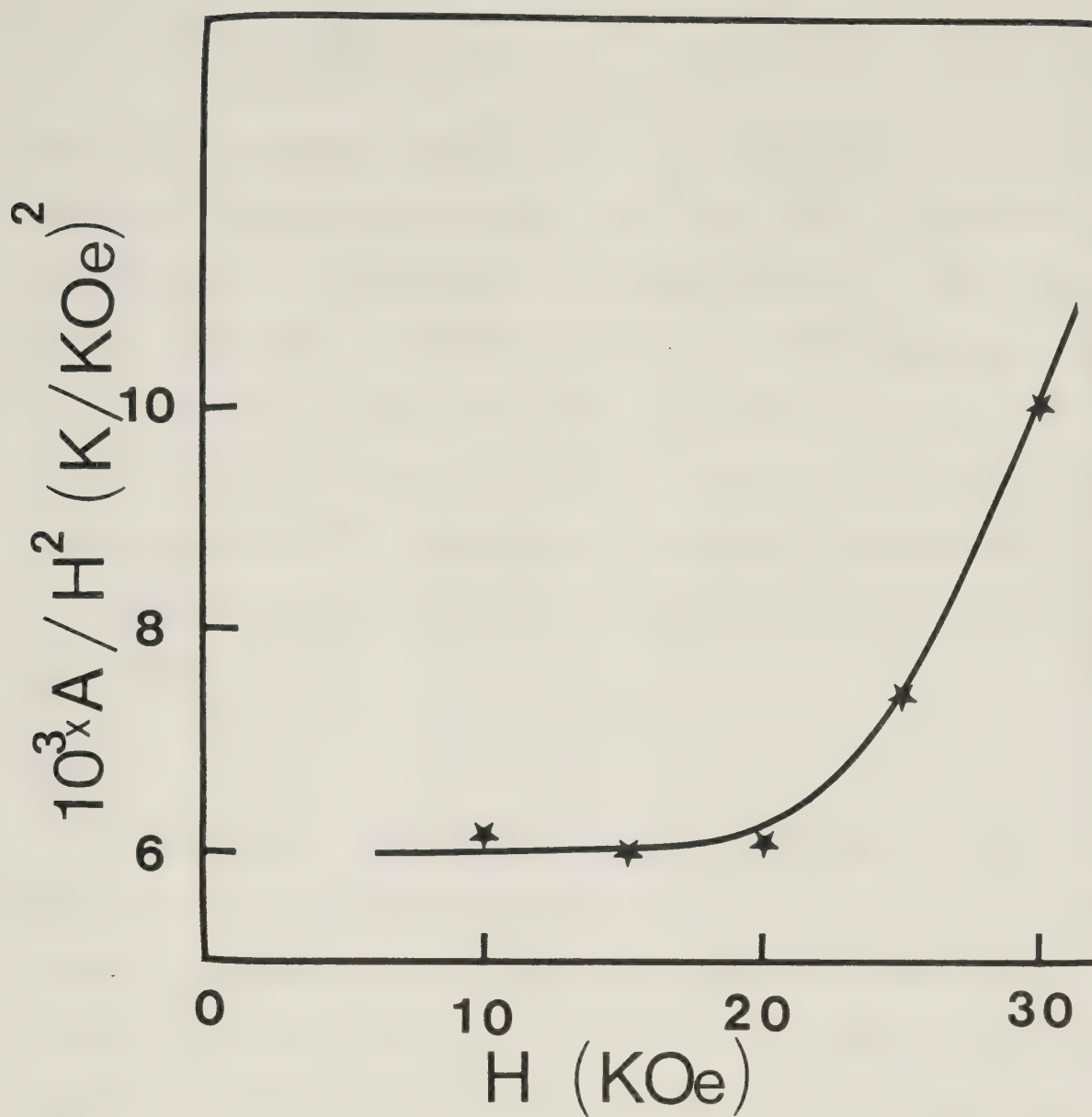


Fig. 4.37 The field dependence of the parameter A/H^2 for PrB_6 .

$$\frac{\Delta\rho}{\rho_0} = \frac{A(H)}{T^2} \quad , \quad (4.11)$$

where the parameter $A(H)$ is found to be proportional to H^{-2} as expected from the isothermal MR (Fig. 4.29). We have found that for $H < 20\text{Koe}$, A remains constant. The values of $A(H)$ and AH^{-2} are given in Table 4.7 for various values of H . Fig. 4.37 shows the field dependence of the parameter A . The increase in A for $H > 20\text{Koe}$ is possibly due to the anisotropic conduction-f-electron interaction, to be discussed along with the transverse magnetoresistance data (TMR).

NdB₆

At higher fields the MR data of single crystal NdB_6 show a linear field dependence for $T < T_N$ (Fig. 4.30) and become negative for $T > T_N$. At very low fields the MR shows a negative peak for $T < T_N$ which vanishes above 7K, whereas no such peak is observed in a polycrystalline sample. It is possible that this negative peak is due to domain alignments. As H increases from zero the domains start aligning with a consequent decrease in the resistance. At the negative peak all domains are expected to have aligned into one single domain and above that field the MR increases as the spin fluctuation increase due to field dominates.

The temperature dependence of MR shown in Fig. 4.34 for various fields is found to be of the form,

Table 4.8 Experimentally determined value of A for
NdB₆ at various fields

H (KOe)	A (K ²)	A/H
10	0.85	0.043
20	0.50	0.049
30	1.15	0.038

Table 4.9 Experimental value of A for GdB₆ at two
temperatures

T (K)	A (KOe ⁻²)	A × T ²
12	1.3×10^{-5}	2.5×10^{-3}
14	1.9×10^{-5}	2.7×10^{-3}

$$\frac{\Delta\rho}{\rho_0} = \frac{A(H)}{T^2} , \quad (4.12)$$

where $A(H)$ is found to be linearly dependent on H as expected from the data in Fig. 4.30. The values of A and A/H found from the data are given in Table 4.8 for various fields and it is seen that A/H is a constant in the field range covered in this study.

GdB₆

The MR of GdB₆ below 11K is complicated because of the lower temperature phase. The behaviour of the MR below 11K will be discussed separately. However, the MR above 12K is very similar to that of other antiferromagnetic REB₆. The field dependence and the temperature dependence of the MR are shown in Fig. 4.31 and Fig. 4.35 respectively. Below T_N the MR has a H^2 dependence and can be expressed as

$$\frac{\Delta\rho}{\rho_0} = A(T) H^2 , \quad (4.13)$$

where $A(T)$ is temperature dependent and the value of $A(T)$ is given in Table 4.9.

The MR of GdB₆ is almost the same for longitudinal and transverse fields as shown in Fig. 4.31, where a very small anisotropy is visible, whereas the MR for $T > T_N$ is negative and is exactly the same for longitudinal and transverse fields. The negative MR for $T > T_N$ is expected in the paramagnetic state due to field-induced alignments of the magnetic moments. In the absence of any crystalline

electric field because Gd^{3+} has $L = 0$ (L = total orbital angular momentum) and is in an S state the anisotropic conduction electron-f-electron interaction is expected to be zero (as discussed in Chapter 2). The anisotropy in TMR and LMR is found to be zero for GdB_6 as expected according to eqn. (4.16) for an S ion (i.e. when $L = 0$).

DyB₆

The MR of DyB_6 is similar to that of NdB_6 for $T < T_N$ but for temperatures close to T_N the higher field MR starts to saturate (Fig. 4.32). The temperature dependence of the MR is like that of NdB_6 for $H < 20K$ but for higher field the temperature dependence is much slower than $1/T^2$. The MR for $T > T_N$ is small but still remains positive. It is expected that the MR just above T_N should be negative because of the field-induced alignments of the magnetic moments in the paramagnetic regime. However, if the normal positive magnetoresistance exceeds the negative magnetoresistance in the paramagnetic phase, then it is possible to have positive MR even for $T > T_N$ as seen in the case of DyB_6 . The MR data for $H < 20Koe$ and $T < T_N$ is found to obey the same relation as NdB_6 , namely,

$$\frac{\Delta\rho}{\rho_0} = \frac{A(H)}{T^2} \quad , \quad (4.14)$$

where $A(H) = A/H$. The values of A and A/H obtained from the data are given in Table 4.10 and it is seen that A/H is a constant.

Table 4.10 Experimentally determined value of the
parameter A for DyB₆ at various fields.

H(KOe)	A(K ²)	A/H
10	1.05	0.05
15	0.90	0.06
20	0.60	0.06

Anisotropy in magnetoresistance

The transverse magnetoresistance (TMR) is not the same as the longitudinal magnetoresistance (LMR) except for GdB_6 where the magnetic Gd^{3+} is in an S-state, i.e. it has spherically symmetric charge distribution. In PrB_6 , NdB_6 and DyB_6 , we know that Pr^{3+} , Nd^{3+} and Dy^{3+} have $L=5, 6$ and 5 respectively in their ground states and therefore asymmetry exists in their charge distributions. Such an asymmetry can cause an anisotropic conduction electron-electron scattering (Fert et al, 1977) depending on the direction of an external magnetic field as discussed in Chapter 2. Hence, a difference in LMR and TMR.

We have measured the TMR along with the LMR already discussed in the previous section. The difference in the LMR and TMR is the anisotropy in the MR,

$$\Delta\rho_{\text{AN}} = \text{LMR} - \text{TMR} = \left(\frac{\Delta\rho}{\rho_0}\right)_{||} - \left(\frac{\Delta\rho}{\rho_0}\right)_{\perp} . \quad (4.15)$$

The experimental $\Delta\rho_{\text{AN}}$ is shown in Figs. 4.38-4.40 at different temperatures as a function of applied field for PrB_6 , NdB_6 and DyB_6 respectively. The main features of the anisotropy curves are (i) $\Delta\rho_{\text{AN}}$ increases with increasing field and decreases with increasing temperatures, (ii) $\Delta\rho_{\text{AN}}$ is a function of H^2 at lower fields as expected from the field dependence of the MR data, (iii) $\Delta\rho_{\text{AN}}$ is negative for PrB_6 and NdB_6 and positive for DyB_6 and it

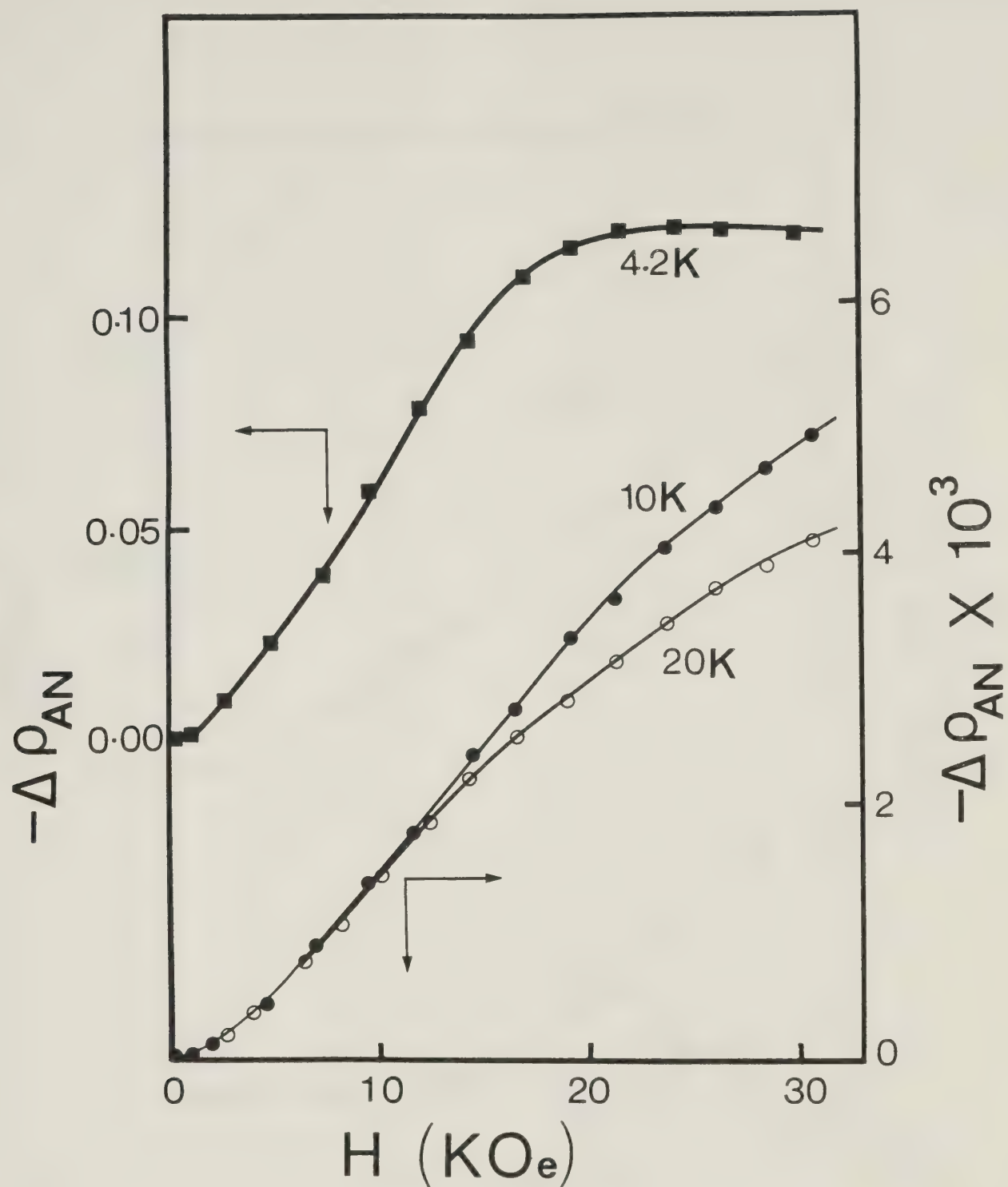


Fig. 4.38 The anisotropy in the magnetoresistance $\Delta\rho_{AN}$ as a function of field (H) at various temperatures for PrB_6 .

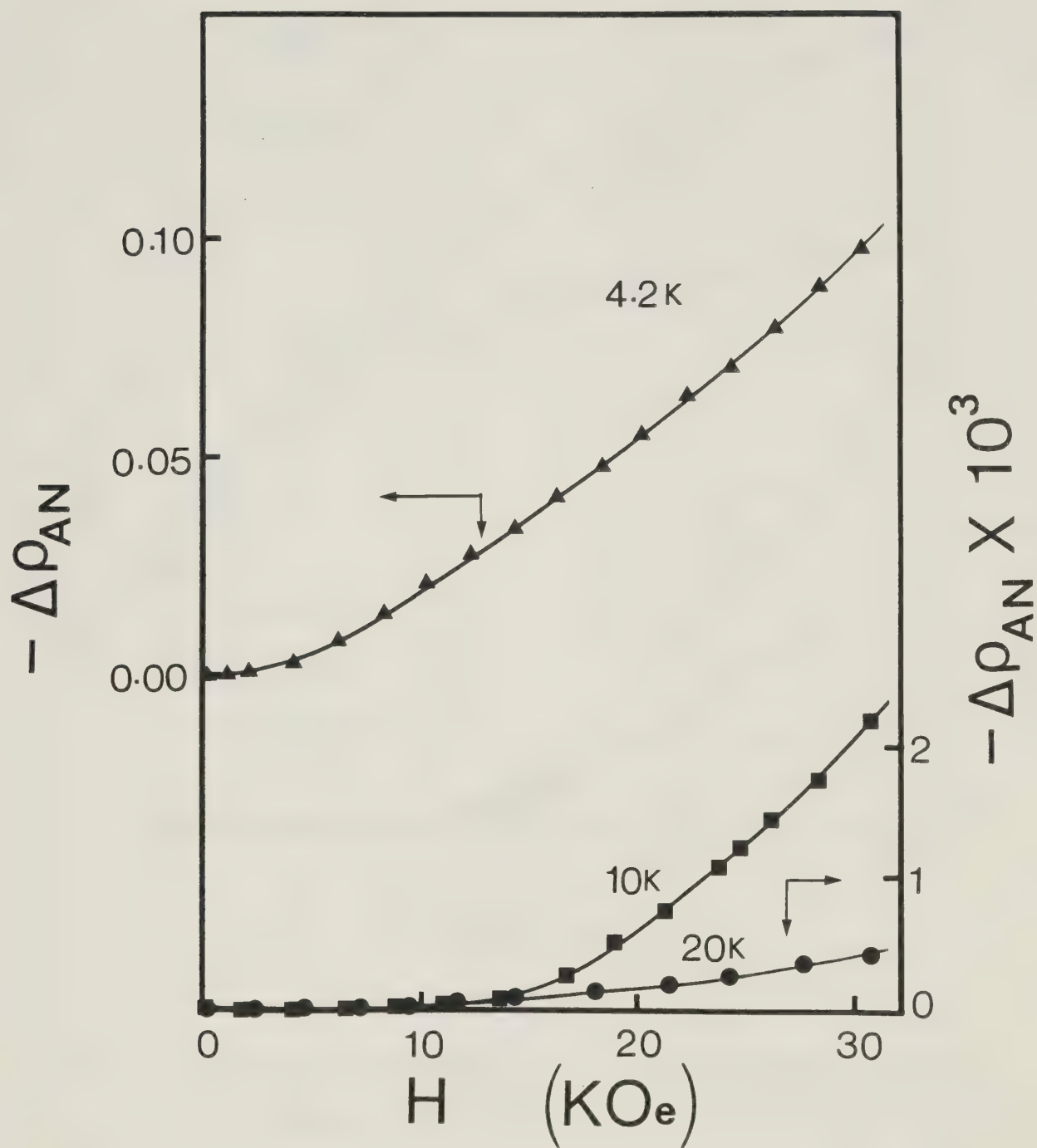


Fig. 4.39 The anisotropy in the magnetoresistance $\Delta\rho_{AN}$ as a function of field (H) at various temperatures for NdB_6 .

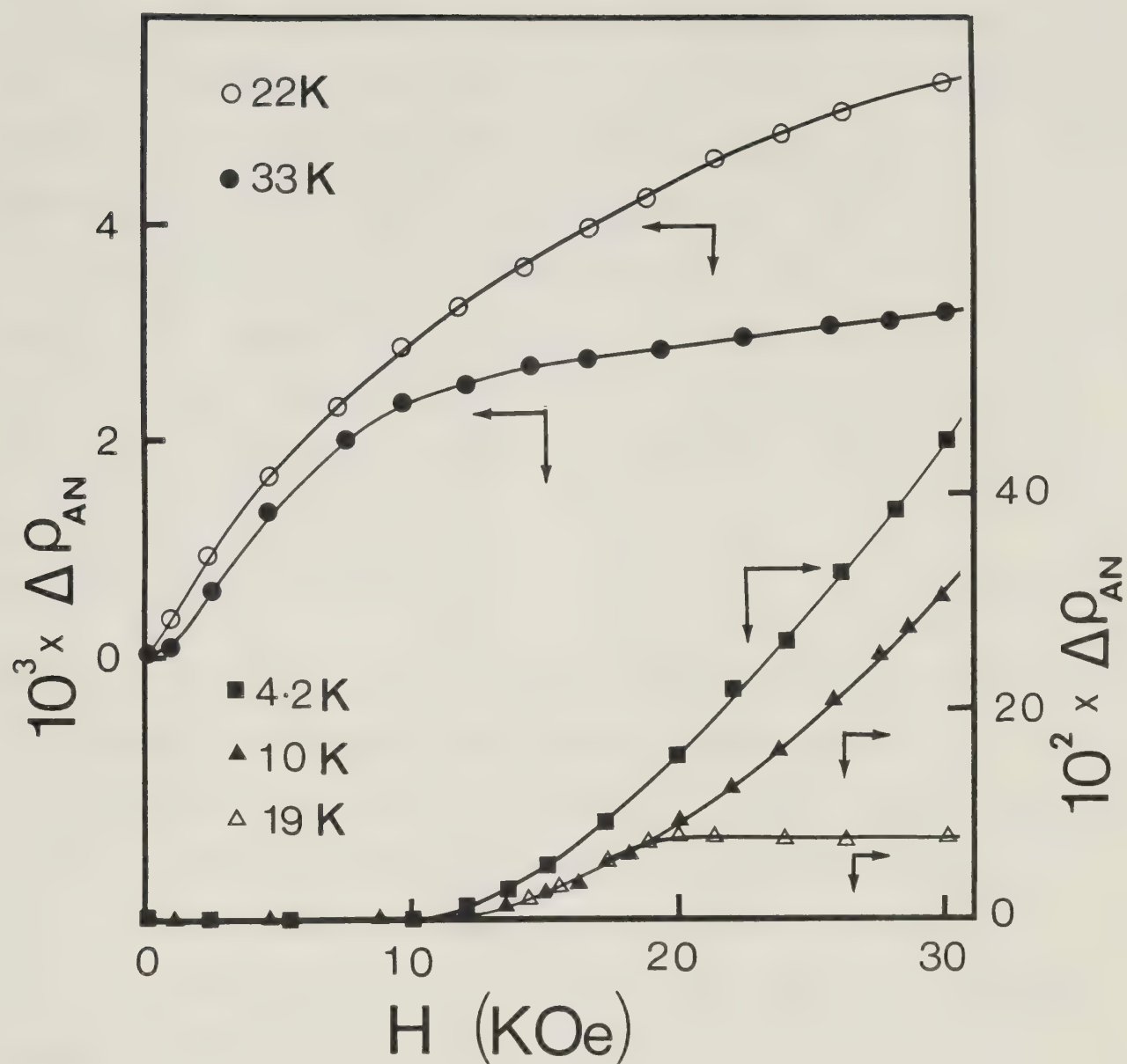


Fig. 4.40 The anisotropy in the magnetoresistance $\Delta\rho_{AN}$ as a function of field (H) at various temperatures for DyB_6 .

tends to saturate at higher fields and higher temperatures.

In the absence of a theoretical study of the MR of antiferromagnetic materials with rare earth ions it is not possible to discuss the above results quantitatively. However, it is possible to correlate these results with the $\Delta\rho_{AN}$ study of very dilute rare earth ions in noble metals (Fert et al, 1977, 1980). In a dilute alloy of rare earth in noble metal with $L \neq 0$ for rare earth ions there will be an anisotropy in the MR. The sign of $\Delta\rho_{AN}$ is given by

$$\Delta\rho_{AN} \propto L(S - \frac{7}{4}) , \quad (4.16)$$

where L = total orbital angular momentum and S is the total spin angular momentum of the magnetic rare earth ion. The above relation is found for anisotropic K-f interactions and to a first approximation taking quadrupolar scattering to be the main source of the anisotropy (see Chapter 2). From the above expression it is expected that for the system with Gd^{3+} ($L = 0$, $S = 7/2$) $\Delta\rho_{AN} = 0$. From the MR data in Fig. 4.31 we do observe such a result. One expects from the above relation that $\Delta\rho_{AN}$ will be negative for Pr^{3+} ($L = 5$, $S = 1$) and Nd^{3+} ($L = 6$, $S = 3/2$) and positive for Dy^{3+} ($L = 5$, $S = 5/2$). The prediction of the signs of $\Delta\rho_{AN}$ for REB_6 is quite consistent with our results. Based on this consistency we believe that the anisotropy in the MR is mainly due to the anisotropic quadrupolar K-f scattering. There is some contribution to $\Delta\rho_{AN}$ probably due to normal

magnetoresistance which is usually small.

Low temperature second phase of GdB_6

The resistivity of GdB_6 below 11K gives a thermal hysteresis which is associated with a low temperature phase transition. The magnetic structure of the low temperature phase is not known. We have measured the resistivity as a function of temperature at a constant field with $H \parallel I$ and $H \perp I$, where I is the sample current. The result is shown in Fig. 4.41. It is interesting to note that the resistance of the sample below 11K still has thermal hysteresis but the resistance has increased for $H \parallel I$ than virgin state and the resistance has decreased for $H \perp I$ in comparison to the virgin state. This shows a strong anisotropy in the resistance which has a dependence on the direction of the magnetic field with respect to sample current.

This anisotropy is very clearly seen in the isothermal MR versus field at $T < 11\text{K}$ in Fig. 4.42 and Fig. 4.43 for $H \parallel I$ and $H \perp I$ respectively. One very dramatic result as seen in Fig. 4.42 and Fig. 4.43 is a large field hysteresis in the resistance. This hysteresis vanishes for $T \geq 12\text{K}$. The MR for $H \parallel I$ increases very rapidly near 6K0e and tends to saturate at about 12K0e. At higher fields the MR increases as in other antiferromagnetic REB_6 . In the case of $H \perp I$ the MR is negative and decreases rapidly and at higher fields starts increasing as expected in an anti-

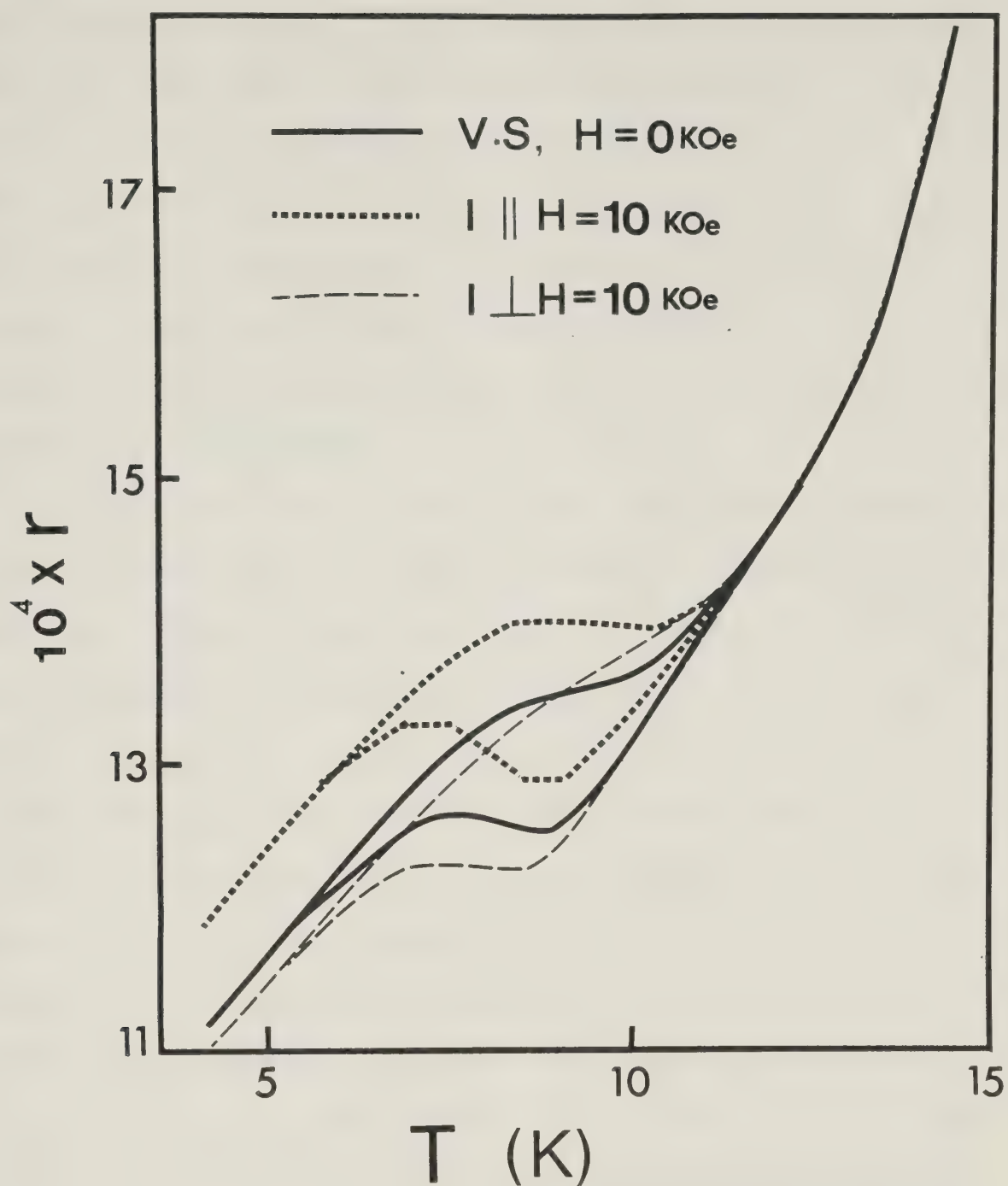


Fig. 4.41 The temperature dependence of resistance (r) of GdB_6 at various fields (H) showing the hysteresis associated with the second low temperature phase. V.S. stands for virgin state, when the specimen is cooled in zero field from room temperature.

ferromagnetic metal. The field hysteresis suggests that there is some kind of magnetic domain alignment. This domain alignment is found to be complete for fields above 10KOE and even when the field is reduced to zero the system remains in that state. It was found that to bring the sample to the virgin state it was necessary to warm the sample above 11K after reducing H to zero and then to cool it down in zero field.

There is some evidence, from the torque measurements by Nozaki et al (1980) on single crystal GdB_6 , that the lower phase of GdB_6 has three equivalent domains and these domains could be changed entirely to one single domain for a magnetic field $H \geq 6.5\text{KOE}$ at 4.2K. This transition is quite sharp in single crystal GdB_6 . For polycrystalline GdB_6 , we do not observe such a sharp transition obviously because of polycrystalline effects. Nozaki et al (1980) have suggested that the conversion between these magnetic domains is similar to the spin-flopping of an antiferromagnet. The question is, why the resistance has such a strong anisotropy depending on the direction of the external magnetic field relative to the sample current for polycrystalline GdB_6 . For fields greater than 10KOE there is complete conversion to a single domain. This conversion of domain has been found by Nozaki et al (1980) to be analogous to the spin-flopping of an antiferromagnet. If this is so then when $H \parallel I$, H is perpendicular to the easy axis of magnetization and I perpendicular

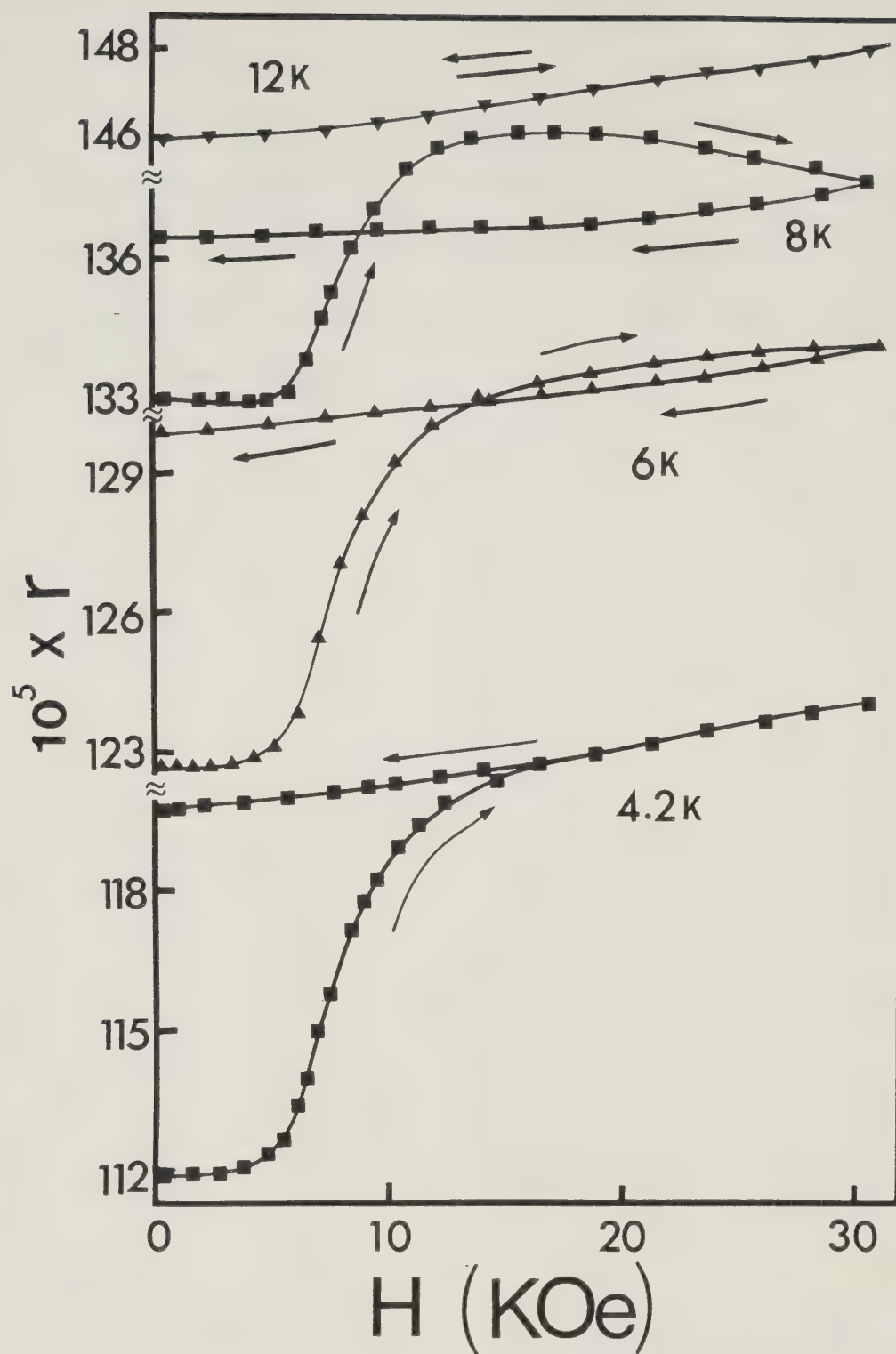


Fig. 4.42 The longitudinal magnetoresistance of GdB₆ as a function of external field (H) at various temperatures for $T \leq 12\text{K}$, showing large field hysteresis in the second low temperature phase of GdB₆.

to the easy axis of magnetization, hence the resistance is expected to increase with increasing field. While for $H \perp I$, again H is perpendicular to the easy axis of magnetization and I is in the plane of the easy axis of magnetization leading to a decrease in resistance with increasing field. This could account for the anisotropy in the MR of GdB_6 in its lower phase.

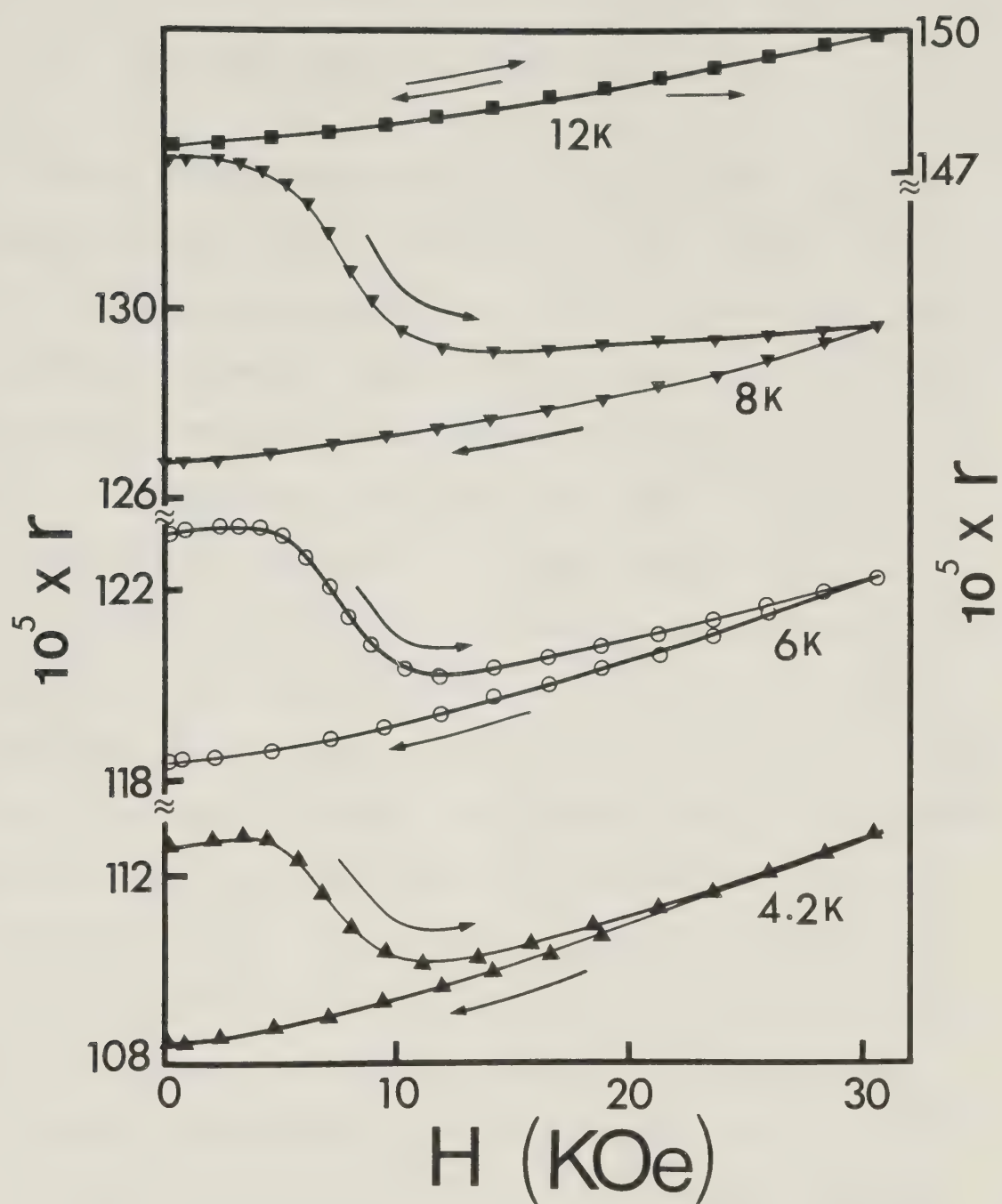


Fig. 4.43 The transverse magnetoresistance of GdB_6 as a function of external field (H) at various temperatures, showing large field hysteresis in the second low temperature phase of GdB_6 .

CHAPTER 5

$[\text{La},\text{Gd}]\text{B}_6$ AND $[\text{La},\text{Dy}]\text{B}_6$ ALLOYS

We have prepared three $[\text{La},\text{Gd}]\text{B}_6$ alloys with concentration of Gd^{3+} ion in the range $0.051 \leq x \leq 0.285$ and two alloys of concentrations $x = 0.03$ and 0.08 . The residual resistivity ratio (RRR) is given in Table 5.1. The correspondence between this ratio and the nominal concentration of the impurity verifies that other impurity scattering was not important in these specimens.

The variation of resistance with temperature in the temperature range from 2K to 20K is shown for $[\text{La},\text{Gd}]\text{B}_6$ and $[\text{La},\text{Dy}]\text{B}_6$ in Fig. 5.1 and Fig. 5.2 respectively, along with the resistance data of non-magnetic LaB_6 . LaB_6 shows no temperature dependence below 30K, hence the variation of resistance in Fig. 5.1 and Fig. 5.2 arises from the substitution of Gd and Dy on some of the La sites. There is no sign of the Kondo effect in the resistivity data. At the lowest temperatures the resistance varies as $\sim T^{3/2}$, which is expected for a spin glass as discussed in Chapter 2. However, in common with resistance measurements on other spin glasses there is no feature in the resistance vs temperature data that can be clearly identified with the transition to the spin glass state. It should be mentioned that the sign of the s-f exchange energy J , believed to be responsible for the properties that arise

Table 5.1 Residual resistivity ratio (RRR) of $[\text{La}, \text{Gd}]\text{B}_6$ and $[\text{La}, \text{Dy}]\text{B}_6$ alloys.

Sample	$\text{RRR} = \rho_{300\text{K}} / \rho_{4.2\text{K}}$
LaB_6	18.0
$[\text{La}_{0.949} \text{Gd}_{0.051}]\text{B}_6$	13.0
$[\text{La}_{0.877} \text{Gd}_{0.123}]\text{B}_6$	8.7
$[\text{La}_{0.715} \text{Gd}_{0.285}]\text{B}_6$	6.2
$[\text{La}_{0.97} \text{Dy}_{0.03}]\text{B}_6$	18.5
$[\text{La}_{0.92} \text{Dy}_{0.08}]\text{B}_6$	18.3

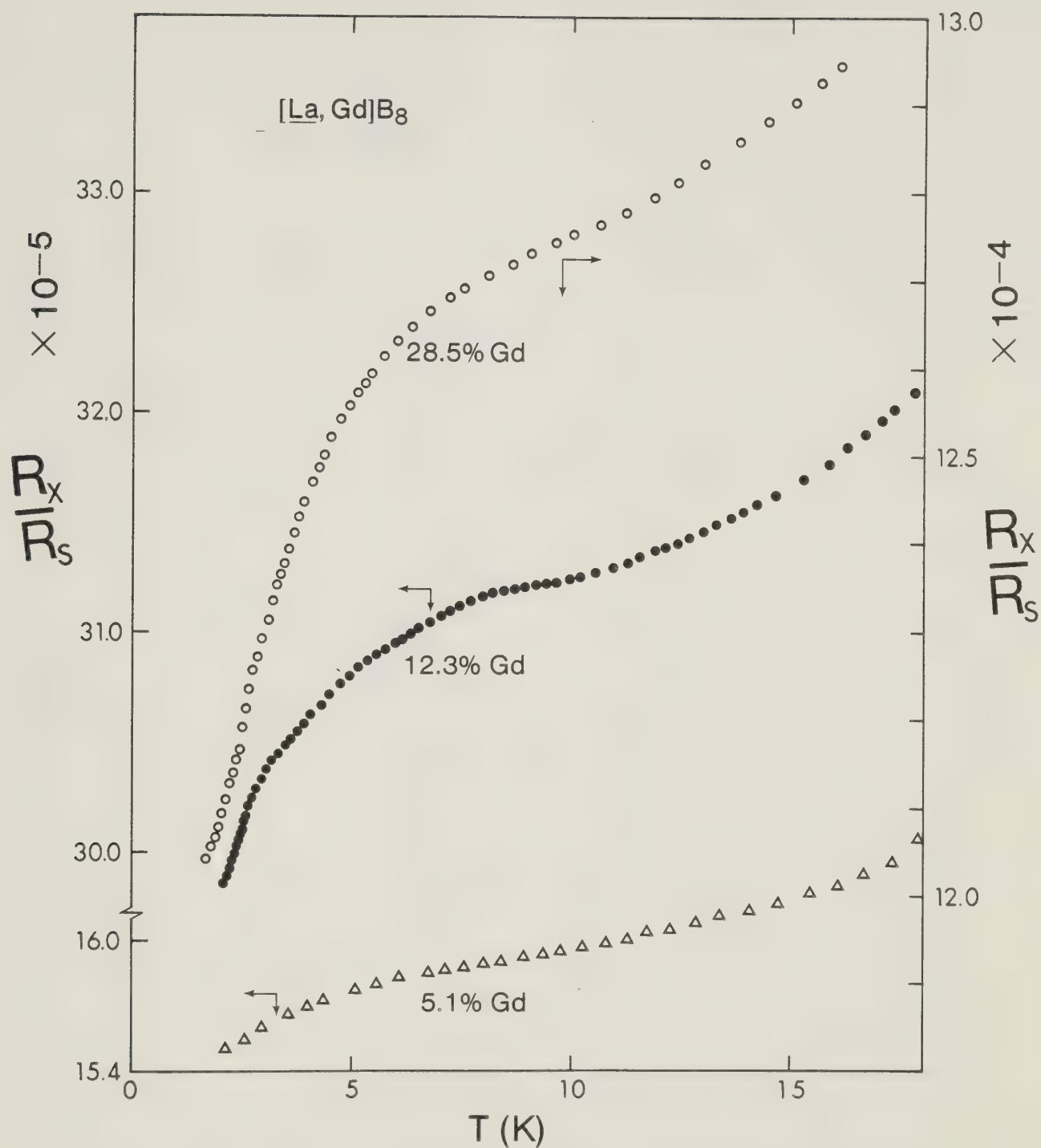


Fig. 5.1 Normalized resistance (R_x/R_s), where R_x is specimen resistance and $R_s = 0.1\Omega$, as a function of temperature (T) for $[\text{La}, \text{Gd}]B_6$.

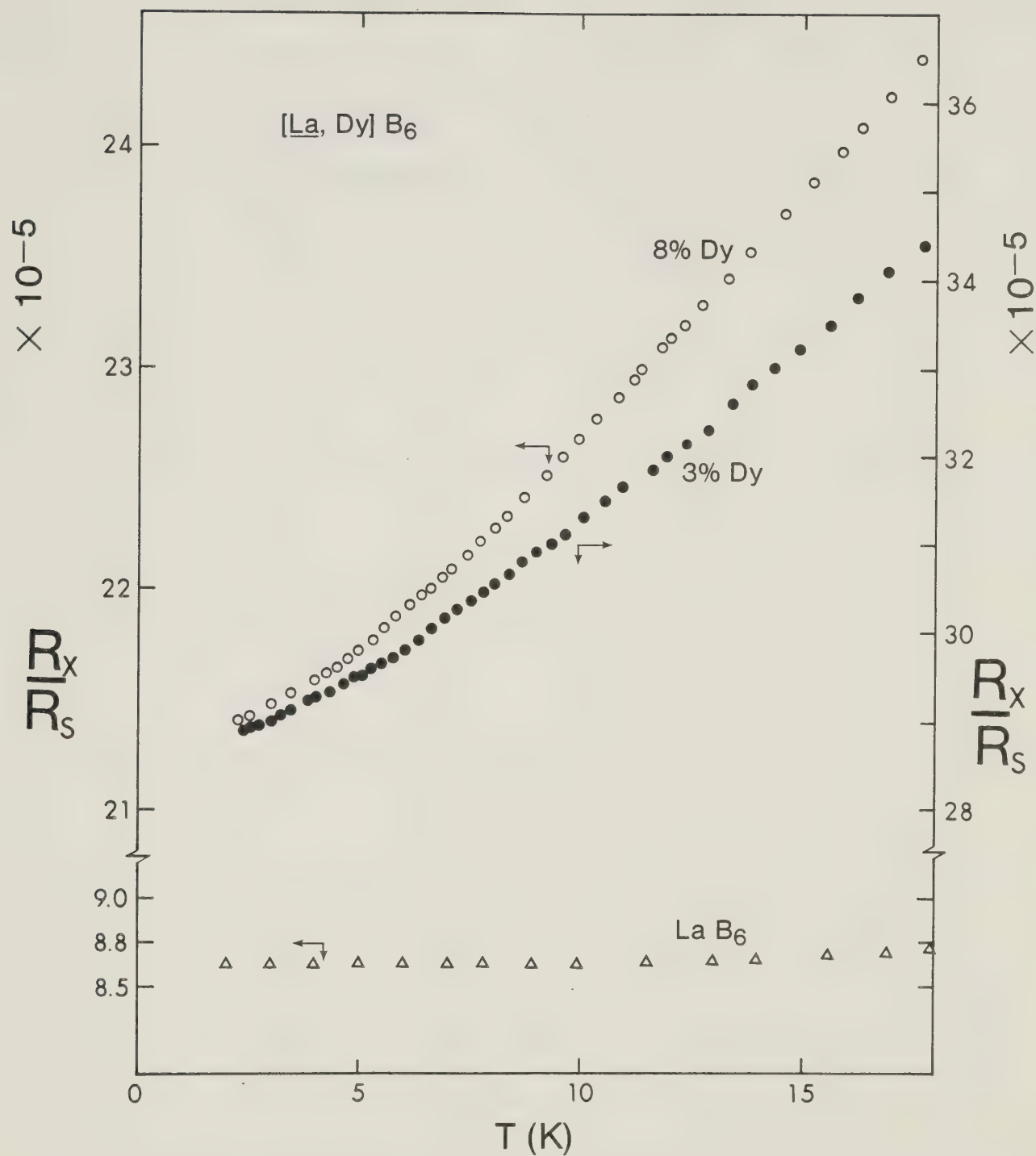


Fig. 5.2 Normalized resistance (R_x/R_s), where R_x is specimen resistance and $R_s = 0.1\Omega$, as a function of temperature (T) for $[La,Dy]B_6$ and LaB_6 .

from the magnetic ions in these materials, has not been determined. Since RKKY interaction is oscillatory in nature, the sign of J depends in a delicate way on the structure and unit-cell size. In the absence of a Kondo effect, it is possible that J is positive, which would produce a "reverse Kondo" effect. The resistance variation would then be obscured in these alloys by possible spin-glass effects even above the freezing temperature.

The TEP data are presented in Figs. 5.3 and 5.4. The main features of the TEP data are as follows: (i) A maximum is observed in the TEP and the temperature at which the maximum occurs, increases with increasing concentration of magnetic ions. (ii) The TEP finally becomes negative. This sign change is characteristic of a spin glass (Fischer, 1980, 1981; and Matho and Béal-Monod, 1974) and its variation with alloy concentration together with the increase in the maximum should be expected. The TEP is almost linear in T with a negative slope for $T > T_{\text{max}}$. The value of T_{max} for different concentrations is given in Table 5.2. To our surprise we observe a spin glass behaviour even for 28% Gd concentration. There is no evidence whatsoever of any long range magnetic order for $[\text{La}, \text{Gd}] \text{B}_6$ alloys with concentration of Gd up to 28 at. %.

It is possible to characterize the systematics in the TEP data by Fig. 5.5. A plausible physical interpretation of the terms of Fig. 5.5 is as follows. The high temperature region, i.e. the region of $T > T_0$, can be described by

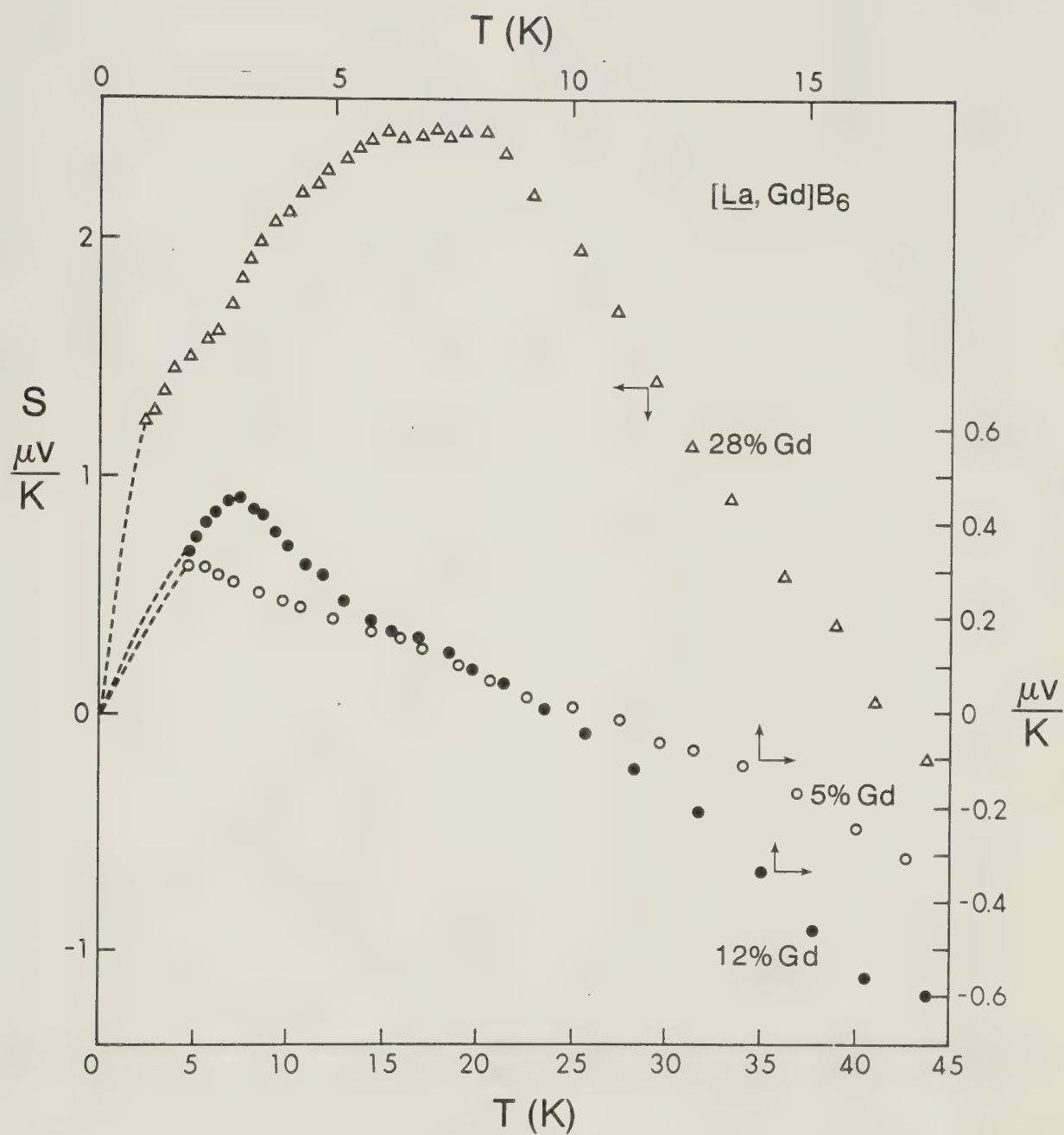


Fig. 5.3 Absolute thermoelectric power (S) as a function of temperature (T) for $[\text{La}, \text{Gd}]\text{B}_6$.

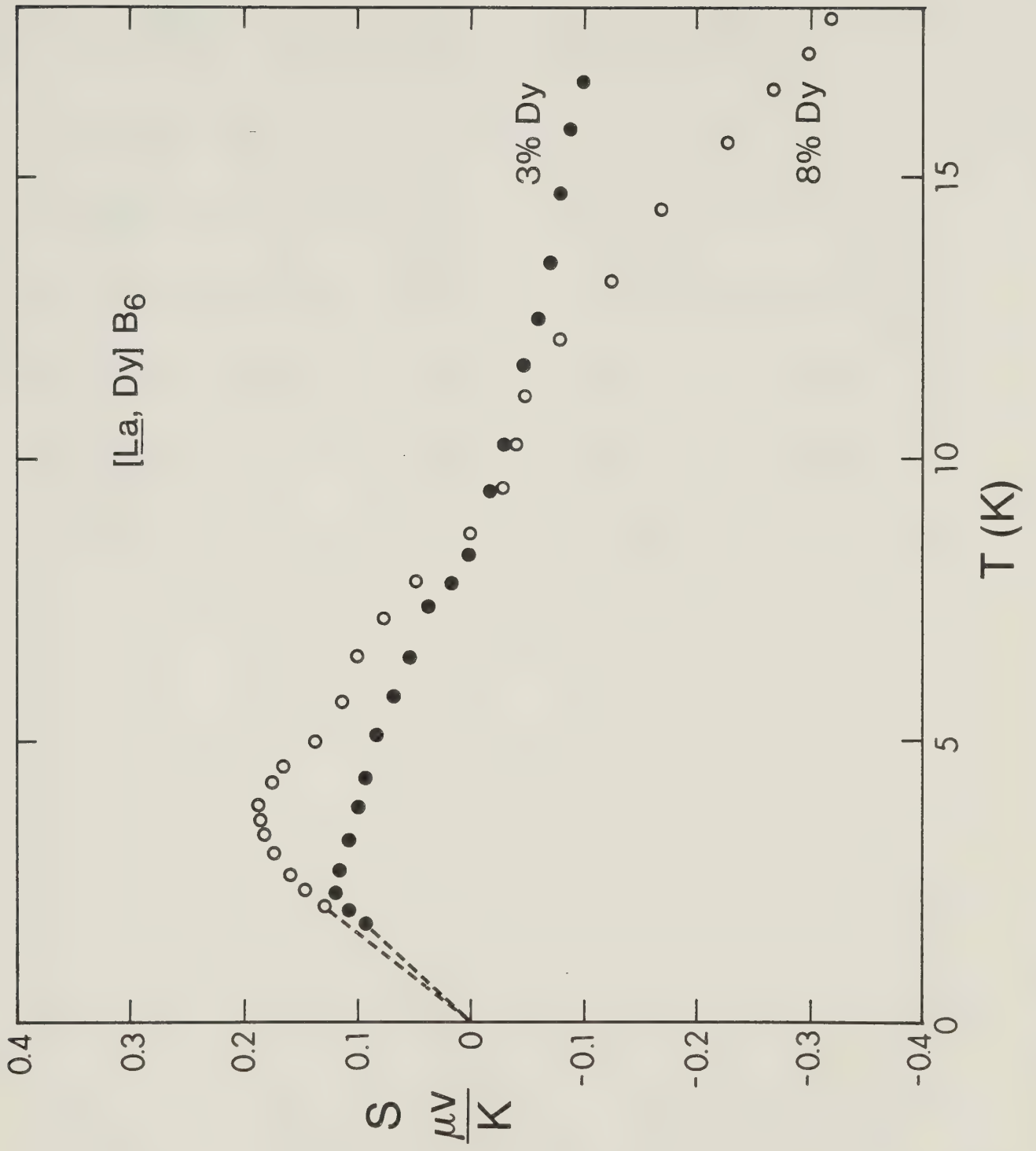


Fig. 5.4 Absolute thermoelectric power (S) as a function of temperature (T) for $[La, Dy]B_6$.

Table 5.2 Experimental values of T_O , T_{\max} and S_{\max} for $[\text{La},\text{Gd}]\text{B}_6$ and $[\text{La},\text{Dy}]\text{B}_6$ spin glasses.

Sample	T_O (K)	T_{\max} (K)	S_{\max} ($\mu\text{V}\text{K}^{-1}$)
$[\text{La}_{0.949}\text{Gd}_{0.051}]\text{B}_6$	10.0	2.1	0.31
$[\text{La}_{0.897}\text{Gd}_{0.123}]\text{B}_6$	9.5	3.0	0.46
$[\text{La}_{0.715}\text{Gd}_{0.285}]\text{B}_6$	41.0	17.0	2.48
$[\text{La}_{0.97}\text{Dy}_{0.03}]\text{B}_6$	8.3	2.3	0.12
$[\text{La}_{0.92}\text{Dy}_{0.08}]\text{B}_6$	8.8	3.8	0.19

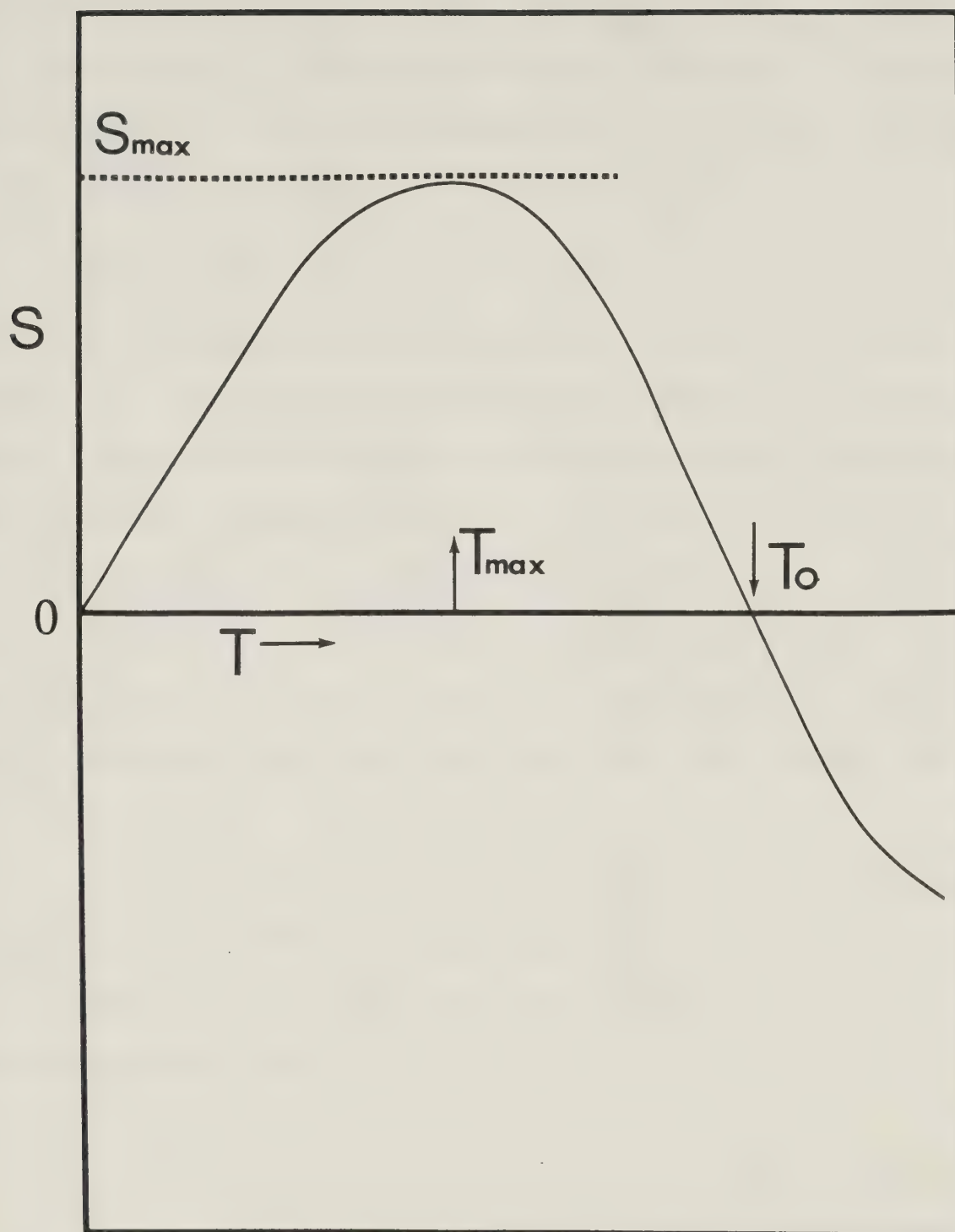


Fig. 5.5 The temperature dependence of the thermoelectric power (S) of dilute magnetic alloys is parameterized in terms of S_{\max} , T_{\max} and T_0 .

a one-impurity regime. For $T < T_0$ the impurity interactions dominate leading to a maximum S_{\max} at T_{\max} . This T_{\max} is expected to be related to the spin-glass freezing temperature T_f . For spin glasses with $J < 0$ (e.g. AuFe etc.) T_0 is related to T_f as

$$T_0 = AT_f ,$$

where A is a constant, which depends on J and the density of states. In the absence of precise knowledge of T_f (which may be found from susceptibility measurements) and correlation between T_0 and T_f for $J > 0$, it is not possible to find the constant (A). However, it is clear that a systematic exists in the TEP data of these spin glasses even when the concentrations of magnetic impurities are very high. These are the first TEP data for spin glasses of $J > 0$ type.

In conclusion, we have observed spin-glass behaviour in resistivity and TEP of $[\text{La,Gd}]B_6$ and $[\text{La,Dy}]B_6$ alloys for concentration of rare earth ion as high as 28 at. % (Ali and Woods, 1983a).

CHAPTER 6

Y-RE ALLOYS

In this chapter we present experimental results and discussion of some dilute yttrium-rare earth alloys. The alloys studied and their residual resistivity ratio are given in Table 6.1.

The variation of resistance ($r = R_x/R_s$) with temperature for YCe (Ce = 3% and 15%) is shown in Fig.6.1. For the 3% Ce alloy we observe a typical Kondo behaviour with a resistance minimum at ~22.2K. But as we increase the concentration of Ce ions, the resistivity behaviour changes. For 15% Ce we observe (Fig. 6.1) that at the lowest temperatures the resistance first increases with T, goes through a small maximum at ~4.5K, then to a minimum at ~7K beyond which it monotonically rises with temperature. Below 4.5K the alloy is showing a spin-glass behaviour and above that, a Kondo effect. A similar effect has been observed in concentrated $\text{La}_{1-x}\text{Ce}_x$ alloys (Zimmer and Schilling, 1978) and dilute AuFe alloys (Mydosh, 1978).

Figure 6.2 shows the thermoelectric power (TEP) as a function of temperature. There is a broad peak at about ~20K for 3% Ce with $S_{\text{max}} \approx 13 \mu\text{V/K}$. This peak is associated with the Kondo temperature $T_K \approx 20\text{K}$ for 3% Ce in Y. A similar broad peak is also found for the 15% Ce alloy at ~17K but the value of $S_{\text{max}} \approx 2.1 \mu\text{V/K}$ which is an order of

Table 6.1 Residual resistivity ratio of Y-RE alloys.

Sample	RRR
$\text{Y}_{0.97}\text{Ce}_{0.03}$	6.0
$\text{Y}_{0.85}\text{Ce}_{0.15}$	4.2
$\text{Y}_{0.97}\text{Sm}_{0.03}$	7.0
$\text{Y}_{0.97}\text{Tb}_{0.03}$	7.7
$\text{Y}_{0.98}\text{Dy}_{0.02}$	13.8
$\text{Y}_{0.90}\text{Dy}_{0.10}$	6.2

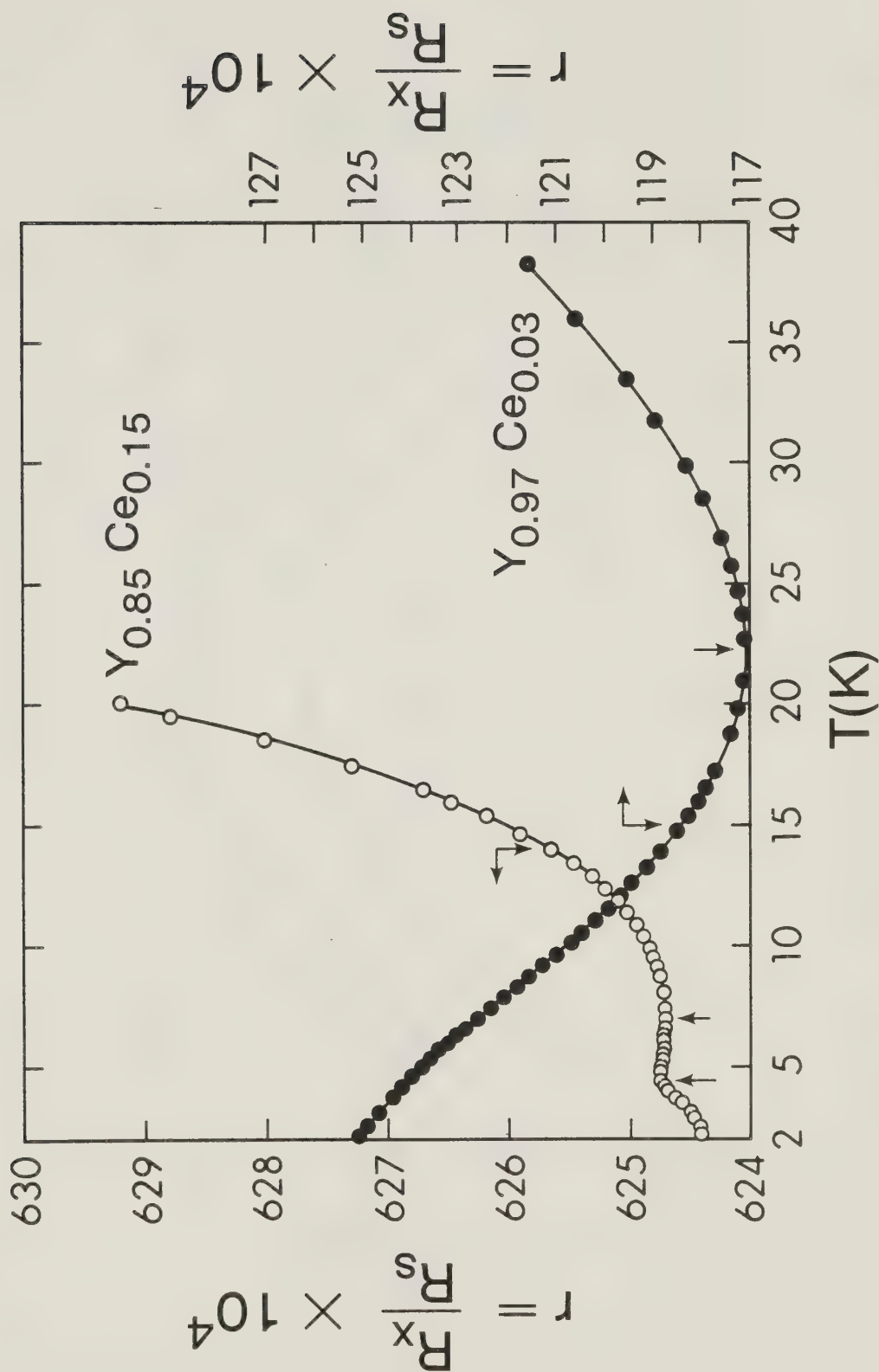


Fig. 6.1 Normalized resistance ($r = R_x/R_s$), where R_x is specimen resistance and $R_s = 0.1\Omega$, as a function of temperature (T) of YCe (Ce = 3% and 15%) alloys.

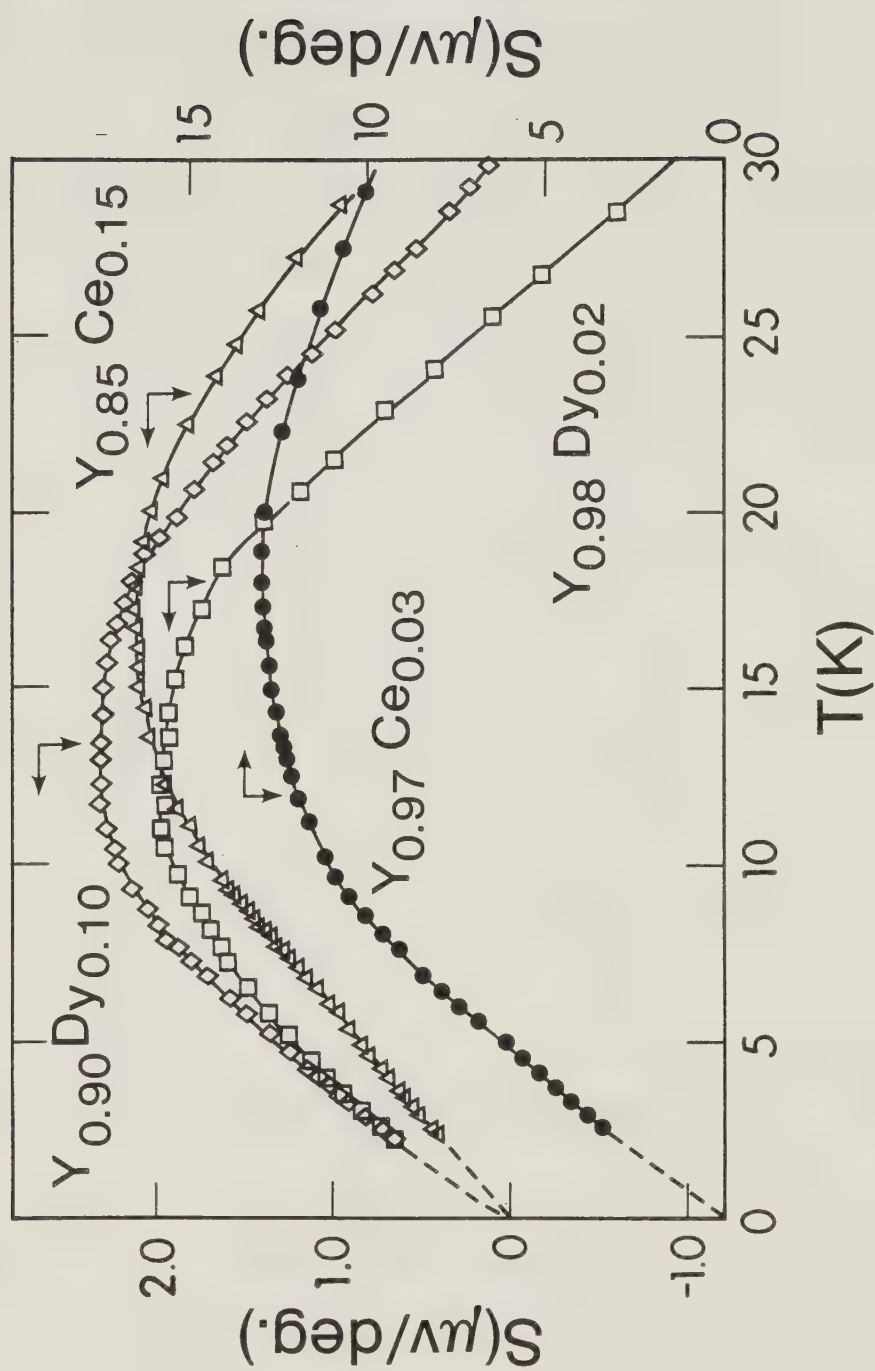


Fig. 6.2 Absolute thermoelectric power (S) of YCe (Ce = 3% and 15%) and YDy (Dy = 2% and 10%) alloys as a function of temperature (T).

magnitude smaller than in the case of 3% Ce alloy. There is change of sign in the TEP at $T_0 \approx 40\text{K}$ for 15% Ce as expected for a spin glass (discussed in Chapter 5) but no such change was found for 3% Ce alloys.

The resistance and TEP data for $\text{Y}_{1-x}\text{Dy}_x$ ($x = 0.02$ and 0.10) are shown in Fig. 6.3 and Fig. 6.2. The resistance increases with T but no sharp phase transition is evident. At lowest temperatures the resistance behaviour is like spin glass which is also evident in Fig. 6.2 where a broad peak in the TEP and a change in sign in S from positive to negative is seen. The values of S_{max} , T_{max} and T_0 are given for each alloy in Table 6.2. For the 10% Dy alloy the resistance increase in T is faster below 6K but no explicit helical ordering of the type suggested by Sarkissian and Coles (1976), is evident.

Results for YSm (3% Sm) and YTb (3% Tb) alloys are shown in Fig. 6.4 and Fig. 6.5. The resistance versus temperature curves for these alloys show clearly a sharp transition from an antiferromagnetic to paramagnetic phase ($T_N = 5.0\text{K}$ and 5.2K for YSm (3%) and for YTb (3%) respectively). Below T_N the resistance increases very rapidly with temperature, whereas the slope of the curve decreases above T_N and becomes almost constant at higher temperatures. The resistance has a temperature dependence of T^3 at $T < T_N$ for both YSm (3%) and YTb (3%) alloys. Such a temperature dependence is expected in an antiferromagnetic alloy below T_N due to spin-wave and conduction-electron interactions.

Table 6.2 Experimental values of S_{\max} , T_{\max} and T_O for Y-RE alloys.

Sample	S_{\max} ($\mu\text{V/K}$)	T_{\max} (K)	T_O (K)
YCe (3%)	13.0	20.0	-
YCe (15%)	2.1	17.0	41.0
YSm (3%)	2.3	15.0	26.8
YTb (3%)	2.0	16.0	28.0
YDy (2%)	2.0	11.0	26.0
YDy (10%)	2.3	13.0	31.0

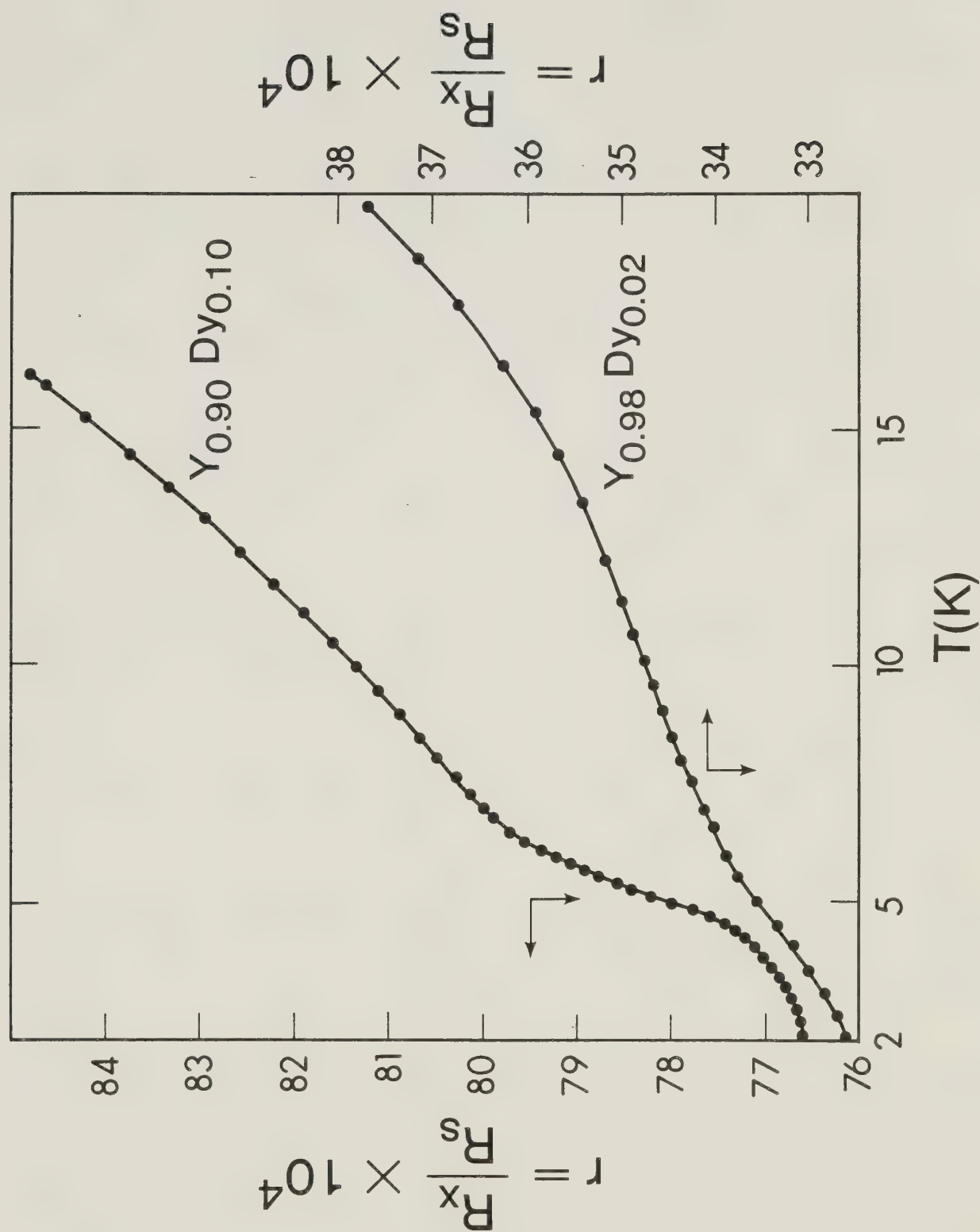


Fig. 6.3 Normalized resistance ($r = R_x/R_s$) as a function of temperature (T) of YDy (Dy = 2% and 10%) alloys.

The effect of dilution down to 3% Sm and Tb in Y is a reduction of T_N as the strength of the interaction between the magnetic moments (RKKY type) is reduced. Sugawara (1965) has observed a similar behaviour from resistivity measurements on dilute YTb alloys and obtained $T_N \approx 5\text{K}$ for an alloy with 2% Tb. Nagasawa and Sugawara (1967) performed susceptibility measurements on a series of dilute YTb alloys and obtained the temperature T_x of the susceptibility maximum. For a 2.7 at.% Tb alloy they obtained $T_x = 11.5\text{K}$ and noted that in dilute alloys T_x does not always correspond to T_N . The sensitivity of their resistivity data was not sufficient for them to locate T_N from the slope change. Sarkissian and Coles (1976) saw a susceptibility maximum at $T_x \approx 12\text{K}$ for a YTb (3% Tb) alloy, but the resistance showed no increase with decreasing temperature below T_x , they identified this as a spin-glass material. Their specimens were chill cast after arc melting, which may have had an effect on the low temperature resistivity and they may have missed a slope change over a narrow temperature range with normal potentiometric measurements. It should also be noted that the TEP shown in Fig. 6.5 has a broad peak for YSm (3% Sm) and YTb (3% Tb) alloys and does not show any evidence of the phase transitions. The TEP data of dilute rare earth alloys can be characterized in the similar way as is done in Chapter 5 for dilute $[\text{La}, \text{Gd}]B_6$ and $[\text{La}, \text{Dy}]B_6$ alloys. The data can be parameterized as shown in Fig. 5.5.

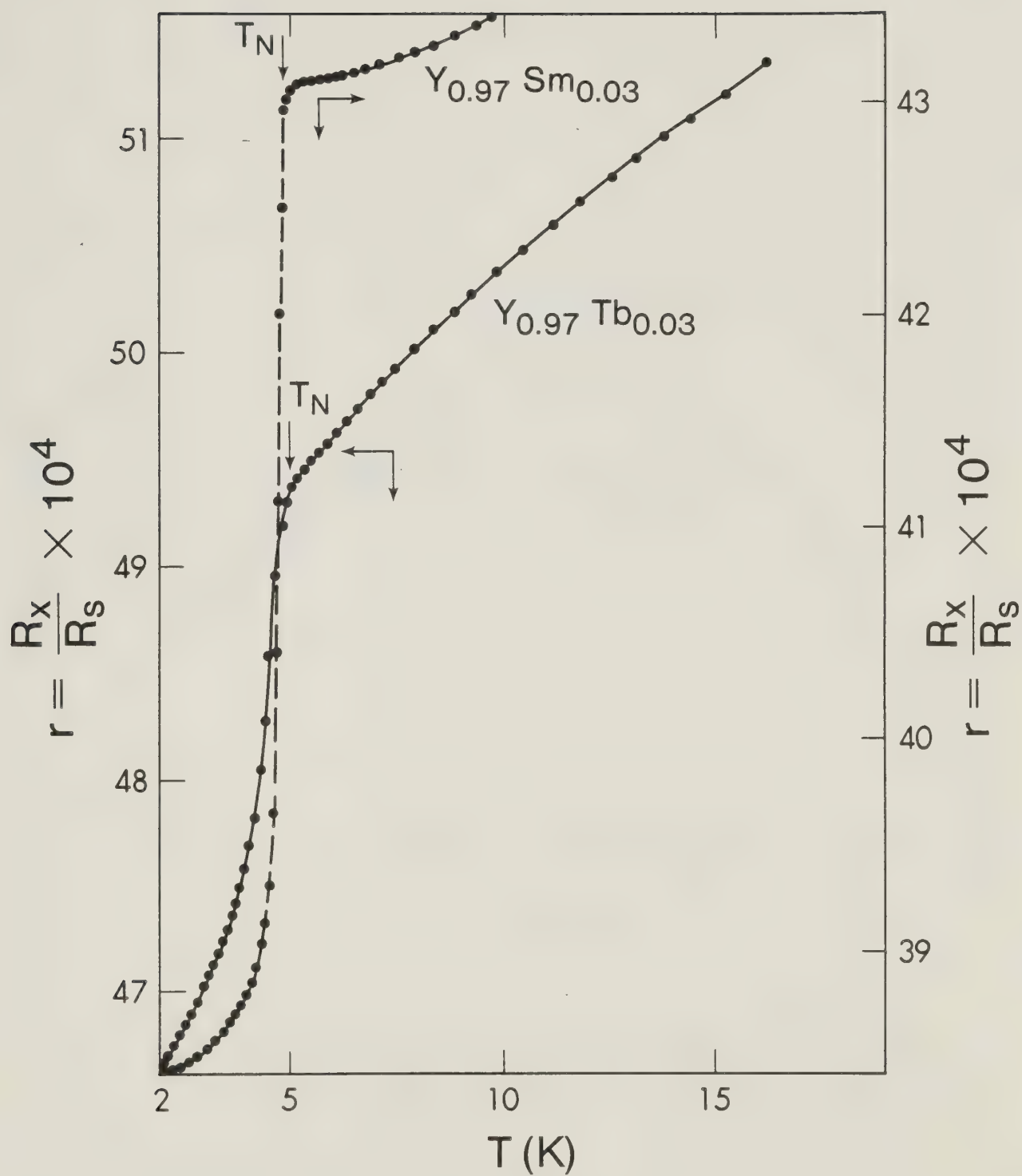


Fig. 6.4 Normalized resistance ($r = R_x/R_s$) as a function of temperature (T) of YSm (3% Sm) and YTb (3% Tb) alloys.

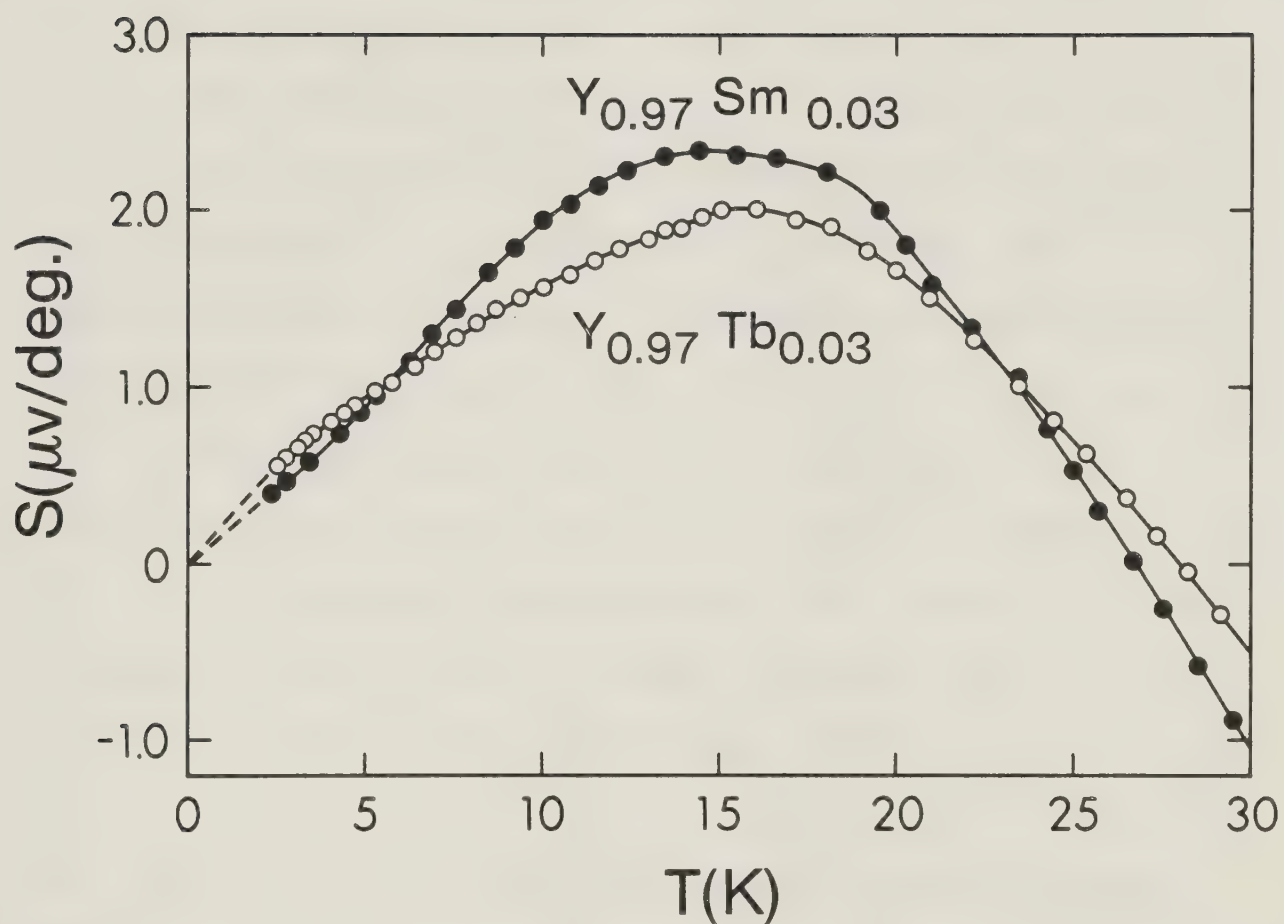


Fig. 6.5 Absolute thermoelectric power (S) of YSm (3% Sm) and YTb (3% Tb) alloys as a function of temperature (T).

From the above results we conclude that we have observed the Kondo effect in a dilute YCe alloy and spin-glass behaviour in more concentrated YCe alloys. Spin-glass behaviour is also found in dilute YDy alloys, but we clearly observe an antiferromagnetic phase at low temperatures in the resistivity of YSm (3% Sm) and YTb (3% Tb). The TEP on the other hand shows no sharp change associated with the phase changes.

Thus here we have dilute rare earth alloys exhibiting three different kinds of magnetic properties, namely (i) Kondo effect, (ii) spin-glass behaviour, and (iii) antiferromagnetic behaviour. To investigate the magnetoresistance (MR) of three kinds of systems we have measured the MR of YCe (3 at. %), YDy (2 at. %) and YTb (3 at. %) alloys. The isothermal MR of YCe (3 at. %) is shown in Fig. 6.6 at different temperatures. The MR of YCe (3 at. %) is negative in the entire range of the external magnetic field and it has a field dependence of H^n ($1 < n < 2$). The MR of dilute magnetic alloys in single impurity regime has been theoretically calculated by Béal-Monod and Weiner (1968) using an isotropic hamiltonian of the form shown in eqn. (2.1). It is found that the MR is negative and for $(g\mu_B H/K_B T) < 1$ the isothermal MR has a H^2 field dependence. This behaviour is exhibited because of the freezing out of the spin-flip scattering due to the alignment of the magnetic moments in an external field. Therefore the MR of YCe (3 at. %) is consistent with the above theory. In Fig. 6.6

only the longitudinal MR is shown but the transverse MR differs only in that it is slightly larger in magnitude.

The magnetoresistance of YDy (2 at. %) in the paramagnetic temperature range is shown in Fig. 6.7. In the paramagnetic phase of a spin glass, that is for temperatures $T > T_f$, it should be possible to treat the MR in the dilute magnetic alloy approximation. We observe from Fig. 6.7 that the MR is negative at low fields for the 4.2K isotherm and for 10K transverse isotherm and becomes positive with increasing field. At higher temperatures the MR remains positive at all values of the field and increases with increasing field as $\sim H^2$. Another interesting feature of the MR data for the YDy (2 at. %) alloy is that the LMR is always greater than the TMR. In the paramagnetic range it is reasonable to treat YDy (2 at. %) alloy as a dilute magnetic alloy in the context of the Béal-Monod and Weiner (1968) theory. We then expect a negative MR with $(\Delta\rho/\rho_0) \propto -H^n$, $1 \leq n \leq 2$. The negative MR at 4.2K and 10K for low fields is caused by the reduction of spin-flip scattering due to field-induced alignment of the magnetic spins as expected in case of a dilute magnetic alloy. The positive MR in YDy (2 at. %) arises from the dominance of the 'normal magnetoresistance' at higher fields and temperatures created by the Lorentz force. At the same time anisotropic scattering between the conduction electrons and f-electrons would produce disagreement with the theory for

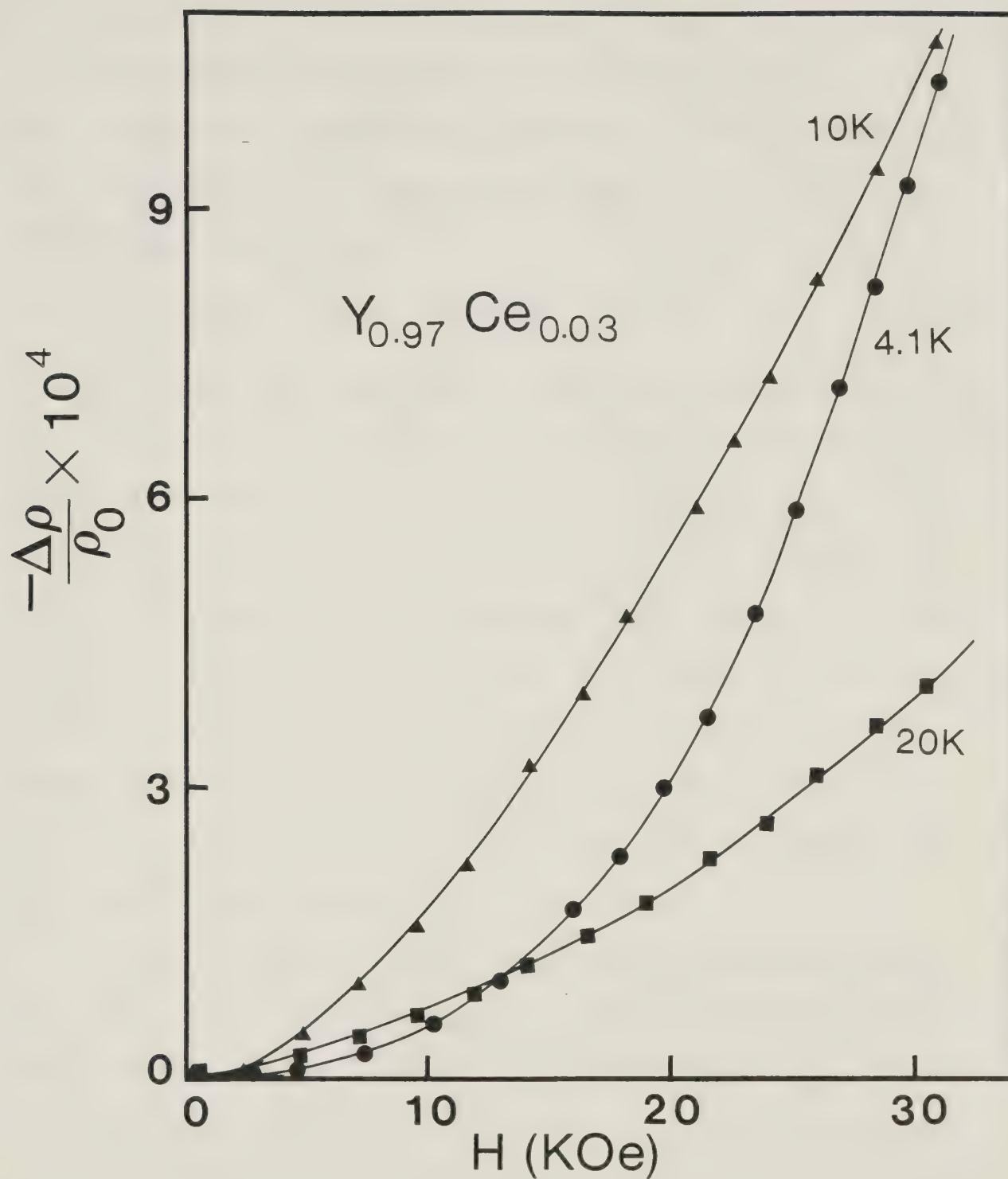


Fig. 6.6 Isothermal magnetoresistance ($\Delta\rho/\rho_0$) versus magnetic field (H) at different temperatures for YCe (3 at. % Ce).

the dilute magnetic alloys with only isotropic scattering (Béal-Monod and Weiner, 1968).

It has been shown by Fert and co-workers (1977, 1974 and 1980) that the anisotropy ($A = \text{LMR} - \text{TMR}$) in the MR of dilute AuRE and AgRE (RE = rare earth) alloys is due to the anisotropic conduction electron-f-electron scattering and it is mainly of quadrupolar type. The sign of the anisotropy changes as

$$A = \text{LMR} - \text{TMR} \propto L \left(S - \frac{7}{4} \right) , \quad (6.1)$$

where L and S are the total orbital angular momentum and the spin of the magnetic ion respectively. Hence for Gd^{3+} ions ($L = 0$) the anisotropy is zero as found for AuGd and AgGd alloys (Friederich and Fert, 1974; and Fert et al, 1980). The sign of A is expected to be positive for Dy^{3+} ($L = 5$, $S = 5/2$) and for YDy (2 at. %) alloys A is observed to be positive at all temperatures. A negative A is observed for YCe (3 at. %) as expected for Ce^{3+} ($L = 3$, $S = 1/2$) from eqn. (6.1), but the difference between LMR and TMR is very small.

The MR data (Fig. 6.8) of the antiferromagnetic YTb (3 at. %) can be discussed in two temperature regimes, one for $T < T_N$ ($T_N \approx 5.2\text{K}$) and the other for $T > T_N$. For the 4.1K isotherm in Fig. 6.8, the MR is positive, increases with increasing field and reaches a maximum at a critical field H_C (at $T = 4.2\text{K}$) $\approx 12\text{KOe}$, and above H_C the MR decreases monotonically with increasing field. The critical field

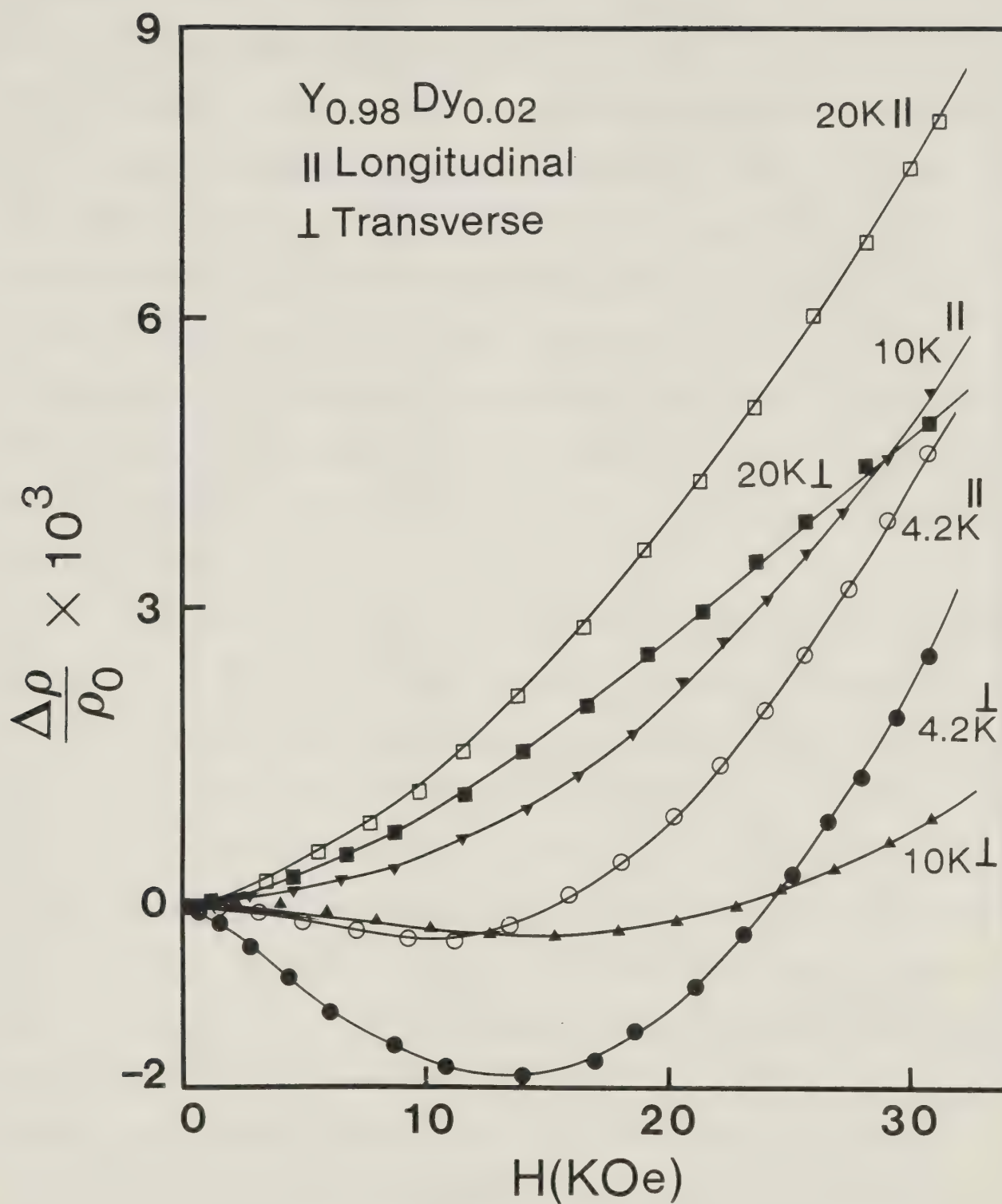


Fig. 6.7 Isothermal magnetoresistance ($\Delta\rho/\rho_0$) versus magnetic field (H) at different temperatures for YDy (2 at. % Dy).

$H_C \approx 12\text{Koe}$ is the field at which the transition from anti-ferromagnetic to paramagnetic phase occurs at 4.2K. The increase in the positive MR with increasing field is consistent with the Yamada and Takada (1973, 1973a) theory. The increase in the MR can be explained as an enhancement in the spin fluctuations with increasing field up to a critical field H_C . This is a mechanism opposite to the ferromagnetic or paramagnetic case where the spins align in the presence of an external magnetic field, causing a suppression in the spin fluctuations and hence a negative MR. That is why above $H_C \approx 12\text{Koe}$ the MR starts decreasing with increasing field as observed for the 4.2K isotherm of YTb (3 at. %) in Fig. 6.8.

The MR of YTb (3 at. %) for the paramagnetic temperatures (i.e. $T > T_N$) is always negative and decreases with increasing field as expected in the paramagnetic phase. The field dependence of the MR is like $(\Delta\rho/\rho_0) \propto -H^n$, ($1 < n < 2$). The anisotropy (A) for $T > T_N$ has a positive sign, that is LMR is greater than TMR. This is consistent with the expectations of eqn. (6.1) for TYb (3 at. %) with Tb^{3+} ($L = 3, S = 3$). A final remark should be made that the anisotropy (A) decreases with increasing temperatures, again qualitatively consistent with the results of Fert and co-workers (1977, 1974 and 1980).

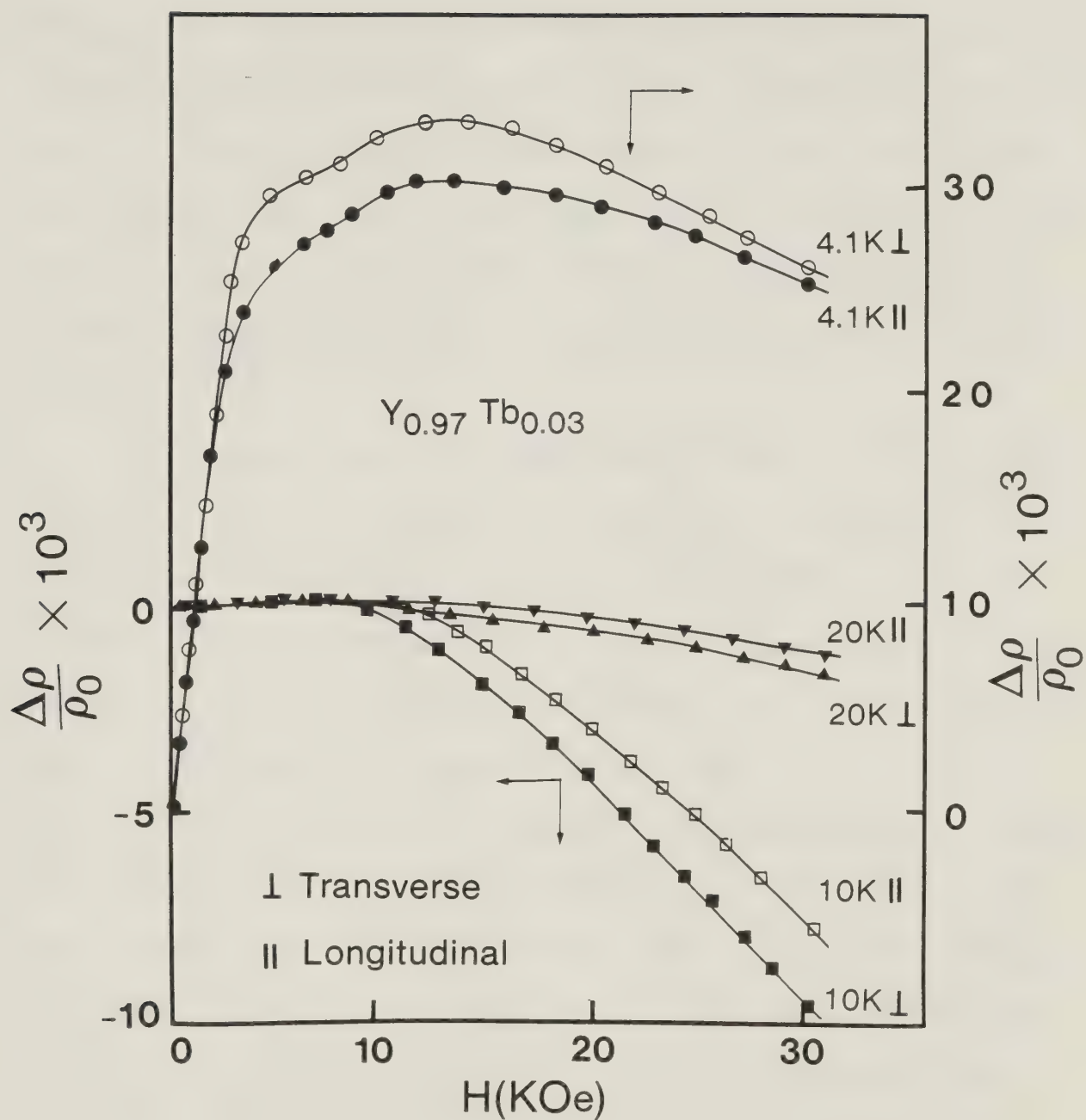


Fig. 6.8 Isothermal magnetoresistance ($\Delta\rho/\rho_0$) versus magnetic field (H) at different temperatures for YTb (3 at. % Tb).

CHAPTER 7

CONCLUDING REMARKS

We have done a systematic study of the low temperature resistivity, thermoelectric power and magnetoresistance of antiferromagnetic Rare Earth Hexaborides (REB_6). CeB_6 , a 'dense Kondo' material, exhibits anomalous behaviour. It is concluded from this study that the 'Kondo Lattice' model gives a qualitative understanding of the experimental resistivity and thermoelectric power results.

At lowest temperatures, where there are no significant excitations of magnons and phonons, we observe a T^2 dependence in the resistivity of all the REB_6 we have studied. This T^2 dependence has been associated with the electron-electron scattering of Baber-type (Ali and Woods, 1984). The magnetic resistivity of the REB_6 in the antiferromagnetic regime has a temperature dependence of either T^3 or T^4 which is in good agreement with the theoretical predictions of Rivier and Mensah (1977). The thermoelectric power of REB_6 has a minimum at low temperatures that is interpreted to be due to the phonon and magnon drag effects. We have estimated experimentally the magnetic contribution to the TEP for $T \gg T_N$. This TEP called the spin-disorder TEP (S_{spd}) by Gratz and Zuckermann (1982) is found to be negative and linear in temperature.

For the first time a systematic experimental study of the magnetoresistance of antiferromagnetic metals with localized magnetic moments has been done in this presentation. We have found that the MR of REB_6 metals (for $T < T_N$) is positive and increases with increasing external magnetic field. This positive MR is interpreted to be because of an enhancement of the spin fluctuations created by the presence of the external magnetic field. Similar results have been found for another antiferromagnetic metal $\text{GdRh}_{1.07}\text{Sn}_{4.21}$ (Ali *et al*, 1984). An anisotropy in the MR has been observed and found to be mainly associated with the anisotropic conduction electron-f-electron interaction.

We have done detailed measurements of resistivity and thermoelectric power in the immediate neighbourhood of T_N (the antiferromagnetic to paramagnetic phase transition temperature) and are able to extract values of α , the critical exponent, for REB_6 compounds (Ali and Woods, 1982). It has been found that there is a linear relationship between the temperature derivatives of the resistivity and the TEP in the vicinity of T_N (Ali and Woods, 1983, 1984a). This is in accordance with the theoretical predictions (Ausloos, 1977) that all transport coefficients have the same temperature dependence in the vicinity of T_N .

We have measured the low temperature electrical resistivity and absolute thermoelectric power of a few alloys of $[\text{La}, \text{Gd}]\text{B}_6$ and $[\text{La}, \text{Dy}]\text{B}_6$ with different concentrations of rare earth ions. The resistance of these alloys varies

as $\sim T^{3/2}$ which is characteristic of spin glasses at low temperatures. The TEP shows a broad positive peak in the lower part of the temperature range and becomes negative at high temperatures, a feature typical of a spin glass. We observe spin-glass behaviour even for 28 atomic percent of Gd^{3+} ion (Ali and Woods, 1983a).

The temperature dependence of resistivity, TEP and MR of dilute $Y_{1-x}RE_x$ ($RE = Ce, Sm, Dy$ and Tb) alloys has been also investigated. YCe ($Ce = 3\%$) exhibits only a typical Kondo effect, whereas YCe ($Ce = 15\%$) shows spin-glass behaviour at low temperatures with a Kondo resistance minimum at $\sim 7K$. For YDy alloys, 2% Dy is sufficient concentration to produce spin-glass behaviour with resistance varying as $T^{3/2}$ at lower temperatures and a broad peak in the TEP with a sign change from positive to negative at a higher temperature. We observe an antiferromagnetic to paramagnetic phase transition in YSm ($Sm = 3\%$) and YTb ($Tb = 3\%$) (Ali and Woods, 1984b).

BIBLIOGRAPHY

- Alexander, S., Helman, J.S. and Balberg, I. (1976), Phys. Rev. B13, 304.
- Ali, N. and Woods, S.B. (1982), J. Appl. Phys. 53, 7905.
- Ali, N. and Woods, S.B. (1983), Solid State Commun. 46, 33.
- Ali, N. and Woods, S.B. (1983a), Solid State Commun. 45, 471.
- Ali, N., Woods, S.B., Kozlowski, G. and Rojek, A. (1984), J. Phys. F. (to be published).
- Ali, N. and Woods, S.B. (1984), Phys. Lett. A (to be published).
- Ali, N. and Woods, S.B. (1984a), J. Low Temp. Phys. 56, 575.
- Ali, N. and Woods, S.B. (1984b), Solid State Commun. 49, 241.
- Andres, K., Graebner, J.E. and Ott, H.R. (1975), Phys. Rev. Lett. 35, 1779.
- Ausloos, M. (1977), Solid State Commun. 21, 373.
- Ausloos, M. (1977a), Physica 86-88B, 338.
- Baber, W.G. (1937), Proc. Roy. Soc. A158, 383.
- Bailyn, M. (1962), Phys. Rev. 126, 2040.
- Bailyn, M. (1967), Phys. Rev. 157, 480.
- Bak, P. and Mukamel, D. (1976), Phys. Rev. B13, 5086.
- Balberg, I. (1977), Physica 91B, 71.
- Balberg, I. and Maman, A. (1979), Physica 96B, 54.
- Béal-Monod, M.T. and Weiner, R.A. (1968), Phys. Rev. 170, 552.
- Berman, R., Brock, J.C.F. and Huntly, D.J. (1964), Cryogenics 4, 223.

- Campbell, I.A., Ford, P.J. and Hamzić, A. (1982), Phys. Rev. B26, 5195.
- Daybell, M.D. (1973), Magnetism, ed. G.T. Rado and H. Suhl, Academic Press, London, V, pp. 121.
- de Gennes, P.G. and Friedel, J. (1958), J. Phys. Chem. Solids 4, 71.
- de Gennes, P.G. (1962), J. Phys. Paris 23, 510.
- Dekker, A.J. (1965), J. Appl. Phys. 36, 906.
- Doniach, S. (1977), Physica 91B, 231.
- Dugdale, J.S. (1977), The Electrical Properties of Metals and Alloys (Edward Arnold Ltd.) Chapter 11.
- Felsch, W. (1978), Z. Phys. B29, 203.
- Fert, A., Asomoza, R., Spanjaard, D. and Friedrich, A., (1977), Phys. Rev. B16, 5050.
- Fert, A. and Levy, P.M. (1977a), Phys. Rev. B16, 5052.
- Fert, A., Asomoza, R., Creuzet, G. and Ousset, J.C. (1980), in Crystalline Electric Field and Structural Effect in f-electron Systems, ed. J.E. Crow et al (Plenum Press, New York) p. 381.
- Finnemore, D.K., Ostenson, J.E. and Stromberg, T.F. (1965), Rev. Sci. Inst. 36, 1369.
- Fischer, K.H. (1979), Z. Phys. B34, 45.
- Fischer, K.H. (1980), J. Magn. Magn. Mat. 15-18, 131.
- Fischer, K.H. (1981), Z. Phys. B42, 245.
- Fisher, M.E. and Langer, J.S. (1968), Phys. Rev. Lett. 20, 665.
- Fisk, Z. (1976), Solid State Commun. 18, 221.

- Fisk, Z. and Johnston, D.C. (1977), Solid State Commun. 22, 359.
- Ford, P.J. and Mydosh, J.A. (1976), Phys. Rev. B14, 2057.
- Ford, P.J. (1982), Contemp. Phys. 23, 141.
- Friederich, A. and Fert, A. (1974), Phys. Rev. Lett. 33, 1214.
- Geballe, T.H., Matthias, B.T., Andres, K., Maita, J.P., Cooper, A.S. and Corenzwit, E. (1968), Science 160, 1443.
- Geldart, D.J.W. and Richard, T.G. (1975), Phys. Rev. B12 5175.
- Gratz, E. (1981), J. Magn. Magn. Mat. 24, 1.
- Gratz, E. and Zuckermann, M.J. (1982), J. Magn. Magn. Mat. 29, 181.
- Gschneider, K.A. (1961), Rare Earth Alloys, New York: Van Nostrand Co.
- Guénault, A.M. (1971), J. Phys. F 1, 373.
- Hacker, H. Jr. and Lin, M.S. (1968), Solid State Commun. 6, 379.
- Hacker, H. Jr., Shimada, Y. and Chung, K.S. (1971), Phys. Stat. Sol. (a) 4, 459.
- Helman, J.S. and Balberg, I. (1978), Solid State Commun. 27, 41.
- Hirst, L.L. (1978), Adv. Phys. 27, 231.
- Hurd, C.M. (1982), Contemp. Phys. 23, 469.
- Ishizawa, Y., Tanaka, T., Bannai, E. and Kawai, S. (1977), J. Phys. Soc. Japan 42, 112.

- Jones, H. and Zener, C. (1934), Proc. Roy. Soc. A 144, 101.
- Jullien, R., Fields, J.N. and Doniac, S. (1977), Phys. Rev. B16, 4889.
- Kaplan, T.A. and Lyons, D.H. (1962), Phys. Rev. 128, 2072.
- Kapoor, A. (1974), Ph.D. Thesis, University of Alberta.
- Kasuya, T. (1950), Prog. Theor. Phys. (Kyoto) 22, 227.
- Kasuya, T. (1956), Prog. Theor. Phys. (Kyoto) 16, 45.
- Kasuya, T. (1959), Prog. Theor. Phys. 22, 227.
- Kasuya, T., Takegahara, K., Aoki, Y., Hanzawa, K., Kasaya, M., Kunii, S., Fujita, T., Sato, N., Kimura, H., Komatsubara, T., Furuno, T. and Rossat-Mignod, J. (1981), in Valence Fluctuations in Solids, eds., L.M. Falicov, H. Hanke and M.B. Maple (North-Holland Pub.) pp. 215.
- Kohler, M. (1938), Ann. Phys. (5), 32, 211.
- Kondo, J. (1962), Prog. Theor. Phys. 27, 772.
- Lacroix, C. and Cyrot, M. (1979), Phys. Rev. B20, 1969.
- Lavagna, M., Lacroix, C. and Cyrot, M. (1982), J. Phys. F 12, 745.
- Lavagna, M., Lacroix, C. and Cyrot, M. (1982a), Phys. Lett. 89A, 154.
- Lee, K.N., Bachmann, R., Geballe, T.H. and Maita, J.P. (1970), Phys. Rev. B2, 4580.
- Lee, K.N. and Bell, B. (1972), Phys. Rev. B6, 1032.
- Leguillon, J.C. and Zinn-Justin, J. (1980), Phys. Rev. B21, 3976.

- Leike, W., Stenglisch, F., Rander, K. and Keiter, H. (1979),
Phys. Rev. B20, 2129.
- Malmström, G. and Geldart, D.J.W. (1980), Phys. Rev. B21,
1133.
- Malmström, G. and Geldart, D.J.W. (1982), J. Phys. C 15,
5799.
- Mannari, J. (1959), Prog. Theor. Phys. (Kyoto) 22, 335.
- Matho, K. and Béal-Monod, M.T. (1974), J. Phys. F 4, 848.
- Matthias, B.T., Geballe, T.H., Andres, K., Corenzwit, E.,
Hull, G.W. and Maita, J.P. (1968), Science 159, 530.
- McAlister, S.P. and Hurd, C.M. (1976), Solid State Commun.
19, 881.
- McAlister, S.P. (1978), J. Appl. Phys. 49, 1616.
- McCarthy, C.M., Tompson, C.W., Graves, R.J., White, H.W.,
Fisk, Z. and Ott, H.R. (1980), Solid State Commun.
36, 861.
- McCarthy, C.M. and Tompson, C.W. (1980), J. Phys. Chem. Sol.
41, 1319.
- Mott, N.F. (1974), Philos. Mag. 30, 403.
- Mydosh, J.A., Ford, P.J., Kawatra, M.P. and Whall, T.E.
(1974), Phys. Rev. B10, 2845.
- Mydosh, J.A. (1978), J. Magn. Magn. Mat. 7, 237.
- Nagasawa, H. and Sugawara, T. (1967), J. Phys. Soc. Japan
23, 711.
- Nickerson, J.C. and White, R.M. (1969), J. Appl. Phys. 40,
1011.
- Nozaki, H., Tanaka, T. and Ishizawa, Y. (1980), J. Phys. C 13, 2751.

- Paderno, Yu.B., Pokrzywnicki, S. and Stalinski, B. (1967),
Phys. Stat. Sol. 24, K73.
- Peschel, I. and Fulde, P. (1970), Z. Phys. 238, 99.
- Richard, T.G. and Geldart, D.J.W. (1977), Phys. Rev. B15,
1502.
- Rivier, N. and Adkins, K. (1975), J. Phys. F 5, 1745.
- Rivier, N. and Mensah, A.E. (1977), Physica 91B, 85.
- Roberts, R.B. (1977), Phil. Mag. 36, 91.
- Rosenbaum, R.L. (1968), Rev. Sci. Inst. 39, 890.
- Rosenbaum, R.L. (1969), Rev. Sci. Inst. 40, 577.
- Ruderman, M.A. and Kittel, C. (1954), Phys. Rev. 96, 99.
- Sarkissian, B.V.B. and Coles, B.R. (1976), Comm. Phys. 1, 17.
- Sato, N., Woods, S.B., Komatsubara, T., Oguro, I., Kunii, S.
and Kasuya, T. (1983), J. Magn. Magn. Mat. 31-34, 417.
- Schrieffer, J.R. and Wolff, P.A. (1966), Phys. Rev. 149, 491.
- Seth, R.S. (1969), Ph.D. Thesis, University of Alberta.
- Sierro, J. Bucher, E., Longinotti, L.D., Takayama, H. and
Fulde, P. (1975), Sol. Stat. Commun. 17, 79.
- Singh, R.L. and Woods, S.B. (1981), J. Low Temp. Phys. 42,
241.
- Sparks, L.L. and Powell, R.L. (1972), J. Res. Nat. Bur.
Stand. (U.S.) - A. Phys. and Chem. 76A, 263.
- Specht, F. (1967), Phys. Rev. 162, 389.
- Stackhouse, B.J. (1977), Ph.D. Thesis, University of
Alberta.
- Sugawara, T. (1965), J. Phys. Soc. Japan 20, 2252.
- Takayama, H. and Fulde, P. (1975), Z. Phys. B20, 81.

- Tsang, E., Baberschke, K., Kästner, J. and Beandry, B.J.
(1980), Z. Phys. B38, 235.
- Umlauf, E., Pepperl, G. and Meyer, A. (1973), Phys. Rev.
Lett. 30, 1173.
- van Deursen, A.P.J., Fisk, Z. and de Vroomen, A.R. (1982),
Sol. St. Commun. 44, 609.
- Westrum, E.F., Jr., Clever, H.L., Andrews, J.T.S. and
Feick, S. (1966), in Rare Earth Research, ed. L.
Eyring, vol. III (New York: Gordon and Breach) pp.597.
- Westrum, E.F., Jr. (1968), in Progress in the Science and
Technology of the Rare Earths, vol. 3, (Oxford:
Pergamon) p. 459.
- Yamada, H. and Takada, S. (1973), Prog. Theor. Phys. 49,
1401.
- Yamada, H. and Takada, S. (1973a), J. Phys. Soc. Japan
34, 51.
- Yoshimori, A. and Sakurai, A. (1970), Prog. Theor. Phys.
Supp. 46, 162.
- Yosida, K. (1957), Phys. Rev. 106, 893.
- Yosida, K. (1957), Phys. Rev. 107, 397
- Ziman, J.M. (1960), Electrons and Phonons (The Clarendon
Press, Oxford).
- Zimmer, F. and Schilling, J.S. (1978), J. Magn. Magn. Mater.
9, 37.

B30422